The Dissertation Committee for Cheng-Ching Wang
certifies that this is the approved version of the following dissertation:

Two Problems in Many-Body Physics

Committee:

_____

Allan Hugh MacDonald, Supervisor

_____

John T. Markert

_____

James Chelikowsky

_____

Qian Niu

_____

Gregory A. Fiete

_____

Bhagawan R. Sahu

Two Problems in Many-Body Physics

by

Cheng-Ching Wang, B.S.;M.S.

DISSERTATION

Presented to the Faculty of the Graduate School of

The University of Texas at Austin

in Partial Fulfillment

of the Requirements

for the Degree of

DOCTOR OF PHILOSOPHY

THE UNIVERSITY OF TEXAS AT AUSTIN

December 2008

Dedicated to my parents and late Master advisor Zhen Ye.

Acknowledgments

I would like first to acknowledge my advisor, Allan H. MacDonald. His diligent attitudes and insights toward research is one of the best I have ever come across. He let me learn not to take things for granted and feel comfortable on uncertainties on the road of science exploration. When I was down at some point, his tolerance and willingness to understand is greatly appreciated. His encouragement also helps strengthen my positive attitudes toward frustration. I also thanks for his tolerance on the freedom to pursue my research interests. I will remember his forgetfulness and the good time working with him at Austin for a long long time. My committee members, Profs. John Markert, Q. Niu, James Chelikowsky, Greg Fiete and Dr. Bhagawan Sahu, are greatly appreciated for their helpful comments and precious time to make everything happen.

There are also several kind persons who make me feel at home in Allan's group when I joined the group at 2002 from the other side of the Pacific Ocean. Joaquin Fernndez-Rossier's enthusiasm to answer my stupid question , Ramin Abolfath's sincerity to discuss my bottleneck on research , and Alvaro Nunez's willingness to share his knowledge on good materials to learn research topics are all deeply appreciated. Jairo Sinova also showed me how to conduct a good research in a disciplined way.

more balanced during these years.

Two Problems in Many-Body Physics

Publication No. _____

Cheng-Ching Wang, Ph.D.
The University of Texas at Austin, 2008

Supervisor: Allan Hugh MacDonald

In this dissertation, the applications of many-body physics in neutral bosons and electronic systems in transition metal oxides are discussed. In the first part of the thesis, I will introduce the concepts of Bose condensation, emphasize the significance of the order parameter in superfluids (macroscopic wave function), and its consequence such as the emergence of exotic vortex states under rotation. Dated back to the importance of the vortex dynamics in the properties of high T_c superconductors, people have introduced a dual vortex description to describe the dynamics of charged bosons in a magnetic field. Similarly, the dual description is adapted to the problems of neutral bosons under rotation. Based on that picture, vortices behave like charges in an effective magnetic field which has been known to demonstrate different quantum phases such as Wigner crystal phase, and fractional quantum Hall liquid phases depending on the relative fraction of the number of bosons and vortices. In this work, we would like to address the validity of the picture by

low energy effective theory. We can identify the origin of the vortex masse and the parameter regimes in which the vortex dual description is appropriate.

In the second part of the dissertation, density functional theory is used to describe the strongly correlated matters with local density approximation and local Hubbard U interaction(LDA+U). We are particularly interested in the interface states in the heterojunction systems of two different perovskite oxides. What we found is that the interface states can be engineered to appear in certain transitional metal oxide layers by controlling the number of positive and negative charged layers, leading to the formation of quantum wells in two dimension. This type of systems ignite the hope to search for broken symmetry states in the interface which can be tunable with chemical doping or electric field doping. Even room temperature superconducting state may or may not exist in the interface is still an intriguing issue.

Table of Contents

List of Tables

List of Figures

xv

Chapter 1

Overview of many-body physics

With the development of quantum mechanics in last century, we should be able to understand what are the consequences due to the interaction between constituent particles such as electrons in solids and cold atoms in atomic traps by solving Schrödinger's equation. However, tremendous degree of freedoms in the many-body system has hindered this possibility. Therefore, different perspective are required to understand the many-body physics. One of the leading Giant, Lev Landau, in condensed matter physics introduce two crucial concepts, fermi liquid theory and the concept of symmetry breaking, which have become the paradigms of condensed matter physics.

1.1 Landau's Fermi liquid picture

Landau's Fermi liquid theory applies to Fermi system whose spectrum of elementary excitations is similar to that of a free Fermi gas. It is assumed that there is a one-to-one correspondence between the states of free Fermi gas and those of the interacting systems; that is, if one takes a state in the non-interacting system and turn on the interaction adiabatically , we will end up with a state of the interacting system. The assumption of one-to-

one correspondence fails if it comes across electronic phase transition (such as Wigner Crystallization, metal-supercoductor transition, metal-insulator transition) when the strength of the interaction is increased. An elementary excitation of the non-interacting system represents an "approximate excitation" of the interacting system (i.e. its "lifetime" is long). Excitations are quasi-particles(and quasi-holes) above a sharply defined Fermi surface. Based on the adiabatic assumption, a broad spectrum of observables can be analyzed without "microscopic" calculation. Both its remarkable success and failure has made Landau Fermi liquid theory a powerful tool in the development of condensed matter physics.

1.2 Landau's symmetry breaking theory

Landau's symmetry breaking theory states that the reason why different phases are different is due to the fact that they have different symmetries which can be described by order parameters. A phase transition is simply a transition that changes the symmetry. Landau's symmetry breaking theory describes almost all of the known phases, such as solid phases, ferromagnetic and antiferromagnetic phases, superfluid phases and all of the phase transition between them. A phase can have a gapless excitations if the ground state of the system which breaks the continuous symmetry of the Hamiltonian of the system. For example, gapless phonons exist in solids because the solid breaks the continuous translational symmetries. The understanding of the excitations is deeply rooted in the symmetry property of the phases.

1.3 Many-body physics as an emergent phenomena

Due to the complexity of many-particle systems, it has become clear that the collective behavior of the system at low energies can be qualitatively very different from the properties of individual particles and sensitive to the quantitative details of the system because of the closeness of different energy scales in the system. Transition metal oxide system[2, 3] is one of the best examples in condensed matter. High-temperature superconducting materials have multiple active competing orders(antiferromagnetic order, superconducting order, and stripe phases) and the transition to different phases are sensitive to the chemical doping. Also, colossal magnetoresistance in manganites is due to the fact that the preformed nanosized ferromagnetic clusters to render the system globally ferromagnetic when the temperature is between the Curie temperature T_c and Neel temperature T_N in the presence of disorders. These facts has led us to view strongly correlated physics as a good example of the emergent phenomena from complexity. Such complex systems exists on the edge of chaos-they can change dramatically and stochastically as a result of small changes in conditions. With the tremendous advance of computation power, there has been enormous efforts trying to understand correlated physics as accurate as possible to have predictive power for what should happen for the interested systems. Density functional theory (DFT), which has been used successfully to explore the ground states of metals, semiconductors, and band insulators, has been combined with static mean field theories such as LDA+U approach and dynamic mean field theory(DMFT). Those developments have

combine Landau's theories into the theories of correlated materials. It is noticed that exotic phases such as topological orders[1, 4, 5] in correlated systems which cannot be described by Landau's paradigms are becoming the frontier in condensed matter research. This is beyond the scope of the dissertation.

Chapter 2

Bose Einstein Condensation

Dated to the early days of twenty century, the indistinguishability of particles has led to the prediction of Bose Einstein condensation(BEC) at low temperature. BEC was first described for an ideal gas of free bosons with mass m and particle number N. The chemical potential μ is obtained from the conditions

$$n_{\mathbf{k}} = \frac{1}{e^{\beta(\epsilon_{\mathbf{k}} - \mu)} - 1}, \sum_{\mathbf{k}} n_{\mathbf{k}} = N, \qquad (2.1)$$

where $\epsilon_{\mathbf{k}} = \frac{\hbar^2 k^2}{2m}$ are the eigen-energies for free bosons and $\beta = \frac{1}{k_B T}$ is related to the inverse of the temperature. The chemical potential μ can only take values less than zero $\mu \leq 0$ because the occupation number $n_{\mathbf{k}}$ must be positive. When $\mu = 0$ at certain temperature T_c, we know the total number of particles in $\mathbf{k} \neq \mathbf{0}$ states will be maxima. Therefore, the number of particles in excited states N_{ex} will behave dramatically different for physics in different dimension d :

$$N_{ex} = \int d\epsilon D(\epsilon) \frac{1}{e^{\beta_c \epsilon} - 1}, \qquad (2.2)$$

where $D(\epsilon) \sim \epsilon^{d/2-1}$ is the density of states. When $d \leq 3$, N_{ex} is macroscopic when temperature is below T_c, this indicates the boson particles do not condensed into $\mathbf{k} = 0$ states. However, for $d = 3$, the macroscopic occupation of

zero momentum state is possible. Notice that this is the conclusion for the case without trapping potentials. With harmonic trapping potential, BEC can take places in lower dimensions $d > 1$ which render the excitements of cold atom physics feasible nowadays[6, 15]. We will generalize the concept of BEC to the interacting boson case and discuss inhomogeneous spatial states such as vortex states in this dissertation.

2.1 Definition of BEC and macroscopic wave function

Let us define the BEC in a more general sense from Leggett's perspective[15]. Consider a system of N identical spinless bosons characterized by the spatial coordinates $\mathbf{r}_i$ $(i = 1, 2, ...N)$, with arbitrary interactions and subject to some external potential which can be time dependent. The system is neither necessarily in thermal equilibrium or in steady state. The many-body wave functions $\Psi(\mathbf{r_1}, \mathbf{r_2}, ..\mathbf{r_N}, t)$ must be symmetric with respect to the interchange of any two particle coordinates. For any given time t, we can define the one-particle reduced density matrix $\rho(\mathbf{r}, \mathbf{r}', t)$ in which the description of the system is given by a statistical mixture of mutually orthogonal many-body states Ψ_N^s with probability p_s :

$$\rho(\mathbf{r}, \mathbf{r}', t) \equiv N \sum_s p_s \int d\mathbf{r_2}...d\mathbf{r_N} \Psi_N^{*(s)}(\mathbf{r}, \mathbf{r_2}...\mathbf{r_N}, \mathbf{t}) \Psi_N^{*(s)}(\mathbf{r}', \mathbf{r_2}...\mathbf{r_N}, \mathbf{t}) \quad (2.3)$$

$$\equiv \langle \hat{\phi}^\dagger(\mathbf{r}, t) \hat{\phi}(\mathbf{r}', t) \rangle$$

where $\hat{\phi}(\mathbf{r}', t)$ is the standard boson field operator. It is clear that the density matrix is hermitian with respect to the indices $\mathbf{r}$ and $\mathbf{r}'$. Therefore, it can be

6

diagonalized with real eigenvalues with orthogonal eigenfunctions $\chi_i(\mathbf{r}, t)$ such that we can expand

$$\rho(\mathbf{r}, \mathbf{r}', t) = \sum_i n_i(t) \chi_i^*(\mathbf{r}, t) \chi_i(\mathbf{r}', t). \qquad (2.4)$$

It is important to note that not only the eigenfunctions χ_i but also the eigenvalue n_i may be functions of time and χ_i need not to be eigenfunctions of any other operators; in particular, eigenfunctions of the single-particle terms in system Hamiltonian. Based on the density matrix, we can say that at any time t, the system shows BEC if one or more of the eigenvalues $n_i(t)$ is macroscopic to the order of the number of particles N. It shows simple BEC when one and only one eigenvalue is of order N, and all the rest being of order 1. Systems showing non-simple BEC(having more than one eigenvalue of order N are said to be fragmented. In the case of simple BEC, the eigenfunction $\chi_i(\mathbf{r}, t)$ corresponds to macroscopic occupation n_i is called the macroscopic wave function.

2.2 Why simple BEC ?

However, in the presence of interactions, simple BEC is not guarantied. Why don't condensed particles share states that are degenerate or at least close in energy? The answer is the exchange energy that makes condensate fragmentation costly. We can use a simple argument to claim that simple BEC is protected by repulsive interaction when system is in equilibrium. The interaction energy in a system of spinless boson particles can be written as

second quantized form as

$$E_{int} = \frac{1}{2} \int d\mathbf{r_1} d\mathbf{r_2} V(|\mathbf{r_1} - \mathbf{r_2}|) \langle \phi^\dagger(\mathbf{r_1}) \phi^\dagger(\mathbf{r_2}) \phi(\mathbf{r_2}) \phi(\mathbf{r_1}) \rangle. \qquad (2.5)$$

If we expand the field operators $\phi^\dagger(\mathbf{r_1})$, $\phi^\dagger(\mathbf{r_2})$ into single particle basis $|\chi_i\rangle$ of the density matrices, the interaction energy can be written as

$$E_{int} = \frac{1}{2} \sum_{ijkl} V_{i,j,k,l} \langle a_i^\dagger a_j^\dagger a_k a_l \rangle. \qquad (2.6)$$

where the matrix element $V_{i,j,k,l}$ in the single particle basis is given by

$$V_{i,j,k,l} = \int d\mathbf{r_1} d\mathbf{r_2} \chi_i^*(\mathbf{r_1}) \chi_j^*(\mathbf{r_2}) V(|\mathbf{r_1} - \mathbf{r_2}|) \chi_k(\mathbf{r_2}) \chi_l(\mathbf{r_1}). \qquad (2.7)$$

For simplicity, we consider the interaction between particles is short ranged with the form $V(|\mathbf{r_1} - \mathbf{r_2}|) = g\delta(\mathbf{r_1} - \mathbf{r_2})$. Therefore, we can rewrite the E_{in} as

$$E_{int} = \frac{g}{2} \sum_{i,j,k,l} \langle a_i^\dagger a_j^\dagger a_k a_l \rangle \int d\mathbf{r} \chi_i^*(\mathbf{r}) \chi_j^*(\mathbf{r}) \chi_k(\mathbf{r}) \chi_l(\mathbf{r}) \qquad (2.8)$$

When $i \neq j$, the average $\langle a_i^\dagger a_j^\dagger a_k a_l \rangle$ is given by

$$\langle a_i^\dagger a_j^\dagger a_k a_l \rangle = \langle a_i^\dagger a_k \rangle \langle a_j^\dagger a_l \rangle + \langle a_i^\dagger a_l \rangle \langle a_j^\dagger a_k \rangle = n_i n_j (\delta_{ik}\delta_{jl} + \delta_{il}\delta_{jk}), i \neq j. \quad (2.9)$$

When $i = j$, the average $\langle a_i^\dagger a_j^\dagger a_k a_l \rangle$ take the value

$$\langle a_i^\dagger a_j^\dagger a_k a_l \rangle = \langle a_i^\dagger a_k \rangle \langle a_i^\dagger a_l \rangle = \delta_{ik}\delta_{il} \langle a_i^\dagger a_i \rangle^2 = (n_i^2 - n_i)\delta_{ik}\delta_{il}, i = j. \qquad (2.10)$$

Therefore, the interaction energy can be rewritten as

$$E_{int} = \frac{g}{2} \sum_{ij} [n_i n_j (2 - \delta_{ij}) - n_i \delta_{ij}] \int d\mathbf{r} |\chi_i(\mathbf{r})|^2 |\chi_j(\mathbf{r})|^2. \qquad (2.11)$$

8

Let consider a special case that there are two degenerate states in which the boson can condense into with occupation numbers n_1 and n_2. Suppose the total number of the system $N = n_1 + n_2$ is large. The interaction energy in this case can be simplified as

$$E_{int} = \frac{g}{2} \sum_{ij} [n_i n_j (2 - \delta_{ij}) - n_i \delta_{ij}] \int d\mathbf{r} |\chi_i(\mathbf{r})|^2 |\chi_j(\mathbf{r})|^2. \qquad (2.12)$$

From the expression, when we have repulsive interaction $g > 0$, the system will favor occupation into a single one-particle state, which can be checked by looking at two-state systems. Equal populations in two states will make the product term in the expression cost more energy due to the effect of the product term $n_i n_j$.

2.3   BEC implies phase coherence

Based on simple BEC argument, the density matrix $\rho(\mathbf{r}, \mathbf{r}', t)$ in the condensed phase χ_i must be able to factorized as the product of the macroscopic wave function and its complex conjugate:

$$\langle \hat{\phi}^\dagger(\mathbf{r}, t) \hat{\phi}(\mathbf{r}', t) \rangle \sim \chi_i^*(\mathbf{r}', t) \chi_i(\mathbf{r}, t) \qquad (2.13)$$

P.W. Anderson further assume that the macroscopic wave function $\chi_i(\mathbf{r}, t)$ is the average of the field operator $\langle \phi(\mathbf{r}, t) \rangle$, i.e. $\langle \phi(\mathbf{r}, t) \rangle = \chi_i(\mathbf{r}, t)$. This can only be so when the condensate state is phase coherent (particle number is not conserved). Based on the phase coherent states, one can construct the path integral formulation to describe boson physics quite successfully. However, it

9

is worthwhile to keep in minds that this assumption is still controversial[7–9] but does not run into serious problems in predicting observable effects.

Chapter 3

Microscopic theory for bosons

In this chapter, we would like to develop the low temperature theory for boson particles including the ground state properties and collective excitations (Bogoliubov excitations). There are various theoretical descriptions which leads to the same conclusions and has mostly been shown in standard textbook in BEC. Here I will motivate the idea with canonical Hamiltonian formulation to derive the mean field ground state of bosons and low energy excited states quantum mechanically. Alternative approaches are those such as variational wave function approach(Appendix A) or path integral formulation (Appendix B) which I will use to study vortex dynamics in condensate.

3.1 Gross Pitaevskii equation

An essential feature of a dilute Bose gas at zero temperature is the existence of a macroscopic wave function('order parameter')Ψ that characterizes the Bose condensate. For a uniform system with N particles in a box of volume V, the order parameter $\Psi = \sqrt{N_0/V}$ reflects the presence of a macroscopic number N_0 of particles in the zero momentum state $\mathbf{k} = 0$, with the remaining particles $N' = N - N_0$ distributed in remaining states ($\mathbf{k} \neq \mathbf{0}$). For

11

nonuniform case due to the existence of vortex states or the inhomogeneous trapping potential V_{tr}, the same idea can also be generalized.

The existence of nonuniform states of a dilute Bose gas can be understood by considering a second-quantized Hamiltonian

$$\hat{H} = \int dV [\hat{\psi}^\dagger (T + V_{tr})\hat{\psi} + \frac{1}{2}g\hat{\psi}^\dagger\hat{\psi}^\dagger\psi\psi], \qquad (3.1)$$

expressed in terms of Bose field operators $\hat{\psi}(\mathbf{r})$ and $\hat{\psi}^\dagger(\mathbf{r})$ that obey boson commutation relations

$$[\psi(\mathbf{r}), \hat{\psi}^\dagger(\mathbf{r})] = \delta(\mathbf{r}, \mathbf{r}'), [\psi(\mathbf{r}), \psi(\mathbf{r})] = [\hat{\psi}^\dagger(\mathbf{r}), \hat{\psi}^\dagger(\mathbf{r}')] = 0. \qquad (3.2)$$

Here $T = \frac{-\hbar^2}{2m}\nabla^2$ is the kinetic energy operator for the particles with mass m, and the inter-particle potential has been approximated by a short-ranged interaction $g\delta(\mathbf{r}-\mathbf{r}')$, where g is a coupling constant with the dimensions of energy $\times$ volume. For a dilute cold gas, only binary collisions at low energy are relevant, and these collisions are characterized by a single parameter, the s-wave scattering length a, independent of the details of the two-particle potentials. The time dependence of the Heisenberg field operator $\hat{\psi}(\mathbf{r}, t) = exp(-i\hat{H}t)\hat{\psi}(\mathbf{r})exp(i\hat{H}t)$ obeys the equation of motion $i\hbar\frac{\partial\hat{\psi}(\mathbf{r},t)}{\partial t} = [\hat{\psi}(\mathbf{r},t), \hat{H}]$, which yields a nonlinear operator equation

$$i\hbar\frac{\partial\hat{\psi}(\mathbf{r},t)}{\partial t} = (T + V_{tr})\hat{\psi}(\mathbf{r},t) + g\hat{\psi}(\mathbf{r},t)\psi(\mathbf{r},t)\psi(\mathbf{r},t). \qquad (3.3)$$

The macroscopic occupation of condensate make it natural to write down the field operator as a sum $\hat{\psi}(\mathbf{r}, t) = \Psi(\mathbf{r}, t) + \delta\hat{\psi}(\mathbf{r}, t)$ of the order parameter $\Psi(\mathbf{r}, t) = <\hat{\psi}(\mathbf{r}, t)>$ which describes the condensate and the quantum

field $\delta\hat\psi(\mathbf{r},t)$ referring to remaining noncondensed particles. To leading order, the time-dependent Gross-Pitaevskii(GP)equation can be derived by neglecting quantum fluctuations entirely :

$$i\hbar\frac{\partial\Psi(\mathbf{r},t)}{\partial t}=[T+V_{tr}+g|\Psi(\mathbf{r},t)|^2]\Psi(\mathbf{r},t) \qquad (3.4)$$

for the condensate wave function $\Psi(\mathbf{r},t)$. If there is no explicit time dependence for the system Hamiltonian $\hat{H}$, the field operator $\hat\psi(\mathbf{r},t)$ reduce the number of particles by one, its matrix element $<\hat\psi(\mathbf{r},t)>\approx<N-1|\hat\psi(\mathbf{r},t)|N>=\Psi(\mathbf{r})e^{-i\mu t}$ oscillates at a frequency corresponding to the chemical potential $\mu\approx E_0(N)-E_0(N-1)$ associated with removing one particle from the ground state with particle number N. Thus the $\Psi(\mathbf{r})$ satisfies the stationary GP equation

$$(T+V_{tr}+g|\Psi|^2)\Psi=\mu\Psi \qquad (3.5)$$

In general, this equation is nonlinear and needs to be solved numerically.

From the time dependent GP equation, we can also identify how the condensate velocity $\mathbf{v}$ relates to the phase field $\phi(\mathbf{r},t)$ of condensate wave function $\Psi(\mathbf{r},t)$. We can write the condensate wave function $\Psi(\mathbf{r},t)=|\Psi|e^{i\phi}$ in terms of the amplitude $|\Psi(\mathbf{r},t)|$ and the phase field $\phi(\mathbf{r},t)$. The condensate density n is defined by $|\Psi(\mathbf{r},t)|^2$.

The number of particles need to conserved in the condensate when neglecting fluctuations; therefore, the continuity equation must be satisfied

$$\frac{\partial n}{\partial t}+\nabla\cdot(n\mathbf{v})=\mathbf{0}. \qquad (3.6)$$

By manipulating the complex conjugate of Eq. (3.4) and the $n = \Psi(\mathbf{r}, t)\Psi^*(\mathbf{r}, t)$, one can identify the form of the condensate velocity is proportional to the gradient of phase field $\phi(\mathbf{r}, t)$

$$v(\mathbf{r}, t) = \frac{\hbar}{m}\nabla\phi(\mathbf{r}, t). \tag{3.7}$$

3.2 Bogoliubov excitations

Now we are going to discuss the elementary excitations due to quantum fluctuations. The eigenstates of the excitations are collective due to the coupling to the condensate which acts as a particle reservoir. In Bogoliubov's approximation, scattering between excitations are completely ignored. This theory is particular good when the system is at low temperature in which the thermal population of excited states are scarce. By substituting $\hat{\psi}(\mathbf{r}, t) = \Psi(\mathbf{r}, t) + \delta\hat{\psi}(\mathbf{r}, t)$ into Eq. (3.3) and keeping the field operators $\delta\hat{\psi}^\dagger$ and $\delta\hat{\psi}$ to leading order in small deviations, one finds the Bogoliubov equations of motion for the fluctuations $\delta\hat{\psi}, \delta\hat{\psi}^\dagger$

$$i\hbar\frac{\partial\delta\hat{\psi}(\mathbf{r}, t)}{\partial t} = [T + V_{tr} + 2g|\Psi|^2]\delta\hat{\psi}(\mathbf{r}, t) + g\Psi^2\delta\hat{\psi}^\dagger(\mathbf{r}, t) \tag{3.8}$$

and

$$-i\hbar\frac{\partial\delta\hat{\psi}^\dagger(\mathbf{r}, t)}{\partial t} = [T + V_{tr} + 2g|\Psi|^2]\delta\hat{\psi}^\dagger(\mathbf{r}, t) + g\Psi^{*2}\delta\hat{\psi}(\mathbf{r}, t) \tag{3.9}$$

Assume the existence of a linear transformation to quasiparticle operators $\hat{\alpha}_j(t)$ and $\hat{\alpha}_j^\dagger(t)$ for a set of normal modes labeled by j

$$\delta\hat{\psi}(\mathbf{r}, t) = e^{-i\mu t}\sum_j'[u_j(\mathbf{r})\hat{\alpha}_j(t) - v_j(\mathbf{r})^*\hat{\alpha}_j^\dagger(t)],$$

14

$$\delta\hat{\psi}^{\dagger}(\mathbf{r}, t) = e^{+i\mu t} \sum_{j}^{\prime} [u_j^*(\mathbf{r})\hat{\alpha}_j^{\dagger}(t) - v_j(\mathbf{r})\hat{\alpha}_j(t)], \tag{3.10}$$

where the prime sum indicates to omit the condensate mode. Here, the quasi-particle operators $\hat{\alpha}_j$ and $\hat{\alpha}_j^{\dagger}$ obeys Boson commutation relations $[\alpha_j, \alpha_k^{\dagger}] = \delta_{j,k}, [\alpha_j, \alpha_k] = [\alpha_j^{\dagger}, \alpha_k^{\dagger}] = 0$ and have simple time dependence $\alpha_j(t) = \alpha_j e^{-iE_j t/\hbar}$ and $\alpha_j^{\dagger}(t) = \alpha_j^{\dagger} e^{iE_j t/\hbar}$ and the time dependence $e^{-i\mu t}, e^{+i\mu t}$ is required due to the appearance of those terms $\Psi^2 \delta\psi^{\dagger}$ and $\Psi^{*2}\delta\psi$ to satisfy Bogoliubov equations of motion at any time t. By direct substitution, we find the following time-independent Bogoliubov equations in matrix form

$$\begin{pmatrix} L & -g\Psi^2 \\ -g\Psi^{*2} & L \end{pmatrix} \begin{pmatrix} u_j \\ v_j \end{pmatrix} = \begin{pmatrix} E_j & 0 \\ 0 & -E_j \end{pmatrix} \begin{pmatrix} u_j \\ v_j \end{pmatrix} \tag{3.11}$$

where the Hermitian operator L is defined as $L = T + V_{tr} - \mu + 2g|\Psi|^2$. Multiply the vector (u_j, v_j) to the above equation and do integration over the whole space $\int dV$, it can be shown that $E_j \int dV(|u_j|^2 - |v_j|^2)$ is real. If the integral $\int dV(|u_j|^2 - |v_j|^2)$ is nonzero, then E_j itself is real. For each solution u_j, v_j with eigenvalue E_j and positive normalization, the Bogoliubov equations always have a second solution v_j^*, u_j^* with eigenvalue $-E_j$ and negative normalization. Physically, the solutions with negative normalization is not physically allowed since it violates the Boson commutation relation for α_j and $\alpha_j^{\dagger}$ we are looking for. The only exception to the requirement of real E_j arises for zero-norm solutions with $\int dV(|u_j|^2 - |v_j|^2) = 0$ and it deserve further analysis when this happens. It can be shown the part of Hamiltonian $\hat{H}$ due to fluctuations $\hat{H}_{BG}$ are diagonal in the Bogoliubov basis $\hat{H}_{BG} = \sum_j^{\prime} E_j \alpha_j^{\dagger} \alpha_j$ [10].

3.3 uniform Bose gas

In this section, we will apply the Bogoliubov's equations to see what we can learn from the microscopic theory. We consider a uniform gas of N interacting bosons contained in a box of volume V . In the homogeneous system , momentum $\mathbf{k}$ is a good quantum number and the trapping potential $V_{tr}(\mathbf{r}) = 0$. Therefore, we can search for the solution for the momentum $\mathbf{k}$ in Eq. (3.11)

$$u_{\mathbf{k}}(\mathbf{r}) = u_{\mathbf{k}}\frac{e^{i\mathbf{k}\cdot\mathbf{r}}}{V^{1/2}} \quad and \quad v_{\mathbf{k}}(\mathbf{r}) = v_{\mathbf{k}}\frac{e^{i\mathbf{k}\cdot\mathbf{r}}}{V^{1/2}}, \tag{3.12}$$

where the normalization factor $1/V^{1/2}$ is introduced explicitly. The chemical potential μ for the condensate wave state $\Psi(\mathbf{r}) = \sqrt{n}$ can be solved by Eq. ((3.5)) by knowing the kinetic energy $T\Psi$ and potential energy $V_{tr} = 0$ make no contribution. As a result, the chemical potential for the uniform system is due to the interaction energy between particles $\mu = gn$ where n is the condensate number density. Therefore, the Bogoliubov equations are

$$\begin{pmatrix} \frac{\hbar^2}{2m} + gn - \epsilon_{\mathbf{k}} & -gn \\ -gn & \frac{\hbar^2}{2m} + gn + \epsilon_{\mathbf{k}} \end{pmatrix} \begin{pmatrix} u_q \\ v_q \end{pmatrix} = 0. \tag{3.13}$$

To have nonzero solutions for $u_{\mathbf{k}}, v_{\mathbf{k}}$, the determinant of the above matrix must vanishes and leads to the condition

$$\epsilon_{\mathbf{k}}^2 = \epsilon_{\mathbf{k}}^0(\epsilon_{\mathbf{k}}^0 + 2gn), \tag{3.14}$$

where $\epsilon_{\mathbf{k}}^0 = \frac{\hbar^2 k^2}{2m}$ is the energy for a free particle with momentum $\mathbf{k}$. As discussed in last section, we only look for solutions with positive Bogoliubov excitation energy $\epsilon_{\mathbf{k}}$ and positive normalization condition $|u_{\mathbf{k}}|^2 - |v_{\mathbf{k}}|^2 = 1$ since

16

this ensures the Boson commutation relation for Bogoliubov quasiparticles. Without loss of generality we may take $u_\mathbf{k}$ and $v_\mathbf{k}$ to be real. With this choice, one finds that

$$u_\mathbf{k}^2 = \frac{1}{2}(\frac{\xi_\mathbf{k}}{\epsilon_\mathbf{k}} + 1) \quad and \quad v_\mathbf{k}^2 = \frac{1}{2}(\frac{\xi_\mathbf{k}}{\epsilon_\mathbf{k}} - 1), \tag{3.15}$$

in which $\xi_\mathbf{k} \equiv \epsilon_\mathbf{k}^0 + gn$. From the excitation energies $\epsilon_\mathbf{k} = +\sqrt{\epsilon_\mathbf{k}^0(\epsilon_\mathbf{k}^0 + 2gn)}$, the energy dispersion $\epsilon_\mathbf{k} = \hbar k c_s$ is phonon-like and gapless at low momentum ($\frac{\hbar^2}{2m} << 2gn$), where $c_s = \sqrt{gn/m}$ is the speed of sound in dilute gas. This indicates the excitations are collective. At high momentum ($\frac{\hbar^2}{2m} >> 2gn$), the excitation energy $\epsilon_\mathbf{k} \rightarrow \frac{\hbar^2}{2m}$ is particle-like showing the Bogoliubov excitations at high energy is free particles.

Let's look at the problem from the free particle basis so that we can interpret the physics more clearly. From the field operators in Eq. 3.10 at $t = 0$, it can be written in free particle basis as

$$\delta\psi(\mathbf{r}) = \sum_\mathbf{k} \frac{e^{i\mathbf{k}\cdot\mathbf{r}}}{V^{1/2}}\hat{a}_\mathbf{k} \quad , \quad \delta\hat{\psi}^\dagger(\mathbf{r}) = \sum_\mathbf{k} \frac{e^{-i\mathbf{k}\cdot\mathbf{r}}}{V^{1/2}}\hat{a}_\mathbf{k}^\dagger. \tag{3.16}$$

In Bogoliubov basis, the field operators can be rewritten as

$$\delta\psi(\mathbf{r}) = \sum_\mathbf{k} u_\mathbf{k}(\mathbf{r})\hat{\alpha}_\mathbf{k} - v_\mathbf{k}^*(\mathbf{r})\hat{\alpha}_\mathbf{k}^\dagger = \sum_\mathbf{k} u_\mathbf{k}(\mathbf{r})\hat{\alpha}_\mathbf{k} - v_{-\mathbf{k}}^*(\mathbf{r})\hat{\alpha}_{-\mathbf{k}}^\dagger$$

$$= \sum_\mathbf{k} u_\mathbf{k}\hat{\alpha}_\mathbf{k} - v_\mathbf{k}\hat{\alpha}_{-\mathbf{k}}^\dagger, \tag{3.17}$$

in which $v_\mathbf{k} = v_{-\mathbf{k}}$ is used. By comparison, $\hat{a}_\mathbf{k} = u_\mathbf{k}\hat{\alpha}_\mathbf{k} - v_\mathbf{k}\hat{\alpha}_{-\mathbf{k}}^\dagger$. One can also derive the following relation by using the symmetry $u_\mathbf{k} = u_{-\mathbf{k}}$ and $v_\mathbf{k} = v_{-\mathbf{k}}$

$$\hat{a}_{-\mathbf{k}} = u_\mathbf{k}\hat{\alpha}_{-\mathbf{k}} - v_\mathbf{k}\hat{\alpha}_\mathbf{k}^\dagger, \quad \hat{a}_\mathbf{k}^\dagger = u_\mathbf{k}\hat{\alpha}_\mathbf{k}^\dagger - v_\mathbf{k}\hat{\alpha}_{-\mathbf{k}}. \tag{3.18}$$
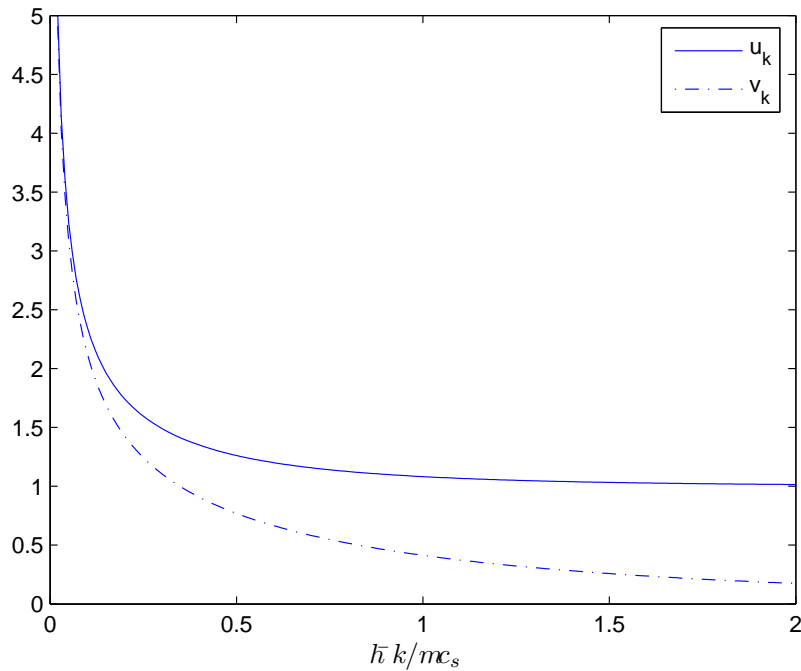
Figure 3.1: The coefficient $u_{\mathbf{k}}$ and $v_{\mathbf{k}}$ as a function of the wave number scaled by mc_s as the dimensionless variable $\hbar k/mc_s$.

By manipulating the above equation and use the normalization $u_{\mathbf{k}}^2 - v_{\mathbf{k}}^2 = 1$, we have the relation

$$\hat{\alpha}_{\mathbf{k}}^{\dagger} = u_{\mathbf{k}}\hat{a}_{\mathbf{k}}^{\dagger} + v_{\mathbf{k}}a_{-\mathbf{k}}. \tag{3.19}$$

The behaviors of $u_{\mathbf{k}}$ and $v_{\mathbf{k}}$ are shown as a function of $\mathbf{k}$ in Fig. 3.1. Therefore, Bogoliubov excitations at large $\mathbf{k}(u_{\mathbf{k}} \to 1, v_{\mathbf{k}} \to 0)$ is equivalent to free particle creations at momentum $\hbar\mathbf{k}$. At small $\mathbf{k}$ in which $u_{\mathbf{k}}, v_{\mathbf{k}}$ are equal in magnitude, Bogoliubov excitations at momentum $\hbar\mathbf{k}$ are excitations of the pairing between particle and hole excitations at momentum $\hbar\mathbf{k}$.

18

3.3.1 Depletion of condensate at zero temperature

In this subsection, we would like to understand one of the observable effects on dilute Bose condensate. Even in the absence of thermal fluctuations, at zero temperature, there is still condensate population depletion due to the interaction effects between particles. We can write the number operator $\hat{N}$ in Bogoliubov basis as

$$\hat{N} = N_0 + \sum_{\mathbf{k} \neq 0} \hat{a}_{\mathbf{k}}^\dagger \hat{a}_{\mathbf{k}} = N_0 + {\sum_{\mathbf{k}}}' v_{\mathbf{k}}^2 + {\sum_{\mathbf{k}}}' (u_{\mathbf{k}}^2 + v_{\mathbf{k}}^2) \hat{\alpha}_{\mathbf{k}}^\dagger \alpha_{\mathbf{k}} - {\sum_{\mathbf{k}}}' u_k v_k (\alpha_{\mathbf{k}}^\dagger \hat{\alpha}_{-\mathbf{k}}^\dagger + \hat{\alpha}_{-\mathbf{k}} \hat{\alpha}_{\mathbf{k}}),$$

(3.20)

where the prime sum indicates the exclusion of condensate state $\mathbf{k} = \mathbf{0}$ and Bose commutation relations for $[\hat{\alpha}_{-\mathbf{k}}, \hat{\alpha}_{-\mathbf{k}}^\dagger] = 1$ is used. The physical interpretation of this expression is that the first term is the number of particles in condensed phase. The second term represents the depletion of the condensate by interactions ($v_{\mathbf{k}}$ is dominant at low momentum $\mathbf{k}$) at zero temperature. The third term are the depletion due to thermal fluctuations. The last term represents the effect due to physical excitations which change the total particle number of the system by external means. For an isolated system, the total number of particle is conserved. The last term can be dropped out. Let us evaluate the second term explicitly and one finds that the number density in excited states is given by

$$n_{ex} = \frac{1}{V} {\sum}' v_{\mathbf{k}}^2 = \int \frac{d\mathbf{p}}{(2\pi\hbar)^3} v_{\mathbf{k}}^2 = \frac{1}{3\pi^2} (mc_s\hbar)^3.$$

(3.21)

19

If we take cold atom system as the example in which the contact interaction is given by $g = 4\pi\hbar^2 a/m$, and one finds

$$\frac{n_{ex}}{n} = \frac{8}{3\sqrt{\pi}}(na^3)^{1/2}, \qquad (3.22)$$

where a is the scattering length which can be generally tuned by Feshbach resonance between atoms. For dilute cold atoms $na^3 \ll 1$, there is not much condensate depletion which shows the validity of the Bogoliubov theoy in the boson dilute gas system.

Chapter 4

Vortices in condensate

4.0.2 Vortex as a topological defect in superfluids

Due to the fact that the superfluid order parameter is described by condensate wave function $\Psi(\mathbf{r}) = \sqrt{n}fe^{i\phi}$ where f is the amplitude and ϕ is the phase field and n is bulk particle density. Quite generally, from the single-valueness of the condensate wave function it follows that around a closed contour the change phase angle must be a multiple of 2π as

$$\triangle\phi = \oint \bigtriangledown\phi \cdot d\mathbf{r} = 2\pi k, \tag{4.1}$$

where k is the integer number(winding number in topology). According to the continuity equation for the condensate, the velocity of the condensate is proportional to the gradient of phase angle $\mathbf{v} = \frac{\hbar}{m}\bigtriangledown\phi$. It follows immediately the circulation Γ of the condensate is also quantized.

$$\Gamma = \oint \mathbf{v} \cdot d\mathbf{r} = k\frac{h}{m}. \tag{4.2}$$

In addition, the velocity field of the condensate must be irrotational, that is, $\nabla\times\mathbf{v} = 0$ unless there are singularities in the velocity field. Those singularities correspond to the vortex lines in the condensate and are solutions of Gross-Pitaevskii equation.

Let us illustrate the case of a single straight vortex line in an otherwise uniform dilute Bose-Einstein condensate with bulk particle density n. This is equivalent to a reduced two dimensional problem since the physics along the direction of the vortex line is frozen. Eq. (4.2) gives the circulating velocity of the vortex line as

$$\mathbf{v}(\mathbf{r}) = \frac{\hbar}{mr}\hat{\theta}; \tag{4.3}$$

this hydrodynamic flow has circular streamlines and a magnitude that diverges as $r \to 0$. The circulation Γ can be transformed with Stokes theorem as $\int da \nabla \times \mathbf{v} = 2\pi\hbar/m$, implying a singular localized vorticity at the center of the vortex core

$$\nabla \times \mathbf{v} = \frac{2\pi\hbar}{m}\delta^2(\mathbf{r})\hat{z}. \tag{4.4}$$

The kinetic energy per unit length of the vortex is

$$\frac{\hbar^2}{2m}\int |\bigtriangledown \Psi|^2 = \frac{\hbar^2 n}{2m}\int d\mathbf{r}\left[(\frac{df}{dr})^2 + \frac{f^2}{r^2}\right], \tag{4.5}$$

where the first term arises from the density variation near the vortex core and the second term is the kinetic energy of the circulating flow. With this kinetic energy functional, the Euler-Lagrange equation yields the nonlinear GP equation for the radial amplitude $f(r)$. The resulting centrifugal barrier forces the amplitude $f(r)$ to vanish linearly to avoid divergence of the kinetic energy for $r \leq \xi$, which characterizes the vortex core, and $f(r) \approx 1$ for $r \gg \xi$. In addition, the particle-current density $|j(\mathbf{r})| = n|f(r)|^2\hbar/mr$ vanishes both far away from the vortex and at the center of the vortex with a maximum near $r \approx \xi$. Defects such as vortices just described are important because

they cannot be made to disappear by any continuous deformation of the order parameter. Any noncontinuous deformation will cost a macroscopic energy to change between states with different topology. The topology stability also implies physical stability from energy considerations.

4.0.3 Vortex phases under rotation

One of the most spectacular manifestations of the existence of a macroscopic wave function describing a Bose-Einstein condensate is the nucleation of quantized vortices when the system is set in rotation. Based on experimental observation that Helium superfluid in rotating bucket experiments with angular velocity $v = \Omega \times \mathbf{r} (\nabla \times \mathbf{v} = 2\Omega)$ shows similar solid-body rotation as classical fluids. However, it is required that superfluid has to be irrotational with the exception that there are phase singularities which are vortices in the superfluids. Based on this argument, Feynman expected the number of vortices lines should contribute to the same circulation as that from a solid-body rotation; that is, $\Gamma = \int d\mathbf{A} \cdot (\nabla \times \mathbf{v}) = N_v h/m$ where h/m is the quanta of the circulation due to a vortex and Stoke's theorem for the integral has been used. Therefore, the number of vortex per area n_v can be estimated as $2\Omega/(h/m)$.

The nucleation of such quantized vortices is an experimental proof of the existence of macroscopic wave function characterizing a Bose-Einstein condensate. Their direct observation is difficult for the Helium superfluid due to the smallness of the size of the vortex core which is on the order of a few angstroms. However, with the advance of low temperature physics and laser

23
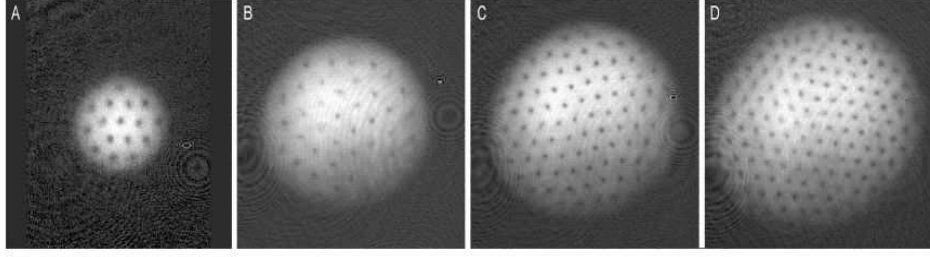
Figure 4.1: Observation of Abrikosov lattices with increasing rotational frequencies of laser stirring field in sodium dilute gases. The examples shown contain approximately (A) 16,(B)32,(C) 80, and (D)130 vortices. The picture is taken from J. R. Abo-Shaeer et al. (W. Ketterle's group).

trapping techniques, another superfluid system with dilute cold atoms become feasible at low temperature in which the vortex core size can be on the order of several microns. This ignite the excitement of vortices physics in superfluids. Large Abrikosov lattices in a rotating BEC in traps has proven the existence of vortices through real space images(Fig. 4.1). .

One of the most exciting many-body physics in boson superfluids is the quantum Hall physics. There are various proposals on realizing lowest Landau level(LLL) physics in mean field regime $N/N_v >> 1$ or correlated regime $N/N_v << 1$ determined by the filling factor of particles and vortices $\nu = N/N_v$ under rotation. In a frame of reference rotating with angular velocity $\Omega\hat{z}$, the Hamiltonian for a particle of mass m in an (isotropic) harmonic trap of natural frequency Ω_0 is

$$H_\Omega = \frac{\mathbf{p}^2}{2m} + \frac{1}{2}m\Omega_0^2\mathbf{r}^2 - (\Omega\hat{z}) \cdot \mathbf{r} \times \mathbf{p}$$
$$= \frac{(\mathbf{p} - m\Omega\hat{z} \times \mathbf{r})^2}{2m} + \frac{1}{2}m[(\Omega_0^2 - \Omega^2)(x^2 + y^2) + \Omega_0^2 z^2] \qquad (4.6)$$

The second form indicates the equivalence of a charge particle $q_{eff} > 0$ experiencing an effective magnetic field $\mathbf{B}_{eff} = \nabla \times \mathbf{A}_{eff} = (2m\Omega/q_{eff})\hat{z}$ where the effective vector potential is given by $\mathbf{A}_{eff} = \frac{m\Omega\hat{z}\times\mathbf{r}}{q_{eff}} = \frac{1}{2}\mathbf{B}_{eff} \times \mathbf{r}$.

When the rotational frequency Ω is close to trapping frequency Ω_0. The physics along the z direction is frozen and the system will live in a two dimensional world. Therefore, the filling factor for the bosons in the effective magnetic fields is given by

$$\nu = \frac{N}{A}\frac{h}{q_{eff}|B_{eff}|} = N/N_v \qquad (4.7)$$

where $N_v = (2m\Omega A)/h$ is the average number of vortices. One may then claim the existence of quantum Hall physics in two dimensional electron gas. Notice that the integer quantum Hall effects are not possible in this system because of the bosonic nature of the particles. Therefore, fractional quantum Hall effects are the main concern in this field. For weak interaction, $gn << \hbar\Omega$ the bosons are restricted to single-particle states in the lowest Landau levels. By exact diagonalization study[16] in this limit $gn << \hbar\Omega$, the ground states of weakly interacting bosons in a rotating trap exhibit both vortex lattices and incompressible vortex liquids. A clear distinction between these phases appears for a large number of bosons N and vortices N_v , and is controlled by the filling fraction ν . Vortex liquid phases appear for $\nu < \nu_c$ including Laughlin states and vortex lattices appear for $\nu > \nu_c$, in which $\nu_c \approx 6$. The mean field regime of LLL physics has been predicted with the mean field theory[17] for the LLLs with traps and realized experimentally[42] when the

rotational frequencies range from $0.99\Omega_0 < \Omega < 0.999\Omega_0$. It is not clear now if particle fractional quantum Hall regimes can be realized in the future because it would require larger rotational speed $\Omega > 0.999\Omega_0$ and smaller particle number N challenging most current experiments [19].

Chapter 5

Effective vortex dynamics in superfluids

Instead of treating boson particles as elementary objects, one can equally well consider vortices to be elementary point objects forming a highly correlated fluid of vortices. Based on this flow of thoughts, the vortex motion is govern by a Hamiltonian with a charge equal to the quantum circulation $\kappa = +2\pi$ interacting with the effective magnetic field $\mathbf{B}_{eff} = -n\hbar\hat{z}$ where n is the particle number density. For a large collection of N_v vortices in a rotating frame with angular velocity Ω, the vortex Hamiltonian reads

$$H_v = \sum_{i=1}^{N_v} \frac{(\mathbf{P}_i - \kappa\mathbf{A}_i)^2}{2m_v} - \Omega(\mathbf{X}_i \times \mathbf{P}_i)_z - \frac{\rho\kappa^2}{2\pi} \sum_{i<j}^{Nv} ln|\frac{\mathbf{X}_i - \mathbf{X}_j}{a_c}|, \qquad (5.1)$$

where a_c is of the order of the vortex core size.

Since this is the dual description of the system of the bosons under rotation we discussed in last chapter, this vortex description should be able to describe the vortex phases correctly under rotation. Based on the vortex Hamiltonian which has the same form as Eq. (4.6) except the long range interaction between vortices, the homogeneous vortex density can be estimated to be $n_v = 2\Omega m/h$ based on plasma analogy. The vortex filling factor $\nu_v = 2\Omega m/hn$ in the dual vortex description is the inverse of the particle filling factor ν. It has been studied that the Laughlin wave functions are still excellent ground

states for the long range interaction. Therefore, we would expect that the vortex Laughlin quantum Hall states will exist when $\frac{1}{\nu_v} = 2, 4, 6, ...$ The work[20] discussed the feasibility of quantum Hall states of vortices in trapped low-density two-dimensional Bose gases with large particle interactions. Motivated by the vortex dual description, we want to answer the questions on what is origin of vortex mass and under what circumstances this vortex Hamiltonian is the correct description.

5.1   Introduction

It has been known that a superfluid can accommodate angular momentum only through vortices[11, 12]. With the rapid progress on Bose-Einstein condensation in ultracold atoms in magnetic traps[13–15, 21] and optical lattices[22, 23], it offers us an alternative to study the vortex physics with superior tunability of system parameters[24–27]. Quantum mechanical aspects of vortices have led to many interesting proposals on vortex lattice melting due to quantum fluctuations and emergence of correlated vortex liquid states[16], phase separation between different vortex states in trapped cold atomic gases because of the inhomogeneity of the condensate density in traps[20], and Vortex-Peierls states in optical lattices, manifestations of the quantum nature of vortices due to geometry frustration[28].

However, the understanding of quantum dynamics for a vortex in neutral superfluids is still controversial[29]. The main concerns are sources of forces on a quantum vortex and effective vortex mass in various circumstances

[30–33]. The consensus is on the existence of Magnus force at zero temperature either from Berry phase argument[34] or hydrodynamic theory[**?**] [**?**]. By Berry phase argument, a vortex behaves like a charged particle in an effective magnetic field due to the background bosons with a given vortex mass[36]. However, the origin of the vortex mass was not well understood and was treated as a phenomenological parameter without much microscopic basis in early works[37]. Although the work[38] proposed that vortex mass may be generated by superfluid compressibility, the microscopic origin based on elementary excitations is not clearly demonstrated and the Magnus force is not considered to be part of their theories. Based on those works, a systematic and microscopic theory for the cyclotron motion of a quantum vortex is still needed. In the preparation of the paper, we are aware of another work[39] making progress toward this direction. The approach they take is based on perturbation theory with rotating pinning potential. They confirm the vortex mass is due to compressibility of the superfluids and the expression of the effective mass may depend on the details of the vortex core.

In this paper, we plan to make a step toward this direction by a different formulation. Our work gives a different perspective and attacks the regime beyond adiabatic limits toward the vortex problem. In general, quantum fluctuations may make the cyclotron mode overly damped and renormalize the effective mass of the vortex. We believe that an unified treatment of the quantum vortex dynamics which takes into account quantum fluctuations is still needed. We take a standard procedure of low-energy effective field theory by

integrating out irrelevant quantum fluctuations but keep relevant vortex translational zero energy modes. Collective vortex cyclotron mode emerges due to the dressing of quantum fluctuations on bare vortex zero modes through nontrivial Berry phase coupling of pure quantum origin. In adiabatic limits where the dynamics of quantum fluctuation is negligible, we reproduce the vortex mass predicted by Duan[38]. It is confirmed the appearance of the vortex mass is due to the density fluctuations (compressibility) and we find that vortex particle picture are more favorable when system size R is much larger than coherence length ξ in superfluids. In addition, we consider the possibility of having the vortex cyclotron mode in optical lattices with bosonic cold atoms by draw analogy between discrete Gross-Pitaevskii equation and a single-band Hubbard model. It is found that when the tunneling energy J is much smaller than on-site interaction energy U, collective dynamics of vortex cyclotron mode can be well approximated by predictions in adiabatic limits.

5.2   Theoretical formulation

5.2.1   Effective action

We consider a dilute interacting bosonic gas in a reduced two-dimensional geometry. The starting point is the partition function for the two-dimensional dilute gas with contact interaction g, written as a coherent-state path integral(See Appendix A) over the fields $\phi^*(\mathbf{x}, \tau)$ and $\phi(\mathbf{x}, \tau)$.

It is given by

$$Z = \int d[\phi^*]d[\phi]e^{-S[\phi^*, \phi]/\hbar} \ , \tag{5.2}$$

30

with the action

$$S[\phi^*, \phi] = \int_0^{\hbar\beta} d\tau \int d^2x \phi^*(\mathbf{x}, \tau) \left[\hbar \frac{\partial}{\partial \tau} - \frac{\hbar^2 \nabla^2}{2m} - \mu + \frac{g|\phi(\mathbf{x}, \tau)|^2}{2} \right] \phi(\mathbf{x}, \tau) \ (5.3)$$

Here, the integration is over all fields periodic on the imaginary-time axis from zero to $\hbar\beta$, with $\hbar$ Planck's constant and $\beta = 1/k_B T$ the inverse thermal energy. In the context of cold atoms, the model can be realized with the harmonic trapping potential with frequency ω_z in the z-direction being sufficiently strong for this approximation to be practically valid. The effective contact interaction strength g is related to the s-wave scattering length a of the atoms by means of $g = 4\pi a \hbar^2/(m d_z)$, with m the mass of an atom. The extent of the system in the z-direction is denoted by d_z and is related to the strong harmonic trapping potential in that direction given by $d_z \sim \sqrt{\hbar/m\omega_z}$. We ignore the effects of trapping potentials at this moment for the clarity of essential physics.

We consider field configurations that consist of a vortex with counter-clockwise phase winding $+2\pi$ surrounded by quantum fluctuations and write

$$\phi(\mathbf{x}, \tau) = \phi_v(\mathbf{x} - \mathbf{r}_v(\tau)) + \delta\phi(\mathbf{x}, \tau), \tag{5.4}$$

where $\phi_v(\mathbf{x})$ is a stationary solution of the Euler-Lagrange equation corresponding to the action in Eq. (5.3), i.e., $\delta S[\phi_v^*, \phi_v]/\delta\phi^* = 0$, containing one vortex at the origin, and $\mathbf{r}_v(\tau)$ is the central position of the vortex in the two dimensional plane. Vortex translation in time is described by $\mathbf{r}_v(\tau)$. However, the fluctuating part of the field $\delta\phi(\mathbf{x}, \tau)$ also contains zero modes that describe the translation of the vortex. For example, a fluctuation $\delta\phi \propto \partial_x \phi_v$ describes

translation of the vortex in the x-direction. Generally, we denote the zero modes responsible for translation of the vortex in the x and y-direction by ϕ_{0i}, with $i \in \{x, y\}$. To avoid double-counting in the functional integral we have to enforce that the fluctuations $(\delta\phi^*, \delta\phi)$ are orthogonal to the zero modes. Hence, the fluctuations are required to obey

$$\langle \phi_{0i} | \delta\phi \rangle \equiv \int d^2x \left[\phi_{0i}^*(\mathbf{x}) \delta\phi(\mathbf{x}, \tau) + \phi_{0i}(\mathbf{x}) \delta\phi^*(\mathbf{x}, \tau) \right] = 0 \ . \qquad (5.5)$$

To enforce the above constraint and, at the same time, introduce the vortex position as a dynamical variable in the function integral we use the Fadeev-Popov procedure [40, 41]. We can rewrite the partition function as:

$$Z = \int d[\mathbf{r}_v] d[\phi^*] d[\phi] \, \delta \left(\langle \phi_{0x} | \delta\phi \rangle \right) \delta \left(\langle \phi_{0y} | \delta\phi \rangle \right) e^{-S[\mathbf{r}_v, \delta\phi^*, \delta\phi]/\hbar} \ . \qquad (5.6)$$

We expand the action up to quadratic order in the fluctuations. The action consists of three parts

$$S[\mathbf{r}_v, \delta\phi^*, \delta\phi] = S_0[\mathbf{r}_v] + S_B[\delta\phi^*, \delta\phi] + S_C[\mathbf{r}_v, \delta\phi^*, \delta\phi] \ . \qquad (5.7)$$

The first term describes that components of the vortex coordinate $\mathbf{r}_v(\tau) = (x_\nu(\tau), y_\nu(\tau))$ are canonical conjugate variables and are responsible for Magnus force [36] which leads to vortex cyclotron motion:

$$S_0[\mathbf{r}_v] = \langle \phi_\nu | \hbar \partial_\tau \phi_\nu \rangle = \frac{1}{2} [\langle \phi_\nu | \hbar \partial_\tau \phi_\nu \rangle - \langle \hbar \partial_\tau \phi_\nu | \phi_\nu \rangle],$$

$$= \frac{\hbar}{2} \int d^2x \, 2iIm[\frac{\partial \phi_\nu^*(\mathbf{x})}{\partial x} \frac{\partial \phi_\nu(\mathbf{x})}{\partial y}] \int d\tau [x_\nu \dot{y}_\nu - y_\nu \dot{x}_\nu].$$

32

When a vortex is considered to be at the center of the space, the order parameter with a vortex is given by $\phi_v(\mathbf{x}) = \sqrt{n_c} f(r) e^{i\theta}$ where n_c is the condensate density far away from the vortex core. Therefore, the spatial integral $\int d^2x \, 2i Im[\frac{\partial \phi_\nu^*(\mathbf{x})}{\partial x} \frac{\partial \phi_\nu(\mathbf{x})}{\partial y}]$ can be evaluated in polar coordinates given by

$$\int d^2x \, 2i Im[\frac{\partial \phi_\nu^*(\mathbf{x})}{\partial x} \frac{\partial \phi_\nu(\mathbf{x})}{\partial y}] = 2i n_c \int_0^{2\pi} d\theta \int_0^R r dr \frac{f}{r} \frac{df}{dr}$$

$$= 4\pi i n_c \int_0^R dr f \frac{df}{dr} = 4\pi i n_c [\frac{f^2}{2}|_0^R] = 2\pi i n_c,$$

where $f(r=0) = 0$ at the vortex core and $f(r=R) = 1$ far away from vortex core has been used. As a result, we can reproduce the action responsible for the Magnus force :

$$S_0[\mathbf{r}_v] = \int_0^{\hbar\beta} d\tau \left[2\pi i n_c \hbar \sum_{i,j \in \{x,y\}} \frac{1}{2} \epsilon^{ij} r_v^i(\tau) \frac{\partial r_v^j(\tau)}{\partial \tau} \right], \tag{5.8}$$

where ϵ^{ij} is the two-dimensional Levi-Civitas tensor.

The quadratic action from quantum fluctuations $S_B[\delta\phi^*, \delta\phi]$ is given by

$$S_B = \frac{1}{2} \int_0^{\hbar\beta} d\tau \int d^2x \, [\delta\phi^*(\mathbf{x},\tau), \delta\phi(\mathbf{x},\tau)] \cdot \left[\begin{pmatrix} \hbar\frac{\partial}{\partial\tau} & 0 \\ 0 & -\hbar\frac{\partial}{\partial\tau} \end{pmatrix} + \mathcal{H} \right] \cdot \begin{bmatrix} \delta\phi(\mathbf{x},\tau) \\ \delta\phi^*(\mathbf{x},\tau) \end{bmatrix},$$

$$\tag{5.9}$$

with the Hamiltonian $\mathcal{H}$

$$\mathcal{H} = \begin{pmatrix} -\frac{\hbar^2\nabla^2}{2m} - \mu + 2g|\phi_v(\mathbf{x})|^2 & g(\phi_v(\mathbf{x}))^2 \\ g(\phi_v^*(\mathbf{x}))^2 & -\frac{\hbar^2\nabla^2}{2m} - \mu + 2g|\phi_v(\mathbf{x})|^2 \end{pmatrix}. \tag{5.10}$$

33

The action that describes the coupling between vortex zero modes and fluctuations through Berry phases is given by

$$S_C[\mathbf{r}_v, \delta\phi^*, \delta\phi] = \frac{1}{2} \int_0^{\hbar\beta} d\tau \int d^2x \sum_{i \in \{x,y\}} [\delta\phi^*(\mathbf{x}, \tau)\partial_i\phi_v(\mathbf{x}) - \partial_i\phi_v^*(\mathbf{x})\delta\phi(\mathbf{x}, \tau)] \, \hbar \frac{\partial r_v^i(\tau)}{\partial \tau} \, .$$

(5.11)

Next, we proceed to integrate out the fluctuations $\delta\phi^*$ and $\delta\phi$. It is crucial to expand the fluctuation fields in the basis $\chi_\alpha \equiv \begin{pmatrix} \chi_\alpha^1 \\ \chi_\alpha^2 \end{pmatrix}$ of the Hamiltonian $\mathcal{H}$ with constraints enforced by the delta functions in the functional integral in Eq. (5.6). We expect three zero energy modes for the Hamiltonian $\mathcal{H}$. The first $\chi_{0p} = (\phi_v, -\phi_v^*)$ is the global phase mode that results from the $U(1)$ invariance of the action in Eq. (5.3). This mode makes no contribution to the dynamics of the vortex and will be shown to be so latter. The other two zero modes describe vortex translation in the two dimensional plane in the absence of pinning potentials. Hereafter, we will refer to the translational modes as zero modes in the discussion. A suitable linear combination makes them equivalent to translation along any direction in the $x - y$ plane. Hereafter, we have $\chi_{0i \in \{x,y\}} \propto (\partial_i\phi_v, \partial_i\phi_v^*)$. One can show those zero energy modes are eigenstates of $\mathcal{H}$ by direction substitution. The other modes (environmental modes) with eigen-energies ϵ_α will be the density modes and phase modes in the presence of the vortex in a superfluid. For the purpose of the latter discussions, we define the quantity $\Gamma_{\alpha'\alpha}$ between any two states α', α as $\Gamma_{\alpha'\alpha} = \langle \chi_{\alpha'}^\dagger | \sigma_z | \chi_\alpha \rangle$ where $\sigma_z = \begin{pmatrix} 1 & 0 \\ 0 & -1 \end{pmatrix}$ with the hermitian property $\Gamma_{\alpha'\alpha} = \Gamma_{\alpha\alpha'}^*$.

34

5.2.2 Adiabatic vortex dynamics and effective mass

Now we show the vortex dynamics in adiabatic approximation. This amounts to neglecting the explicit time dependence of environmental modes in the action of fluctuations $S_B[\delta\phi^*, \delta\phi]$. We expand the microscopic action S in the basis of the fluctuation Hamiltonian $\mathcal{H}$; that is, $\begin{pmatrix} \delta\phi(\mathbf{x}, \tau) \\ \delta\phi^*(\mathbf{x}, \tau) \end{pmatrix} = \sum_\alpha c_\alpha(\tau)\chi_\alpha(\mathbf{x})$. Therefore, we have

$$S_B[c^*, c] = \int_0^{\hbar\beta} d\tau \sum_\alpha \epsilon_\alpha c_\alpha^*(\tau) c_\alpha(\tau) \ . \tag{5.12}$$

The coupling part of the total action becomes

$$S_C[\mathbf{r}_v, c^*, c] = \frac{1}{2} \int_0^{\hbar\beta} d\tau \sum_{i \in \{x, y\}} \left[\sum_\alpha c_\alpha^*(\tau)\Gamma_{i\alpha} - \Gamma_{i\alpha}^* c_\alpha(\tau) \right] \hbar \frac{\partial r_v^i(\tau)}{\partial \tau} \ , \tag{5.13}$$

with

$$\Gamma_{i\alpha} = \int d^2 x \left[\left(\chi_\alpha^1(\mathbf{x})\right)^* \partial_i \phi_v(\mathbf{x}) - \left(\chi_\alpha^2(\mathbf{x})\right) \partial_i \phi_v^*(\mathbf{x}) \right] \ . \tag{5.14}$$

Integration over fluctuation amplitude $c_\alpha^*(\tau)$ and $c_\alpha(\tau)$ can be performed by Gaussian integral. The effective action of the vortex is then given by

$$S_{\text{eff}}[\mathbf{r}_v] = \int_0^{\hbar\beta} d\tau \left[2\pi i n_c \hbar \sum_{i,j \in \{x,y\}} \frac{1}{2} \epsilon^{ij} r_v^i(\tau) \frac{\partial r_v^j(\tau)}{\partial \tau} + \frac{1}{2} m_v \left(\frac{\partial \mathbf{r}_v}{\partial \tau} \right)^2 \right] \ , \tag{5.15}$$

with the effective mass of the vortex

$$m_v = \hbar^2 {\sum_\alpha}' \frac{|\Gamma_{x\alpha}|^2}{2\epsilon_\alpha} = \hbar^2 {\sum_\alpha}' \frac{|\Gamma_{y\alpha}|^2}{2\epsilon_\alpha} \ . \tag{5.16}$$

Note that the coupling $\Gamma_{i\alpha}$ has the dimension of the inverse of length, m_v indeed has the dimension of mass. The prime on the summation denotes omission

of the zero modes, as required by the constraint. In addition, the effective magnetic field can be identified by writing down the semiclassical equation of motion for the effective action in imaginary time and make the Wick rotation $\tau \longrightarrow it$ to real time. The equation of motion is like a positive charge $e = +1$ in an effective magnetic field $-B_{eff}\hat{z}$ where the strength of the magnetic field B_{eff} is given by $B_{eff} = 2\pi\hbar n_c$. Therefore, the cyclotron frequency of a vortex in adiabatic limit is given by $\omega_c = eB_{eff}/m_{eff}$. The adiabatic picture confirm the vortex-charge duality[36]and the presence of Magnus force $\mathbf{F}_M = -2\pi\hbar n_c[\frac{d\mathbf{r}_v}{dt} \times \hat{z}]$ for a vortex in a superfluid.

To make analytical progress, we approximate the excited states of the Hamiltonian $\mathcal{H}$ by plane waves. This is a good approximation as long as we are interested in low energy fluctuations in which the vortex is creating slow-varying non-uniformity. The environmental modes in the presence of the vortex are phase and density fluctuations given respectively by

$$\chi_{\mathbf{k}}^{\theta} = \frac{1}{\sqrt{n_c V}} i \begin{pmatrix} \phi_v \\ -\phi_v^* \end{pmatrix} e^{i\mathbf{k}\cdot\mathbf{x}} \tag{5.17}$$

with the energy $\epsilon_{\mathbf{k}}^{\theta} = \hbar^2 \mathbf{k}^2/2m$ and

$$\chi_{\mathbf{k}}^{\rho} = \frac{1}{\sqrt{n_c V}} \begin{pmatrix} \phi_v \\ \phi_v^* \end{pmatrix} e^{i\mathbf{k}\cdot\mathbf{x}} , \tag{5.18}$$

with the energy $\epsilon_{\mathbf{k}}^{\rho} = \epsilon_{\mathbf{k}} + 2gn_c$ where V represents the area of the system. When $\mathbf{k} = \mathbf{0}$, the modes include global phase mode and density mode respectively. We proceed to evaluate the couplings $\Gamma_{x\mathbf{k}}$. The spatial derivative of the condensate wave function containing a vortex at the center is approximated

36

by

$$\partial_x \phi_v(\mathbf{x}) = i\sqrt{n_c}f\left(\left|\frac{\mathbf{x}}{\xi}\right|\right)e^{i\theta_v(\mathbf{x})}\partial_x\theta_v(\mathbf{x}) + \sqrt{n_c}e^{i\theta_v(\mathbf{x})}\partial_x f\left(\left|\frac{\mathbf{x}}{\xi}\right|\right), \qquad (5.19)$$

where θ_v is the phase of the vortex. The function $f(|\mathbf{x}/\xi|)$ is zero in the origin and equal to one for $x \gg \xi$, where ξ is the coherence length that sets the size of the vortex core. Consider the vortex coupling with phase fluctuations, which is given by

$$\Gamma^\theta_{\mathbf{k}x} = \frac{-i}{\sqrt{n_c V}} \int d^2\mathbf{x}[\phi_v^*\partial_x\phi_\nu + \phi_v\partial_x\phi_\nu^*]e^{-i\mathbf{k}\cdot\mathbf{x}}. \qquad (5.20)$$

At $k = 0$, the coupling $\Gamma^\theta_{\mathbf{k}x}$ has no effects on the vortex mode because the long wavelength fluctuations cannot resolve the presence of the vortex at all. This implies the global phase fluctuations has no contribution to the vortex effective mass. Therefore, we can safely disregard the global phase mode in the expression of the effective mass.

Therefore, we go to next order in k to see what will be the effects by the truncated expansion $e^{-i\mathbf{k}\cdot\mathbf{x}} \approx 1 - ikr\cos\theta - ikr\sin\theta$. Vortex zero modes couple with phase fluctuations through the compressibility of the bosons inside the vortex core:

$$\Gamma^\theta_{\mathbf{k}x} \approx -2\frac{i}{\sqrt{n_c V}}n_c\int_0^\xi rdrd\theta f\frac{\partial f}{\partial r}(-ikr)\cos^2\theta = -\frac{1}{2\sqrt{n_c V}}n_c\pi\xi^2 k, \qquad (5.21)$$

where $f = r/\xi$ is taken inside the vortex core and the contribution out of the vortex core is negligible because the density is uniform along radial direction

37

$\partial_r f = 0$ at $r > \xi$. Cautions should be taken while doing the above expansion. In general, it is problematic in evaluating the coupling at a distance larger than the coherence length ξ, in which $\frac{r}{R} < |\mathbf{k} \cdot \mathbf{r}| < \frac{r}{\xi}$ is not guaranteed to be a small parameter for $r > \xi$ even when the wave-number of the phase fluctuations is small ($0 < k << 1/\xi$). The expansion can be used here because there is no contribution of phase fluctuations outside the vortex core, which is shown by the vanishing of the factor $\frac{\partial f}{\partial r}$. This justifies the small expansion of $e^{-i\mathbf{k} \cdot \mathbf{x}}$ in k inside the vortex core for the fact that $k\xi$ is much smaller than one. From our estimation, we see a nice linear dependance in k_x when $k\xi << 1$ and the coupling with vortex mode increases with the vortex core size. If the vortex core physics is totally neglected, we will not have any coupling due to the phase fluctuations. Higher order correction terms with odd powers in k_x will change the linear dependance Γ_{kx}^{θ} at $k\xi \simeq 1$. It is straightforward to see the corrections are always opposite in sign to the linear term so that we should expect a decrease of $|\Gamma_{kx}^{\theta}|$ with respect to k_x when $k\xi \simeq 1$.

As far as the Berry phase coupling with density fluctuations is concerned, we need to evaluate the coupling careful by treating the regions $\mathbf{k} \cdot \mathbf{r} < 1$ and $\mathbf{k} \cdot \mathbf{r} > 1$ separately.

$$\Gamma_{\mathbf{k}x}^{\rho} = \frac{1}{\sqrt{n_c V}} \int d^2 \mathbf{x} [\phi_v^* \partial_x \phi_\nu - \phi_v \partial_x \phi_\nu^*] e^{-i\mathbf{k} \cdot \mathbf{x}}. \tag{5.22}$$

In polar co-ordinate, $\Gamma_{\mathbf{k}x}^{\rho}$ has the form :

$$\Gamma_{\mathbf{k}x}^{\rho} = 2i \frac{1}{\sqrt{n_c V}} n_c \int_0^R r dr d\theta f^2 \frac{\partial \theta}{\partial x} e^{-ikr\cos\theta - ikr\sin\theta}. \tag{5.23}$$

38

We made the observation at the long wavelength regime $k\xi << 1$ that spatial coupling out of the vortex core cannot be evaluated by the expansion as we have done in phase fluctuations because the coupling is not zero due to the gradient of phase outside the vortex core. Therefore, it is necessary to treat the coupling $\Gamma^{\rho}_{\mathbf{k}x}$ rigorously. In general, the factor $e^{-ikr\cos\theta - ikr\sin\theta}$ contains even and odd angular harmonics. Since the gradient of phase $\frac{\partial\theta}{\partial x} = -sin\theta/r = -1/r[\frac{e^{i\theta} - e^{-i\theta}}{2i}]$ is made of the angular harmonics with $l = +1$ and -1, we only need to keep $l = +1$ and $l = -1$ in the factor $e^{-ikr\cos\theta - ikr\sin\theta}$ when evaluating $\Gamma^{\rho}_{\mathbf{k}x}$ which involves the integration over angle θ.

Let us carry out the details of the vortex coupling with density fluctuations here. In general, we can expand the angular exponential functions in terms of the spherical Bessel functions of first kind as

$$e^{iz\cos\theta} = J_0(z) + \sum_{n=-\infty}^{n=+\infty} i^n J_n(z)e^{in\theta}, e^{iz\sin\theta} = J_0(z) + \sum_{m=-\infty}^{m=+\infty} J_m(z)e^{im\theta} \quad (5.24)$$

, where n, m are integers other than zero and $J_{n,m}$ are Bessel functions of first kind with order n, m. With the identity $J_{-n}(z) = (-1)^n J_n(z)$ and the orthogonality $\int_0^{2\pi} d\theta e^{i(m-n)\theta} = 2\pi\delta_{m,n}$, we only need to keep the terms dependent on $e^{i\theta}$ and $e^{-i\theta}$ in integral; that is, $\int d\theta e^{-ikr\cos\theta - ikr\sin\theta} = \int d\theta 2i[\cos\theta + \sin\theta]J_0(-kr)J_1(-kr)$. By direct substitution, the coupling with density fluctuations are evaluated as :

$$\Gamma^{\rho}_{\mathbf{k}x} = \frac{4\pi n_c}{\sqrt{n_c V}}[\int_0^R dr f^2 J_0(-kr)J_1(-kr)], \quad (5.25)$$

The function $\Gamma^{\rho}_{\mathbf{k}x}$ will be zero when $k = 0$ in agreement with the conclusion

39

of the original expression and get smaller when $k \to \infty$ due to random phase cancelation of two oscillatory functions.

Reliable evaluation of the function analytically becomes very hard when $kr \simeq 1$. To make further progress, we can divide the integrals into two regimes for $r > r_c = 1/k$ and $r \le r_c$ for a given k based on asymptotic forms of Bessel functions in two different regions respectively. Notice that the separation into two regions is only reasonable when $1/R < k << 1/\xi$ such that $\xi << 1/k < R$. Facilitated by the asymptotic forms of Bessel functions for small arguments $kr \ll 1$

$$J_0(-kr) \sim 1, J_1(-kr) \sim (-kr/2), \tag{5.26}$$

and large arguments $kr \gg 1$

$$J_0(-kr) \sim \sqrt{\frac{2}{\pi k r}} \cos(kr - \pi/4), J_1(-kr) \sim -\sqrt{\frac{2}{\pi k r}} \cos(kr - \pi/2 - \pi/4). \tag{5.27}$$

Therefore, we can evaluate coupling with density fluctuations with the integral $\int_0^R dr J_0 J_1 = [\int_{1/k}^R + \int_0^{1/k}][dr J_0 J_1]$. Use the asymptotic forms of the Bessel functions, a term depends on k^{-1} emerge and other terms with higher power in k are generated when $1/R < k << 1/\xi$ as

$$\int_\xi^R dr f^2 J_0(-kr) J_1(-kr) \simeq \int_\xi^{1/k} dr(-kr/2) + \frac{1}{\pi k} \int_{1/k}^R dr [\frac{\cos(2kr)}{r}], \tag{5.28}$$

$$= \frac{1}{4} k \xi^2 - \frac{1}{4k} + \frac{1}{\pi k} \int_{1/k}^R dr [\frac{\cos(2kr)}{r}]. \tag{5.29}$$

40

Inside the vortex core,

$$\int_0^\xi dr\, f^2 J_0(-kr) J_1(-kr) \simeq \int_0^\xi dr[-kr/2]\frac{r^2}{\xi^2} = -\frac{k\xi^2}{8}. \qquad (5.30)$$

As a result, Γ_{kx}^ρ is given by

$$\Gamma_{kx}^\rho \simeq \frac{4\pi n_c}{\sqrt{n_c V}}\{\frac{1}{8}k\xi^2 - \frac{1}{4k} + \frac{1}{\pi k}\int_{1/k}^R dr[\frac{\cos(2kr)}{r}]\}. \qquad (5.31)$$

Notice that we should not take the analytical results literally. The optimized value of the cut-off r_c can be off from $1/k$ by some factor γ. The above expression is to show the k dependance in continuum limit. Here we see the divergence of Γ_{kx}^ρ when $k \to 0$ and the contribution of vortex core is negligible. This indicates that the vortex mode only couple strongly with long wavelength density fluctuations outside the vortex core. Now we can estimate the effective mass due to phase fluctuations and density fluctuations respectively.

With phase fluctuations at $1/R < k << 1/\xi$, ordinary small k expansion is enough to get reliable estimation by direct substitution of Eq. (5.21) into Eq. (5.16):

$$m_\nu^\theta = \frac{1}{2}\hbar^2 \sum_{\mathbf{k}} |\Gamma_{\mathbf{k}x}^\theta|^2/\epsilon^\theta = \frac{1}{2}\hbar^2 \frac{V}{4\pi^2}\int d^2k \frac{|\Gamma_{\mathbf{k}x}^\theta|^2}{(\hbar^2/2m)k^2} = \frac{1}{32}mn_0\pi\xi^2(1 - \frac{\xi^2}{R^2}). \qquad (5.32)$$

With density fluctuations at $1/R < k << 1/\xi$, we substitute Eq. (5.31) into Eq. (5.16):

$$m_\nu^\rho = \frac{1}{2}\hbar^2 \sum_{\mathbf{k}} |\Gamma_{\mathbf{k}x}^\rho|^2/\epsilon^\rho \simeq \frac{1}{2}\hbar^2 \frac{V}{4\pi^2}\int d^2k \frac{|\Gamma_{\mathbf{k}x}^\rho|^2}{2gn} = \frac{1}{4}mn_0\pi\xi^2\ln\frac{R}{\xi} + \frac{1}{16}mn_0\pi\xi^2. \qquad (5.33)$$

41

For a point vortex in which the vortex core size is zero $\xi = 0$, we see the vortex mass due to vortex core has no contribution $m_\nu^\theta = 0$ and $m_\nu = \frac{1}{4} m n_0 \pi \xi^2 \ln \frac{R}{\xi}$. The effective mass of the vortex coordinate arises from the Berry phase coupling with the quantum fluctuations of density and phase of the superfluid. The effect of the phase fluctuations will be considered to be less important than density fluctuations because the motion of the vortex generates phase disturbance of the superfluid order parameter, which couples with density fluctuations due to the quantum nature that the phase and density are conjugate variables, in the large area outside the vortex core having much more overlap with vortex mode. However, the coupling with phase fluctuations will only be limited to the area inside the vortex core, where the motion of the vortex creates density disturbance, which couples with the phase fluctuations of environmental modes. The vortex mass due to compressibility of a superfluid is supported by our theory. For a system with finite vortex core ξ, the mass due to phase fluctuations are always negligible when $\frac{m_v^\theta}{m_v^\rho} \ll 1$; that is, when $8\pi \ln \frac{R}{\xi} \gg 1$. This condition can usually be satisfied as long as the interaction between atoms are strong enough. Therefore, the vortex mass is mainly due to the compressibility (density fluctuations) of the superfluid. In our derivation, the details of vortex core structure is only linear in radius. This will not change our conclusion as long as the system size is large compared to vortex core size.

5.2.3   Dissipative action beyond adiabatic limit

We have shown that we can reproduce the commonly accepted expression of the effective mass in boson superfluids and vortex-particle duality in adiabatic approximation. The next step is to evaluate the adequacy of the adiabatic approximation. In general, beyond adiabatic approximations, we need to include the dynamics of quantum fluctuations by reserving all the off-diagonal Berry phase terms in the action Eq. (5.9). We can expand fluctuation fields $c_\alpha(\tau) = \sum_n c_\alpha[-i\omega_n]e^{-i\omega_n\tau}$, $c_\alpha^*(\tau) = \sum_n c_\alpha[i\omega_n]e^{i\omega_n\tau}$ in Matsubara frequencies $\omega_n = \frac{2\pi n}{\beta\hbar}$, where n are integers. Quantum dissipative action of a vortex can be derived by integration of multi-dimensional Gaussian integral over $c_\alpha[-i\omega_n]$ and $c_\alpha^*[i\omega_n]$:

$$S_{\text{eff}}[\mathbf{r}_v] = \beta\hbar \sum_n \pi i\hbar n_c(-i\omega_n)\epsilon^{jk} r_v^j[+i\omega_n]r_v^k[-i\omega_n] + \hbar^2\omega_n^2 M r_v^j[+i\omega_n]r_v^k[-i\omega_n],$$

$$(5.34)$$

where Einstein's convention for Levi-Civitas ϵ^{jk} is used, the kernel $M \equiv \frac{1}{2}\sum_{\alpha',\alpha} K_{\alpha',\alpha}\Gamma_{r_v^i,\alpha'}\Gamma_{r_v^i,\alpha}^*$ is defined and the matrix $K_{\alpha',\alpha}$ is given by the inverse of the matrix $[2\epsilon_\alpha\delta_{\alpha',\alpha} - i\hbar\omega_n\Gamma_{\alpha',\alpha}]$ which contains the effects of the renormalization of vortex effective mass and the quantum dissipation of the vortex zero mode. The quantity $\Gamma_{\alpha',\alpha} = \int d^2x[\chi_{\alpha'}^{1*}(\mathbf{x})\chi_\alpha^1(\mathbf{x}) - \chi_{\alpha'}^{2*}(\mathbf{x})\chi_\alpha^2(\mathbf{x})]$ represents the Berry phase coupling between fluctuations which are ignored in adiabatic theory. By Eqs. (5.17) and (5.18), states of phase fluctuations and density fluctuations can be well approximated as plane waves $e^{i\mathbf{k}\cdot\mathbf{x}}$ smoothly modified

43

by vortex fields. Then we can replace state labels $[\alpha', \alpha]$ by momentum labels $[\mathbf{k}', \mathbf{k}]$. We can divide Berry phase coupling between fluctuations $\Gamma_{\mathbf{k}',\mathbf{k}}$ into different categories. It can be shown by using Eqs. (5.17) and (5.18) that Berry phase couplings between one mode in phase fluctuations and the other mode in density fluctuations with momentums $\mathbf{k}'$ and $\mathbf{k}$ are given by

$$\Gamma^{\rho\theta}_{\mathbf{k}',\mathbf{k}} = 2i\delta_{\mathbf{k}',\mathbf{k}}, \Gamma^{\theta\rho}_{\mathbf{k}',\mathbf{k}} = -2i\delta_{\mathbf{k}',\mathbf{k}}$$

while the couplings among phase fluctuations and density fluctuations themselves vanish:

$$\Gamma^{\rho\rho}_{\mathbf{k}',\mathbf{k}} = 0, \Gamma^{\theta\theta}_{\mathbf{k}',\mathbf{k}} = 0.$$

Therefore, the matrix $K_{\alpha',\alpha}$ is given by $K_{\alpha',\alpha} = K_{\mathbf{k}'}\delta_{\mathbf{k}',\mathbf{k}}$ where the matrix $K_{\mathbf{k}'}$ is given by

$$K_{\mathbf{k}'} = \begin{pmatrix} 2\epsilon^{\theta}(|\mathbf{k}'|) & -2\hbar\omega_n \\ 2\hbar\omega_n & 2\epsilon^{\rho}(|\mathbf{k}'|) \end{pmatrix}^{-1} = \frac{1}{4(\epsilon^{\theta}\epsilon^{\rho} + \hbar^2\omega_n^2)} \begin{pmatrix} 2\epsilon^{\rho}(|\mathbf{k}'|) & -2\hbar\omega_n \\ 2\hbar\omega_n & 2\epsilon^{\theta}(|\mathbf{k}'|) \end{pmatrix} \tag{5.35}$$

To study the damping effect, we need to do Wick rotation $i\omega_n \rightarrow \omega + i\delta$ where $\delta \rightarrow 0$ with respect to the effective action. It is noticed that the poles of the matrix elements $K_{\mathbf{k}'}[-i\omega_n \rightarrow -\omega - i\delta]$ are the Bogoliubov modes with the excitation energy $E_b = \sqrt{\frac{\hbar^2 k^2}{2m}(\frac{\hbar^2 k^2}{2m} + 2gn_c)}$. At low energy $k \ll 2gn_c$, the excitations are collective phonon modes with the energy spectra $E_p(k) = \hbar k c$.

Next we derive the quantum action of a vortex in superfluids analytically. The analytical expression of the kernel M at low $\mathbf{k}$ and $\omega < \frac{c}{\xi}$ (phonons) can be derived as the following. In Matsubara's frequencies,

$$\frac{1}{2}\sum_{\mathbf{k}} \Gamma_{x\mathbf{k}} K_{\mathbf{k}}[-i\omega_n]\Gamma^*_{x\mathbf{k}} = \frac{1}{2}\sum_{\mathbf{k}} \begin{pmatrix} \Gamma^{\theta}_{x\mathbf{k}}{}^* & \Gamma^{\rho}_{x\mathbf{k}}{}^* \end{pmatrix} K_{\mathbf{k}}[-i\omega_n] \begin{pmatrix} \Gamma^{\theta}_{x\mathbf{k}} \\ \Gamma^{\rho}_{x\mathbf{k}} \end{pmatrix}$$

$$= \frac{1}{4} \sum_{\mathbf{k}} \frac{1}{E_b^2(k) - (i\hbar\omega_n)^2} [2gn_c|\Gamma_{x\mathbf{k}}^{\theta}|^2 + \frac{\hbar^2 k^2}{2m}|\Gamma_{x\mathbf{k}}^{\rho}|^2$$

$$+\hbar\omega_n({\Gamma_{x\mathbf{k}}^{\rho}}^*\Gamma_{x\mathbf{k}}^{\theta} - \Gamma_{x\mathbf{k}}^{\rho}{\Gamma_{x\mathbf{k}}^{\theta}}^*)],$$

where the Bogoliubov excitation energy at low $\mathbf{k}$ is given by the phonon dispersion $E_b = \hbar k (gn_c/m)^{1/2} = \hbar k c$ and c is the speed of sound in the superfluid. At low $\vec{k}$, the last term vanishes by direct substitution. In real time formulation, we replace $i\omega_n$ by $\omega + i\delta$ where $\delta \to 0$.

Therefore, density fluctuations and phase fluctuations contribute both to the kernel $M = M_\theta + M_\rho$ in real frequencies .

The first term M_θ describes the contribution from the phase fluctuations $\Gamma_{x\mathbf{k}}^{\theta}$ and can be written in frequencies:

$$M_\theta = \lim_{\delta \to 0} \frac{1}{8} \sum_{\mathbf{k}} \left[\frac{1}{E_b(k) - E - i\delta} + \frac{1}{E_b(k) + E + i\delta} \right] \frac{2gn_c|\Gamma_{x\mathbf{k}}^{\theta}|^2}{E_b(k)}$$

$$= \frac{\pi g n_c^2 \xi^4}{64 c^4 \hbar^2} \int_{c/R}^{c/\xi} d\omega' \left[\frac{\omega'^2}{\omega' + \omega} + P[\frac{\omega'^2}{\omega' - \omega}] + i\pi\omega^2\delta(\omega' - \omega) \right]. \qquad (5.36)$$

The second term M_ρ describes the contribution from the density fluctuations $\Gamma_{x\mathbf{k}}^{\theta}$:

$$M_\rho = \lim_{\delta \to 0} \frac{1}{8} \sum_{\vec{k}} \frac{1}{E_b(k)} \left[\frac{1}{E_b(k) - E - i\delta} + \frac{1}{E_b(k) + E + i\delta} \right] \frac{\hbar^2 k^2}{2m}|\Gamma_{x\mathbf{k}}^{\rho}|^2$$

$$= \frac{\pi \xi^2 n_c m}{16 \hbar^2} \int_{c/R}^{c/\xi} d\omega' \left[\frac{1}{\omega' + \omega} + P[\frac{1}{\omega' - \omega}] + i\pi\delta(\omega' - \omega) \right]. \qquad (5.37)$$

From those expressions, we recognize the appearance of imaginary part which does not exist in adiabatic theory. This indicates the damping is due to

collective phonon excitations because of the Berry phase coupling between density and phase fluctuations. In addition, the real part of $M_\theta(\omega)$ and $M_\rho(\omega)$ deviates from the adiabatic expression $M_\theta(\omega = 0)$ and $M_\rho(\omega = 0) = \frac{\pi \xi^2 n_c m}{8\hbar^2} \ln \frac{R}{\xi}$. Therefore, the effects of mass renormalization and quantum dissipation are completely captured in the kernel $M(\omega)$:

$$
\begin{aligned}
M(\omega) = \frac{n_c m \pi \xi^2}{16\hbar^2} \{ & 0.25\{1 - \frac{\xi^2}{R^2} + \frac{\xi^2 \omega^2}{c^2} [2 + \ln | \frac{1/\xi^2 - \frac{\xi^2 \omega^2}{c^2}}{1/R^2 - \frac{\omega^2}{c^2}} |] \\
& + i\pi \frac{\xi^2 \omega^2}{c^2} \} + \ln | \frac{1/\xi^2 - \frac{\omega^2}{c^2}}{1/R^2 - \frac{\omega^2}{c^2}} | + i\pi \}.
\end{aligned}
\tag{5.38}
$$

Notice that M_θ due to vortex core can be safely neglected in most circumstances when $\frac{c}{R} < \omega \ll \frac{c}{\xi}$. In addition, phonon excitations make the vortex dynamics away from adiabatic limit with the kernel $M(\omega)$ being replaced by $M_\rho(\omega)$:

$$
M_\rho(\omega) = \frac{n_c m \pi \xi^2}{16\hbar^2} \{ \ln | \frac{1/\xi^2 - \frac{\omega^2}{c^2}}{1/R^2 - \frac{\omega^2}{c^2}} | + i\pi \},
\tag{5.39}
$$

where $\ln | \frac{1/\xi^2 - \frac{\omega^2}{c^2}}{1/R^2 - \frac{\omega^2}{c^2}} | \approx 2 \ln \frac{R}{\xi} - \ln | 1 - \frac{\omega^2}{c^2 R^2} |$. As can be seen from the above expression, adiabatic theory is a good approximation when its predicted cyclotron mode lies shallowly in low energy phonon seas with the condition $\frac{R}{\xi} \gg 1$ where the imaginary part of M_ρ can be neglected. When the cyclotron mode lies deeply inside phonon seas with high energy, the real part of M_ρ get reduced making the damping effects become not negligible. In summary, we found that the damping and mass renormalization of the vortex mode is due to the immersion of vortex mode inside phonon seas. The adiabatic vortex cyclotron mode can be well defined only when the condition that the adiabatic vortex cyclotron mode lies shallowly in phonon sea.

46

Now we evaluate the validity of treating a point vortex in superfluids like a charge particle in an effective magnetic fields induced by background bosons based on adiabatic theory. The adiabatic cyclotron frequency is given by $\omega_c = 2\pi\hbar n_c/m_v$. The vortex mass is given by $m_v = m_v^\rho = \frac{1}{4}mn_c\pi\xi^2\ln\frac{R}{\xi}$. Therefore, the frequency ω_c is given by $\omega_c = 8\frac{\hbar}{m\xi^2\ln\frac{R}{\xi}}$. To estimate the validity of the adiabatic theory in continuum limit, we require that the adiabatic cyclotron frequency ω_c much smaller than $\frac{c}{\xi}$; that is,

$$\omega_c = 8\frac{\hbar}{m\xi^2\ln\frac{R}{\xi}} \ll \frac{c}{\xi} = \frac{\sqrt{2}}{2}\frac{\hbar}{m\xi^2}. \tag{5.40}$$

Equivalently, $\frac{R}{\xi} \gg 11.3137$. Therefore, we can conclude that the vortex-particle duality is valid in large systems with strong interaction, where the ratio $\frac{R}{\xi}$ is macroscopic. With the advent of Feshbach resonance [21] in cold atoms, the contact interaction g and therefore vortex core size ξ has a wide range of tunability that is not available in other superfluid systems. It will be interesting to observe how vortex dynamics goes from adiabatic to dissipative regime when the ratio $\frac{R}{\xi}$ becomes mesoscopic. The trap to vortex core size ratio $\frac{R}{\xi}$ in standard experimental setup[42] is around 10, which seems to be near the border of both regimes.

5.3 Numerical model

5.3.1 Mapping between discrete GP equation and mean field Hubbard Hamiltonian

With the rapid growth of cold atom physics in optical lattices, it offers us the opportunity to realize vortex-charge duality by tunable system

parameters, such as interaction between atoms, optical potential depth and period. In optical lattices[22, 23], low energy physics can be captured by one-band Hubbard model when the optical lattices are deep enough so that the nearest-neighbored hopping of atoms from site to site is valid and the on-site interaction is small enough. The standard Bose-Hubbard model with negligible trapping potential is given by:

$$H_{BH} = -J \sum_{<i,j>} b_i^\dagger b_j + \frac{U}{2} \sum_j b_j^\dagger b_j^\dagger b_j b_j - \mu b_j^\dagger b_j. \qquad (5.41)$$

Here $< i, j >$ represents the nearest neighbors, J is the hopping energy and U is the interaction energy when two atoms are at the same sites and μ is the chemical potential to enforce number conservation of atoms in optical lattices. In mean field approximation , boson creation and annihilation operators can be replaced by the superfluid order parameter ϕ; that is, $b_i^\dagger = \phi_i^*, b_j = \phi_j, b_j^\dagger = \phi_j^*$ and $b_j^\dagger b_j^\dagger b_j b_j = |\phi_j|^2 |\phi_j|^2$. Therefore, the energy functional E_{SF} is given by $E_{SF} = -J \sum_{<i,j>} \phi_i^* \phi_j + U \sum_j \phi_j^* \phi_j^* \phi_j \phi_j - \mu \phi_j^* \phi_j$. The mean field state ϕ_j is determined by the minimization of the energy functional given by $\frac{\delta E_{SF}}{\delta \phi_j} = 0$. Therefore, the effective Hamiltonian H_{SF} for the mean field ϕ_j is given by $H_{SF} = -J \sum_{<i \neq j>} \phi_i + U |\phi_j|^2 \phi_j$. The expression has exactly the same mathematical structure as the effective Hamiltonian H_{GP} in discrete Gross-Pitaevskii (GP) equation given by :

$$H_{GP} \psi_{i,j} = [-\frac{\hbar^2}{2m} \nabla^2 + g |\psi_{i,j}|^2] \psi_{i,j} = \mu \psi_{i,j}, \qquad (5.42)$$

in cartesian coordinates where $\nabla^2 \psi_{i,j}$ is given by $\frac{\psi_{i+1,j} + \psi_{i-1,j} + \psi_{i,j+1} + \psi_{i,j-1} - 4\psi_{i,j}}{D^2}$ in which D is the lattice constant and g is the contact interaction of atoms.

By comparison, we can see the correspondence between H_{GP} and Hamiltonian H_{SF} via the relation $J \leftrightarrow \frac{\hbar^2}{2mD^2}$ and $U \leftrightarrow g$. Therefore, the numerical study of the discrete GP equation will not only help us to understand the vortex physics in continuum limit but also shed some lights on the vortex dynamics in optical lattices. Here we estimate the parameters to observe adiabatic vortex dynamics in optical lattices. Two physical constraints are required. On one hand, one needs to make sure that the system is safely in superfluid phase and not in Mott-insulating phase. The criteria for a system with one atom per site ($\bar{n} = 1$) on average ($N_a = N_{site} = N$) is given by [23]

$$\frac{U}{J} < 5.8z,$$

where z is the number of nearest neighbors at each site. In terms of lattice parameters, it is given by

$$\frac{g\bar{n}}{\frac{\hbar^2}{2mD^2}} \approx \frac{D^2}{\xi^2} < 5.8z,$$

in which $\bar{n} = 1$. As a result, the first criteria is given by

$$\frac{D}{\xi} < 2.4083\sqrt{z}. \tag{5.43}$$

where n is the number density of the condensate away from the vortex.

On the other hand, even in the superfluid phase, the vortex has to be in adiabatic regime so that quantum fluctuations have less effects on vortex dynamics. By the conclusion we have reached in this report, the adiabatic vortex dynamics is valid when the condition $\frac{R}{\xi} \gg 11.3137$ is satisfied. In

49

lattices, the condition can be written as

$$\frac{L}{\sqrt{2}\xi} = \frac{(\sqrt{N}-1)D}{\xi} \gg 11.3137.$$

Then the second criteria in optical lattices is given by

$$\frac{D}{\xi} \gg \frac{16}{\sqrt{N}}. \tag{5.44}$$

As a result, the adiabatic vortex dynamics can survive in optical lattices when the system length scale $\frac{D}{\xi}$

$$\frac{16}{\sqrt{N}} \ll \frac{D}{\xi} < 2.4083\sqrt{z}. \tag{5.45}$$

Based on this criteria, it is beneficial to have large lattices to have a wide range of tunability for the parameter D/ξ while keeping the system in superfluid regime $D/\xi < 2.4083\sqrt{(z)}$. In terms of system energy scales $\frac{\mu}{E_D}$ where $E_D = \hbar^2/2mD^2$, the criteria can also be written as

$$\frac{256}{N} \ll \frac{\mu}{E_D} < 2.4083\sqrt{zN}. \tag{5.46}$$

In the context of cold atoms, the chemical potential μ is determined largely by the background harmonic magnetic traps. Therefore, by tuning the geometry or size of the background trap and the optical lattice constant D, it would be interesting to study the vortex dynamics.

5.3.2   Numerical procedure

We calculate elementary excitations with the vacuum state being the mean field solution with a vortex of phase winding 2π in a square lattice by

matrix diagonalization. Theoretical formulation we introduced previously can be set up analogously in discrete manners. The following numerical procedures are taken. We employ imaginary time scheme to find the mean field state $\psi_\nu(\mathbf{x})$ with a vortex at the center of space while conserving the total number of particles in iterations. Discrete GP equation in imaginary time is diffusive and can be represented by

$$\frac{\psi_{i,j}^{n+1} - \psi_{i,j}^n}{\epsilon} = H_{GP}\psi_{i,j}^n, \tag{5.47}$$

where i, j are labels for the two-dimensional lattice points, the label n represents the counts of the imaginary time evolution step ϵ. An iterated equation for the updated wave function $\psi_{i,j}^{n+1}$ is set up by writing ψ^{n+1} on the left-handed side and ψ^n on the right-handed side of the GP equation. By choosing appropriate value of ϵ and conserving the normalization $\int d^2\mathbf{x}|\psi_{i,j}^{n+1}|^2 = N_a$, where N_a is the total number of atoms. An ansatz $\psi = fe^{i\theta}$, where $\theta = \arctan(y/x)$, can be used. To conserve the phase winding 2π in the plaquette of the computational domain and discrete rotational symmetry, we use the boundary condition which satisfies discrete rotational symmetry:

$$\psi(x, \frac{L}{2}) = e^{i\pi(1-\frac{x}{L})}\psi(x, -\frac{L}{2}), \psi(\frac{L}{2}, y) = e^{-i\pi(1-\frac{x}{L})}\psi(-\frac{L}{2}, y), \tag{5.48}$$

where the origin is chosen at the center of the computational domain as well as the center of the vortex core. Notice that the boundary conditions can be absorbed into the system Hamiltonian H_{GP} through $\nabla^2\psi^n$ by direct substitution of the boundary condition into discrete GP equation. Finally, the iteration will converge to the mean field state with a vortex in such a lattice.

Quantum fluctuations above the vortex ground state can be described by the hermitian Hamiltonian:

$$\mathcal{H} = \begin{pmatrix} -\frac{\hbar^2\nabla^2}{2m} - \mu + 2g|\phi(\mathbf{x},\tau)|^2 & g\left(\phi_v(\mathbf{x})\right)^2 \\ g\left(\phi^*(\mathbf{x})\right)^2 & -\frac{\hbar^2\nabla^2}{2m} - \mu + 2g|\phi(\mathbf{x},\tau)|^2 \end{pmatrix}. \quad (5.49)$$

Rewrite $\mathcal{H}$ in a matrix form by finite difference methods, elementary excitations in space domain can be solved by direct matrix diagonalization. Bogoliubov excitations can be solved numerically with similar procedure except that it is the non-hermitian Bogoliubov Hamiltonian $\mathcal{H}_B = \sigma_z\mathcal{H}$, where σ_z is the z-Pauli spin matrix, to be diagonalized with the eigenvectors $[u(\mathbf{x}), v(\mathbf{x})]^T$ satisfying the normalization condition $\int d^2x |u(\mathbf{x})|^2 - |v(\mathbf{x})|^2 > 0$.

In the numerical calculations, we always have global phase mode with zero energy and the other two degenerate states (vortex zero modes) taking the second lowest energy states of $\mathcal{H}$. Because the simulation domain is finite in space, the vortex zero modes cannot have zero energy as expected for infinite system. Also, we only have quantized energy levels. To make connection with calculations in continuum limit, we can replace summation over states $\sum_\alpha$ by the integration over spectral density of states $\int dE D(E)$, where $D(E) = \sum_\alpha \delta(E - E'_\alpha)$. In continuum, the Dirac's delta function is given exactly by $\delta(E - E'_\alpha) = \frac{-1}{\pi} Im[\frac{1}{E-E'_\alpha+i\delta}]$, where $\delta \to 0$. In the finite lattice model, the same expression can be used by replacing δ with the energy of the order of energy quanta $E_L = \frac{\hbar^2}{2mL^2}$ to mimic the numerical data in continuum.

5.3.3 Numerical results

In this section, we intend to show in which situation adiabatic vortex cyclotron motion can survive in the presence of quantum fluctuations and suggest the possibility to realize the vortex charge duality picture in dilute cold atoms in optical lattices. We use the numerical cases with $N = 46^2$ sites, lattice spacing $D = 1$, and system length $L = 45D$ in our numerical demonstration. Taking advantage of the analogy between discrete GP equation and single-band Hubbard model in optical lattices, we denote system parameters in a reduced form. The energy $E_D = \frac{\hbar^2}{2mD^2}$ is the energy quanta associated with lattice spacing D in discrete GP equation. The reduced energy $E_R = E/\mu$ is scaled by the chemical potential μ. The reduced interaction $g_R = gN_a/E_D$ and the corresponding $U_R = UN_a/J$ in optical lattices are given simultaneously so that readers can interpret the results for both situations.

In Fig. 5.1, we show the spectral density of states of quantum fluctuations. We expect to see the features of phase and density modes which are the basis of the Hamiltonian $\mathcal{H}$ for quantum fluctuations. The energy difference between the phase fluctuations $\epsilon_{\mathbf{k}}^\theta = \frac{\hbar^2 \mathbf{k}^2}{2m}$ and density fluctuations $\epsilon_{\mathbf{k}}^\rho = \frac{\hbar^2 \mathbf{k}^2}{2m} + 2gn_c$ with the same $\mathbf{k}$ is given by $2gn_c = 2\mu$. In continuous system, the energy density of states $D(E)$ are independent of energy. However, in finite model, we would expect this is only valid at low energy part of those fluctuations because the Van Hove singularities due to lattice spacing which is expected to change the high energy spectrum.

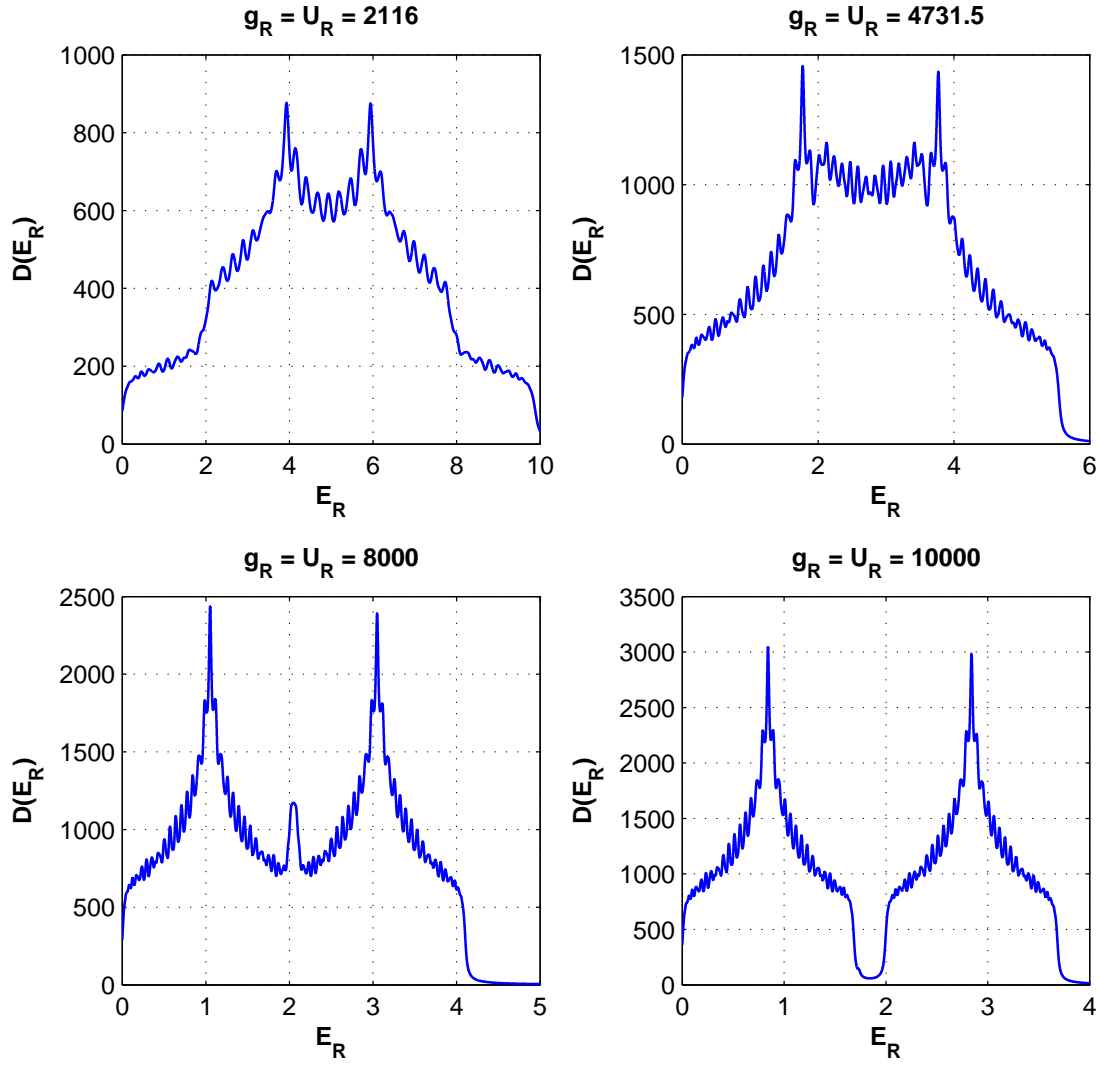As can be seen in the numerical data, two peaks in the spectrum rep-

Figure 5.1: Spectral density of states $D(E_R)$ of quantum fluctuations versus the energy E_R with different interaction strength g_R

resent the Van Hove singularities. The energy difference is set by the energy gap 2μ). The energy difference between the phase and density fluctuations are more clearly seen with large interaction strength $g_R = U_R = 10000$ because the energy scales of phase and density fluctuations are completely well separated; that is, all the phase fluctuations have lower energies than all the density fluctuations. For intermediate interaction $g_R = U_R = 8000$, high energy part of phase fluctuations have similar energy as that of density fluctuations, which can be seen from a small peak at the energy $E_R \approx 2$. For the case with weak interaction $g_R = U_R = 2116$, the states of the phase fluctuations strongly overlap with that of the density fluctuations with the accumulation of the density of states at some energies, which is shown at the energies ranging from $E_R = 2$ to $E_R = 8$.

In Fig. 5.2, we show the spectral density of the vortex effective mass in adiabatic limits. The vortex mass is given by $m_\nu = \sum_\alpha \frac{|\Gamma_{\alpha x}|^2}{\epsilon_\alpha} = \int dE_R \frac{dm_\nu(E_R)}{dE_R}$. In theory, we would expect that the effective mass of the vortex is mainly due to the coupling of the vortex zero modes with density fluctuations. We observe in the figure that the spectral contents of the effective mass all have a strong peak in the low energy part of density fluctuations at the energy $E_R = 2$ for different interactions. In addition, we expect that the contribution of the vortex mass from phase fluctuations will be less important at large interaction g_R (small vortex core), as shown in subplots (c) and (d). In subplots (a) and (b), we observe the development of mass at low energy part of phase fluctuations $E_R \approx 0$. Even so, the phase fluctuation contribution is always
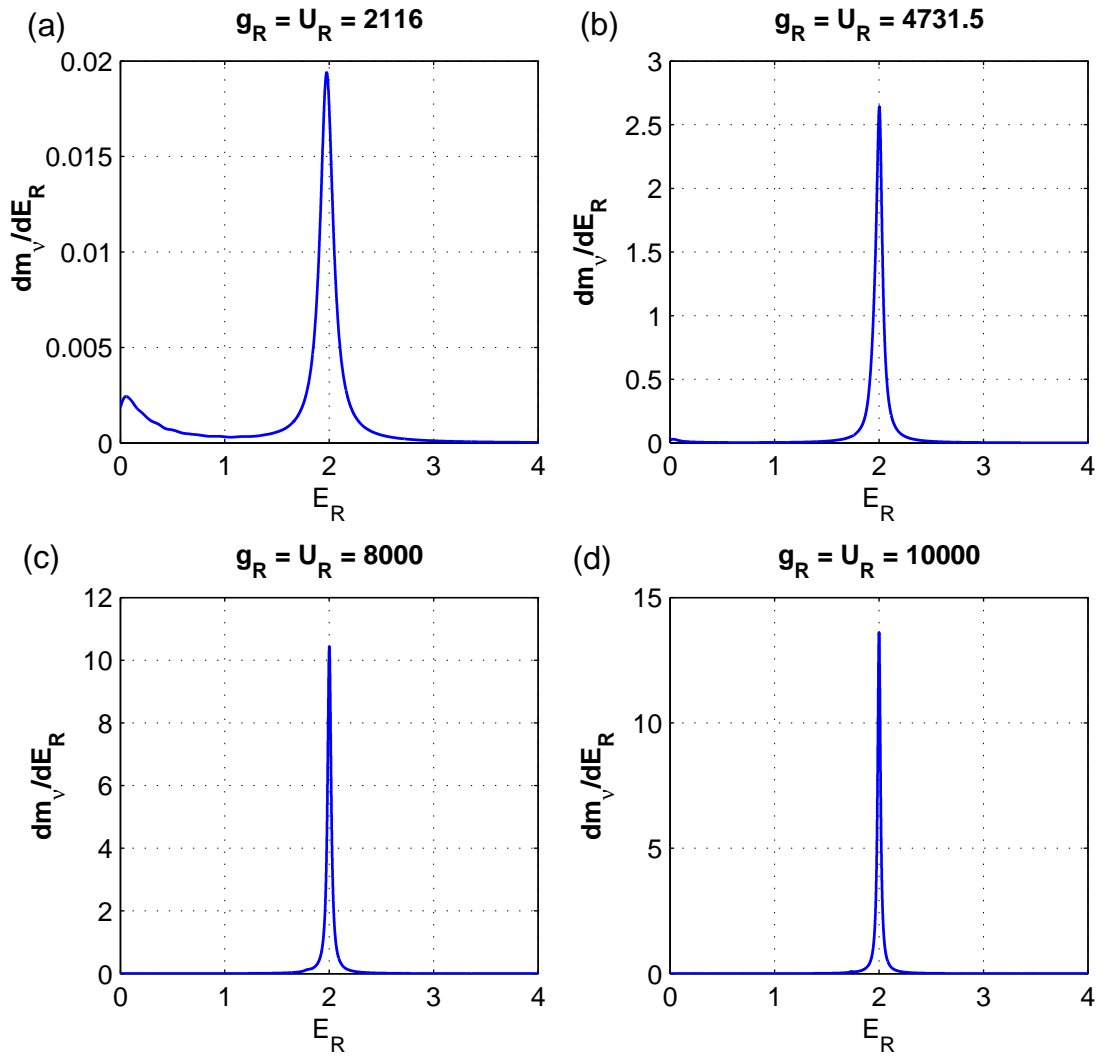
Figure 5.2: Vortex mass energy density $\frac{dm_v(E_R)}{dE_R}$ versus the reduced energy E_R with different interaction

negligible. This confirms the vortex mass is mainly due to compressibility of the superfluid. In addition, we also check that the Berry phase coupling $|\Gamma_{x\alpha}|^2$ and $|\Gamma_{y\alpha}|^2$ between the vortex mode with other modes are dominant by low energy density fluctuations.

In Fig. 5.3, we show the density of states $D_B(E)$ of Bogoliubov excitations which are poles of the vortex effective action beyond adiabatic theory due to Berry phase coupling between phase and density fluctuations. Bogoliubov excitations are phonons at low energies. We expect the density of state is linear at low energies because of the linear phonon dispersion in two dimensional space. In addition, there is a singularity, heritage of the Van Hove singularities of density and phase fluctuations, at the estimated energy $E_{BD} = [E_D(E_D + 2gn_c)]^{1/2}$. As a result, the estimated peak position of Van Hove singularity at the reduced energy E_{BD}/E_D increases with the interaction g and E_{BD}/μ decreases with the interaction considering the energy $\frac{\hbar^2 k_D^2}{2m}$ and n_c are fixed in our numerical simulations. From the numerical subplots, we see the density of states are approaching linear phonon density of states at low energies and the Van Hov singularity peaks are shifting toward low E_R, showing the trend we have explained.

In Fig. 5.4, we show the emergence of collective cyclotron mode. Because the full action of our system in Matsubara frequencies is quadratic, the action can be written compactly as this form $S[-i\omega_n] = \sum_{\alpha,\alpha'} a_{\alpha'}^*[-i\omega_n]K_{\alpha',\alpha}a_\alpha[i\omega_n]$, where Berry phase coupling between different modes make the matrix $K_{\alpha',\alpha}$ off-diagonal in the basis of the Hamiltonian $\mathcal{H}$ and $a_\alpha, a_{\alpha'}$ are mode ampli-
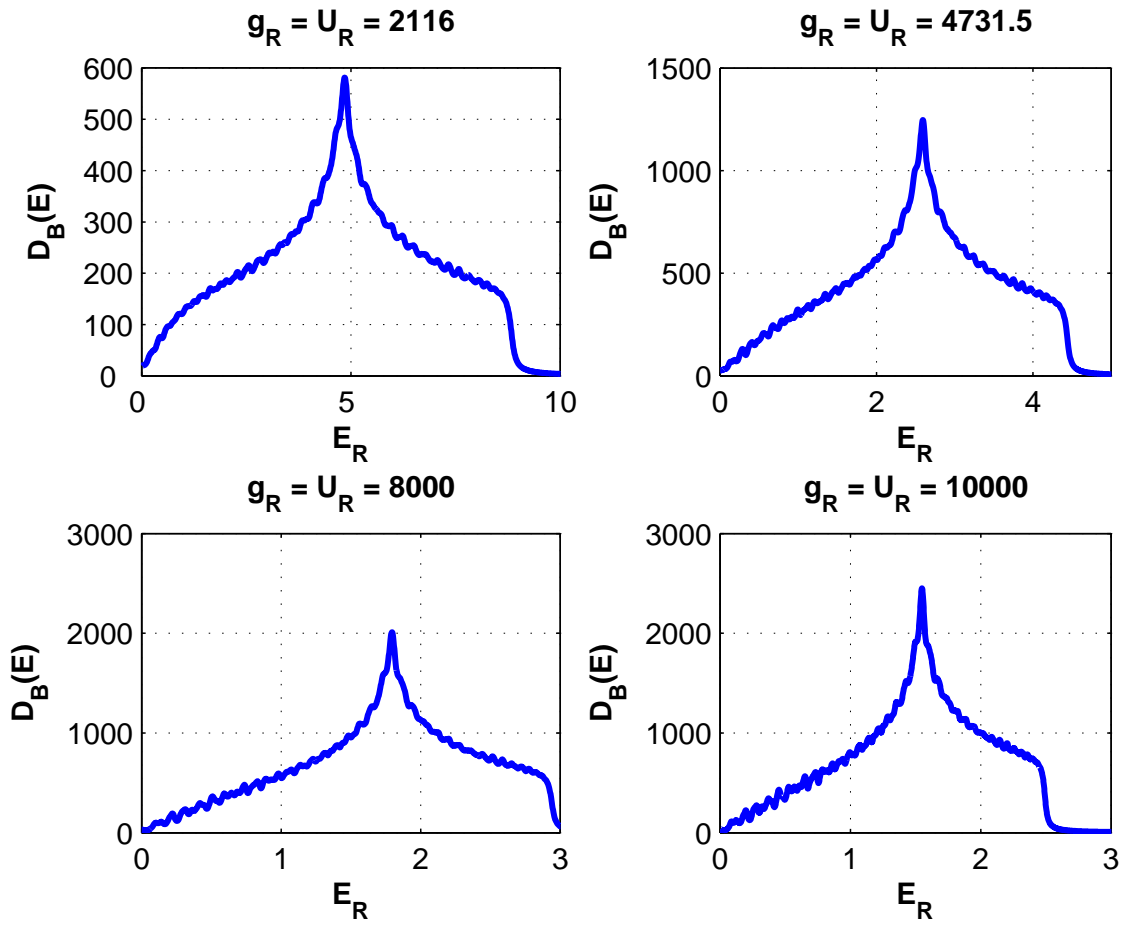
57

Figure 5.3: Spectral density of states of Bogoliubov excitations $D_B(E_R)$ with different interaction strength g_R
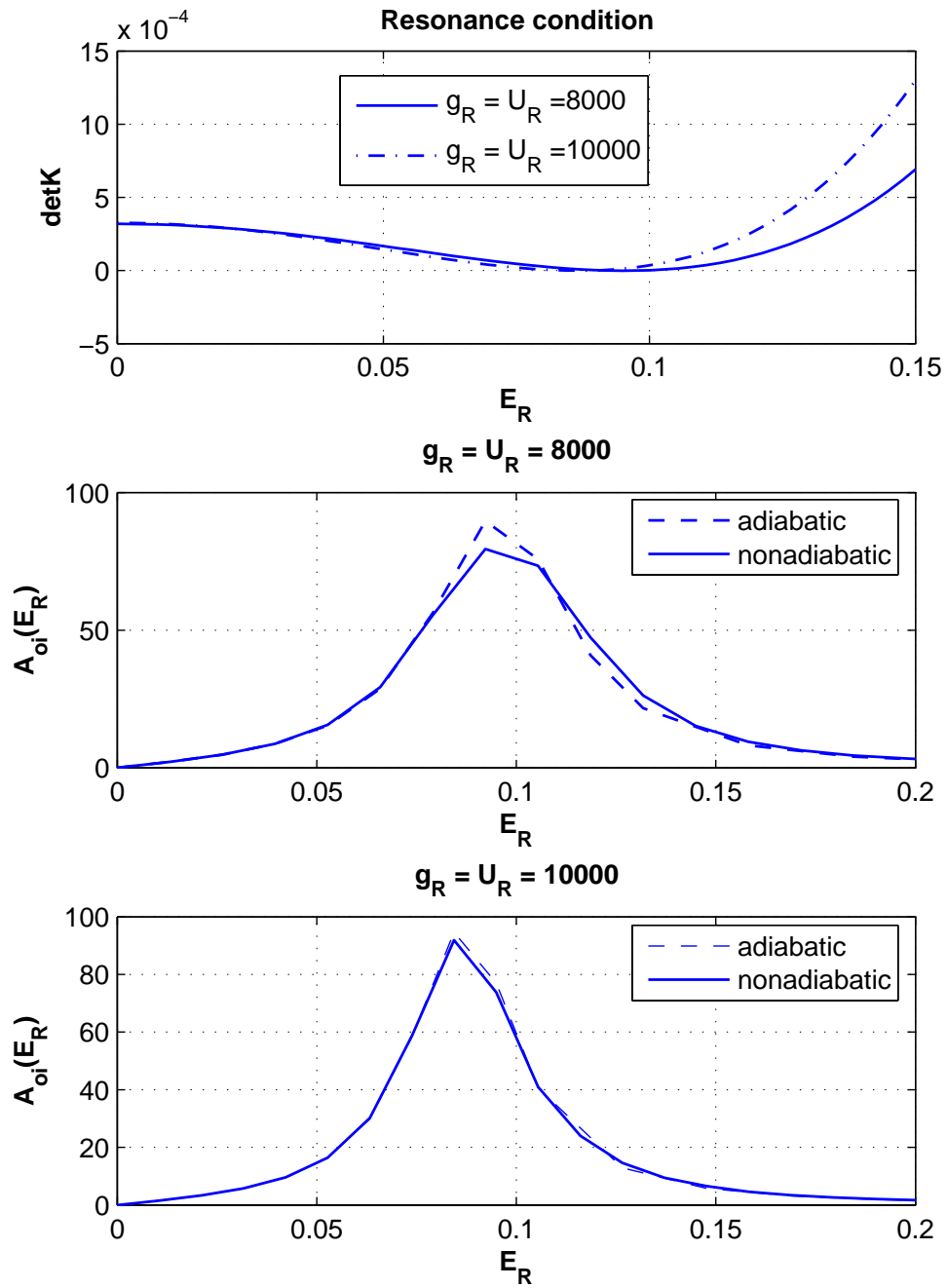
Figure 5.4: Comparison of cyclotron modes in adiabatic and non-adiabatic situation

tudes. Retarded correlation functions $G_\alpha^R[\omega] = K_{\alpha,\alpha}^{-1}[i\omega_n \to \omega + i0^+]$ including vortex zero modes $0i$ can be solved by matrix inversion of the matrix $K_{\alpha',\alpha}$. We can demonstrate the existence of the cyclotron mode by the imaginary part of the vortex position-position correlation function $A_{0i}[\omega] = -\frac{1}{\pi}ImG_{0i}^R$ where $G_{0i}^R = < x_\nu(\omega)x_\nu(-\omega) > = < y_\nu(\omega)y_\nu(-\omega) >$. In subplot (a), we show the adiabatic resonant conditions of the vortex cyclotron modes at which $detK(i\omega_n \to \omega) = 0$. It is observed that cyclotron resonances are located at the energy $E_R \approx 0.09$ for the case $g_R = 8000$, and $E_R \approx 0.08$ for the case $g_R = 10000$. We would expect to see the emergence of the adiabatic cyclotron mode at those resonant positions in the response function $A_{0i}[\omega]$. Similarly, we can turn off the adiabatic approximation in our calculations. In subplots (b) and (c), we see strong peaks right at those positions. As far as the peak position and width of the cyclotron peak are concerned, the agreement between adiabatic cyclotron peak and realistic cyclotron peak with the same g_R is better at stronger interaction g_R. This supports our theoretical speculation that adiabatic theory is favorable when the interaction g_R or U_R is large enough to make system macroscopic $\frac{L}{\xi} \gg 1$. It is also observed that the non-adiabatic cyclotron peaks are damped more for the case with $g_R = 8000$ than the case $g_R = 10000$ when the respective adiabatic resonance peaks are compared. Examine the corresponding adiabatic cyclotron peaks with the Bogoliubov spectrum in Fig. 3(c) and Fig. 3(d). The cyclotron peak in the case with the interaction $g_R = 10000$ lies lower in the low energy part of the Bogoliubov spectrum and therefore the damping effect is less substantial. This

60

agrees with the picture we have in our theoretical predictions.

5.4 Discussions and Conclusions

We establish a theoretical formalism to study quantum vortex dynamics going beyond the adiabatic approximation in which the dynamics of quantum fluctuations are completely ignored. The low energy effective action for vortex motion is derived by integrating out phase and density fluctuations of quantum nature. Magnus force, vortex effective mass, and quantum dissipation of a vortex in superfluids can all be captured in the same framework systematically. In adiabatic limit, analytical calculations on adiabatic vortex effective mass including vortex core are treated carefully. It is confirmed that the vortex mass is mainly due to the compressibility of the superfluids[38] when vortex core size is much smaller than system size. Beyond adiabatic limits, we discuss the effects of vortex mass renormalization and quantum dissipation of the vortex cyclotron mode. Based on analytical results, we draw the following conclusions. The vortex-charge duality picture only emerges when the adiabatic approximation is valid. The vortex mass is mainly due to the density fluctuations and the damping of the vortex cyclotron mode is weak when the system is macroscopic $\frac{R}{\xi} \gg 1$. Based on the analogy between discrete GP equation and single band Hubbard model, we can also claim that the adiabatic vortex dynamics is valid when the ratio UN_a/J is large in cold atoms with optical lattices.

However, cautions need to be taken when generalizing the vortex-charge

61

duality picture in mesoscopic systems such as trapped cold atom system. When the superfluid is mesoscopic, the vortex mass due to phase fluctuations are not negligible. The details of the vortex core structure may play an important role in the estimation of the vortex mass. With the capability of tuning boson inter-action and thus vortex core size in cold atom systems via Feshbach resonance, superfluid systems may go from mesoscopic to macroscopic regimes by tuning the vortex core size with fixed system size. Therefore, we suggest to observe the crossover of vortex dynamics from the adiabatic regime to non-adiabatic regime for cold atoms in optical lattices . To observe the phenomena in our numerical demonstration experimentally, extra efforts are needed to guarantee the system is in superfluid phase and well described by single band Hubbard model through the tunability of the depth and period of the optical lattices.

Chapter 6

Interaction electrons

In solids, many-body Schrödinger equation $i\hbar\frac{\partial\Psi}{\partial t} = H\Psi$ in principle can exhaust the physics of electrons by assuming the ions are stationary with the Hamiltonian:

$$H = -\sum_i \frac{\hbar^2}{2m}\nabla_i^2 - \sum_{i,I} \frac{Z_I e^2}{|\mathbf{r_i} - R_I|} + \frac{1}{2}\sum_{i\neq j} \frac{e^2}{|\mathbf{r_i} - \mathbf{r_i}|} \qquad (6.1)$$

where $\mathbf{R} = \{R_I, I = 1, ..., P\}$ is a set of P nuclear coordinates, $\mathbf{r} = \{\mathbf{r}_i, i = 1, ..., N\}$ is a set of electron coordinates, and Z_I are number of nuclear charges. Since the electrons are fermions, the total wave function has to be antisymmetric when any two of the electron coordinates are exchanged. However, the enormous electron degree of freedoms render the problem intractable when the number of electron is still small especially when the spin and orbital degree of freedoms are all considered in real materials. For example, if the number of electron is N and each electron has two spin flavors, the Hilbert space of the whole electron system will have the dimension of 2^N. Today's most powerful computers can handle up to the order of $N = 10$ electrons. The only feasible way is to solve the problem under certain approximations such as various kind of mean field approximations with certain kind of single-particle pictures

in minds. In this chapter, we will introduce the art of solving many-electron problems from the perspective of density functional theory (DFT).

6.1 Density functional theory

In 1964, Hohenberg and Kohn formulated and proved a theorem[43] that put DFT on solid mathematical basis. The foundation of the DFT is based on the Hohenberg-Kohn thereom which states that the electron charge density of a system's ground state uniquely determines the external potential and all observable properties of the system. However, Kohn-Sham equation makes the DFT calculation to be practical by employing non-interacting system as a reference system to approximate kinetic density functional for the electrons accurately.

6.1.1 The Hohenberg-Kohn theorem

Theorem : The external potential is uniquely determined by the electronic density and vice versa, besides a trivial additive constant. Let's discuss the case in which the ground state is nondegenerate.

By Eq. (6.1), it is obvious the charge density $n(\mathbf{r})$ is the functional of external potential $V_{ex}(\mathbf{r})$ (attractive potential from ions or external static fields) through ground-state wavefunction Ψ. We can also give a simple proof that external potential $V_{ex}(\mathbf{r})$ is a unique functional of density $n(\mathbf{r})$ as follows. Assume that there exists another potential $V_{ex}'(\mathbf{r})$ with ground state wave function Ψ' which leads to the same density $n(\mathbf{r})$. Now clearly Ψ' cannot

be equal to Ψ since they satisfy different Schrödinger equation due to the difference of external potentials. Hence, if we denote the Hamiltonian and ground-state energies associated with Ψ and Ψ' by H, H' and E, E'. We have by the minimal property of the ground state,

$$E' = \langle \Psi'|H'|\Psi' \rangle < \langle \Psi|H'|\Psi \rangle = \langle \Psi|H + V'_{ex} - V_{ex}|\Psi \rangle, \qquad (6.2)$$

so that

$$E' < E + \int d\mathbf{r}[V'_{ex} - V_{ex}]n(\mathbf{r}). \qquad (6.3)$$

Interchanging primed and unprimed quantities, we find similar equation that

$$E < E' + \int d\mathbf{r}[V_{ex} - V'_{ex}]n(\mathbf{r}). \qquad (6.4)$$

Addition of Eqs. (6.3) and (6.4) leads to the inconsistency

$$E' + E < E + E'. \qquad (6.5)$$

Thus $V_{ex}(\mathbf{r})$ has to be an unique functional of $n(\mathbf{r})$; since $V_{ex}(\mathbf{r})$ fixes H we see that the full many-particle ground state is a unique functional of $n(\mathbf{r})$. Note that the same conclusion can be drawn from ground state with degeneracies[44].

The variational Principle : The problem of determining the ground-state energy and density in a given external potential would be given by the minimization of energy density functional restricted by the conservation of electrons $\int d\mathbf{r}n(\mathbf{r})$.

Because of the ground-state properties, any other density profile $\tilde{n}\mathbf{r}$ other than ground-state density profile $n(\mathbf{r})$ will yield a higher energy. Therefore, the ground state energy can be determined by the variational principle :

$$\delta\{E_v[n] - \mu \int d\mathbf{r}\,n(\mathbf{r})\} = 0, \qquad (6.6)$$

which leads to the generalized Thomas-Fermi equation:

$$\mu = \frac{\delta E_v[n]}{\delta n} = V_{ex}(\mathbf{r}) + \frac{\delta F[n]}{\delta n}. \qquad (6.7)$$

The knowledge of $F[n]$ implies the knowledge of the solution of the full many-body Schrödinger equation. It has to be remarked that $F[n]$ is a universal functional which does not depend explicitly on the external potential. It depends only on electronic density. In the Hohenberg-Kohn formulation, $F[n] = \langle\Psi|\hat{T}+U_{ee}|\Psi\rangle$, where Ψ is the ground-state wave function and $F[n]$ consists of kinetic energy functional $\langle\Psi|\hat{T}+U_{ee}|\Psi\rangle$ and potential energy functional due to electron correlation U_{ee}. These two theorems form the mathematical basis of DFT.

6.1.2 Reference system and Kohn-Sham equation

While the Hohenberg-Kohn theorem rigorously establishes the density as a variable to find the ground-state energy, it does not provide us with any useful computational scheme, which is able to calculate the kinetic energy functional accurately other than making rough local density approximation from free electron gas known as Thomas-Fermi approximation. Kohn and

Sham's idea is to use a noninteracting reference system and look for an external potential V_R such that the noninteracting system has the same ground-state density as the real, interacting system. Once the density is obtained, we can use it in the interacting energy functional or in some approximation of it.

By Hohenberg-Kohn theorem, there exists a unique functional for the non-interacting reference system given by

$$F_R[n] = T_R[n] + \int V_R(\mathbf{r})n(\mathbf{r})d\mathbf{r}. \tag{6.8}$$

The ground-state density of this system is easily obtained. It is simply

$$n_R(\mathbf{r}) = \sum_{i=1}^{N} |\phi_i(\mathbf{r})|^2, \tag{6.9}$$

where we occupied the N single-particle orbitals, which satisfy the Schrödinger-like equation

$$[\frac{-\hbar^2}{2m}\nabla^2 + V_R(\mathbf{r})]\phi_i(\mathbf{r}) = \epsilon_i\phi_i(\mathbf{r}), \epsilon_1 \leq \epsilon_2 \leq ...., \tag{6.10}$$

and have the N lowest eigenvalues ϵ_i. We next ask if we can determine the form that V_R must take in order for the noninteracting system to have the same ground-state density as the interacting system in the external potential $V_{ex}(\mathbf{r})$. The strategy we use is to solve for the density using the reference system and then insert this density into the energy functional for the interacting system.

The interacting functional $F_{KS}[n]$ can be classified into different pieces as:

$$F_{KS}[n(\mathbf{r})] = T_R[n(\mathbf{r})] + \frac{1}{2}\int d\mathbf{r}d\mathbf{r}'\frac{n(\mathbf{r})n(\mathbf{r}')}{|\mathbf{r} - \mathbf{r}'|} + E_{xc}[n], \tag{6.11}$$

where $T_R[n(\mathbf{r})]$ is the kinetic energy part of the functional constructed from non-interacting electrons, the second term is the Hartree potential, and E_{xc} is the exchange-correlation energy which absorbs the error due to approximating exact $T[n(\mathbf{r})]$ by that of the non-interacting reference system. The term E_{xc} contains all the knowledge about electron interactions beyond the Hartree term. The density functional form for E_{xc} can be approximated by local density approximation(LDA) or more accurate schemes which have become a highly specialized area in physics and chemistry.

Therefore, we can find the ground state density from Eq. (6.7) from variational principle by replacing $F_[n]$ by $F_{KS}[n]$ for the interacting system and $F[n]$ by $F_R[n]$. As a result, the ground state density satisfy the equations :

$$\mu_{KS} = \frac{\delta T_R[n]}{\delta n(\mathbf{r})} + \int \frac{n(\mathbf{r}')}{|\mathbf{r} - \mathbf{r}'|} d\mathbf{r}' + V_{ex}(\mathbf{r}) + v_{xc}[n(\mathbf{r})], \qquad (6.12)$$

and

$$\mu_R = \frac{\delta T_R[n]}{\delta n(\mathbf{r})} + V_R(\mathbf{r}), \qquad (6.13)$$

where the exchange-correlation potential is defined as $v_{xc}[n(\mathbf{r})] \equiv \frac{\delta E_{xc}[n]}{\delta n(\mathbf{r})}$. Therefore, the effective potential for the reference system V_R must satisfy

$$V_R = (\mu_R - \mu_{HK}) + V_{ex}(\mathbf{r}) + \int \frac{n(\mathbf{r}')}{|\mathbf{r} - \mathbf{r}'|} d\mathbf{r}' + v_{xc}(\mathbf{r}). \qquad (6.14)$$

The chemical potential difference $\mu_R - \mu_{HK}$ can be taken as zero since it is trivial for the determination of ground-state charge density. To implement the self-consistent Kohn-Sham scheme. First, we choose an initial form of charge density $n(\mathbf{r})$ and substitute into Eq. (6.14) to find a trial form of V_R. Then

we solve the Kohn-Sham equation (Eq. (6.10)) for the single-particle wave functions $\phi_i(\mathbf{r})$ and use Eq. (6.9) to find the updated density for $n(\mathbf{r})$ until the convergence of the density has been reached.

The extension of density functional theory to the spin-polarized electrons is straightforward. In spin density functional theory, the total energy is written as

$$F_{KS}[n_\uparrow, n_\downarrow] = T_R[n_\uparrow, n_\downarrow] + \int n(\mathbf{r})v_{ext}(\mathbf{r})d\mathbf{r} + \frac{1}{2}\int\int\frac{n(\mathbf{r})n(\mathbf{r}')}{|\mathbf{r} - \mathbf{r}'|} + E_{xc}[n_\uparrow, n_\downarrow],$$
(6.15)

with

$$T_R[n_\uparrow, n_\downarrow] = -\frac{\hbar^2}{2m}\sum_{s=1}^{2}\sum_{i=1}^{N_s}\langle\phi_{i,s}|\nabla^2|\phi_{i,s}\rangle,$$
(6.16)

in which occupation number for different spin components N_s need to be determined by filling the lowest eigenstates for the Kohn-Sham orbitals $\epsilon_{i,s}$.

6.2   LSDA approximation

In order to have a workable Kohn-Sham scheme, the local density approximation can be used to approximate the exchange-correlation energy E_{xc}. The local density approximation has been for a long time the most widely used approximation to E_{xc}. The main idea is to consider a general inhomogeneous electronic system as locally homogeneous, and then to use the exchange-correlation hole(Appendix C) corresponding to the homogeneous electron gas, which is known to an excellent accuracy. The extension of the LDA to spin-polarized systems is the local spin density approximation (LSDA),

which basically consists of replacing the exchange-correlation energy with a spin-polarized expression:

$$E_{xc}^{LSDA}[n_\uparrow(\mathbf{r}), n_\downarrow(\mathbf{r})] = \int [n_\uparrow(\mathbf{r}) + n_\downarrow(\mathbf{r})]\epsilon_{\mathbf{xc}}^{\mathbf{h}}[\mathbf{n}_\uparrow(\mathbf{r}), \mathbf{n}_\downarrow(\mathbf{r})]\mathbf{dr}$$

$$= \int n(\mathbf{r})\epsilon_{xc}^{h}[n(\mathbf{r}), \zeta(\mathbf{r})]d\mathbf{r}, \tag{6.17}$$

where $\zeta(\mathbf{r})$ is the magnetization density. The common practice in LSDA is to interpolate between the fully-polarized (ϵ_{xc}^{F}) and unpolarized (ϵ_{xc}^{U}) exchange-correlation energy densities using some interpolation function:

$$\epsilon_{xc}^{h}[n, \zeta] = f(\zeta)\epsilon_{xc}^{F}[n] + [1 - f(\zeta)]\epsilon_{xc}^{U}[n].$$

One of the widely used versions for the form of $f(\zeta)$ is given by Perdew and Wang ([45]) which includes the effects going beyond random phase approximation by fitting Monte-Carlo's data from Ceperley and Aldler ([46]).

6.3 LSDA+U approximation

Strongly correlated materials are examples where the DFT under LDA approximation will not produce even the right physics qualitatively. Such systems contains transition metal ions or rare-earth metal ions with partially filled d or f shells. By the band picture implemented by LSDA, the systems will have metallic type of electronic structure and tend to be ferromagnetic. However, in reality, those systems tend to be Mott insulators and antiferromagnetic with a correlation gap at the Fermi surface.

The idea of LDA+U follows closely to the spirit of Anderson model, the electrons can be separated into two subsystems: localized d or f electrons for which screened Coulomb $d - d$ interaction should be taken into account by a term $\frac{1}{2}U \sum_{i \neq j} n_i n_j$ (n_i are d-orbital occupancies) as in a mean-field approximation, and delocalized s, p electrons which could be described by LDA. Let us consider a d ion as an open system with a fluctuating number of d electrons due to hybridization with itinerant electrons in solids. However, LDA has treated the d electrons as itinerant. We need to subtract this energy off. If we assume that the coulomb energy of $d - d$ interactions as a function of total number of d electrons N given by LDA is a good approximation(discussed in [47]), then the correct expression for the energy is $E_{dc} = UN(N-1)/2$. As a result, we need to substrate the energy E_{dc} to avoid double counting and we have the LDA+U functional:

$$E = E_{LDA} - UN(N-1)/2 + \frac{1}{2}U \sum_{i \neq j} n_i n_j. \tag{6.18}$$

The orbital energy ϵ_i are derivatives of eq. (6.19) with respect to orbital occupation n_i :

$$\epsilon_i = \frac{\partial E}{\partial n_i} = \epsilon_{LDA} + U(\frac{1}{2} - n_i). \tag{6.19}$$

This states that correlation shifts the LDA orbital energy by $-U/2$ for occupied orbitals ($n_i = 1$) and by $U/2$ for unoccupied orbitals ($n_i = 0$). Similarly, we have the orbital dependent potential:

$$V_i(r) = V_{LDA} + U(\frac{1}{2} - n_i). \tag{6.20}$$

71

To further construct a quantitatively sound calculation scheme, one needs in a more general way an orbital basis set and to take into account the direct and exchange Coulomb interactions inside a partially filled d atomic shells.

Various versions of LSDA+U exist[48–50], the anchor thoughts are similar. The idea is to subtract $d - d$ Coulomb energy E_{dc} from LSDA energy functional and replace it with Hubbard-like interaction which includes the direct and exchange interaction for different spin components as

$$E_{LSDA+U} = E_{LSDA} - E_{dc} + E_{Hubbard}. \qquad (6.21)$$

The version of LSDA+U due to S. L. Dudarev et al.[50] bridges the orbital-dependent formulation by Anisimov et al.[48] with the rotationally invariant functional proposed by Liechtenstein et al.[49] while retaining the simplicity of the first and the covariance under rotation. We will focus on Dudarev's version, which has known to reproduce the electronic properties of Nickel oxides successfully, in this dissertation because this is the scheme we used in our calculation on transition metal oxide interface physics.

The Hubbard model Hamiltonian which include direct and exchange interactions can be written as this form

$$\hat{H}_{Hubbard} = \frac{\bar{U}}{2} \sum_{m,m',\sigma} \hat{n}_{m,\sigma} \hat{n}_{m',-\sigma} + \frac{\bar{U} - \bar{J}}{2} \sum_{m \neq m',\sigma} \hat{n}_{m,\sigma} \hat{n}_{m',\sigma}, \qquad (6.22)$$

where the summation is performed over projections of the angular momentum ($m, m' = -2, -1, ..., 2$ in the case of d electrons) and $\bar{U}$ and $\bar{J}$ are the spherically averaged matrix elements of the screened Coulomb electron-electron interaction. The first term describe the interaction between different spins in

the d orbitals and second term states that the effective interaction between liked-spins in different d orbitals enforcing Hund's rule is reduced. The form of the E_{dc} should be only expressed as total number of d electrons and can be conjectured as that of the expectation value of $\hat{H}$ for an integer number of d electrons as

$$E_{dc} = \frac{\bar{U}}{2} \sum_{\sigma} N_{\sigma} N_{-\sigma} + \frac{\bar{U} - \bar{J}}{2} \sum_{\sigma} N_{\sigma}(N_{\sigma} - 1), \tag{6.23}$$

where $N_{\sigma} = \sum_{m} n_{m,\sigma}$ is the total number of d electrons with a given projection of spin σ.

The expression of $E_{Hubbard}$ is given by the expectation value of the Hubbard Hamiltonian with mean field approximation with noninteger occupation number as

$$E_{Hubbard} = \frac{\bar{U}}{2} \sum_{m,m',\sigma} n_{m,\sigma} n_{m',-\sigma} + \frac{\bar{U} - \bar{J}}{2} \sum_{m \neq m',\sigma} n_{m,\sigma} n_{m',\sigma}, \tag{6.24}$$

where $n_{m,\sigma}$ is the occupation number of the mth d state. Therefore, we arrive at the LSDA+U functional:

$$E_{LSDA+U} = E_{LSDA} + \frac{\bar{U} - \bar{J}}{2} \sum_{\sigma,m} (n_{m,\sigma} - n_{m,\sigma}^2). \tag{6.25}$$

From the expression, we observe that correlation shifts the LSDA orbital energy $\epsilon_{m\sigma} = \frac{\partial E_{LSDA+U}}{\partial n_{m\sigma}}$ by $-(\bar{U} - \bar{J})/2$ for occupied orbitals ($n_{m,\sigma} = 1$) and by $(\bar{U} - \bar{J})/2$ for unoccupied orbitals ($n_{m\sigma} = 0$). In rotational invariant form, by noticing that the required matrix construction should be diagonal in the spherical harmonics representation, we arrive at

$$E_{LSDA+U} = E_{LSDA} + \frac{\bar{U} - \bar{J}}{2} \sum_{\sigma} [Trn^{\sigma} - Tr(n^{\sigma}n^{\sigma})],$$

$$= E_{LSDA} + \frac{\bar{U} - \bar{J}}{2} \sum_{\sigma} \left[\left(\sum_{j} \rho_{jj}^{\sigma} \right) - \left(\sum_{j,l} \rho_{jl}^{\sigma} \rho_{lj}^{\sigma} \right) \right]. \qquad (6.26)$$

Chapter 7

Transition metal oxides and interfaces

In this chapter, we will introduce the background knowledge for transition metal oxides. Transition metal oxides (TMO) make up one of the most fascinating classes of inorganic materials. They show an extremely wide range of phenomena and do not fit easily into a simple theoretical framework. For these reasons, they have been one of the primary playgrounds for the condensed matter community to decipher the underlying principles in solids. The wide array of properties seen in TMOs is due to the close proximity of their various energy scales. Small changes in experimentally accessible parameters – such as temperature, pressure, and doping – are often enough to subtly rearrange the order of the energy scales, thereby radically changing the properties of these materials. With the advance of oxide molecular beam epitaxy(Oxide MBE), it becomes feasible to grow high quality heterostructures with well-defined layers in laboratory particularly for perovskites compounds ABO_3 and to probe the electronic states of the materials by different techniques. One of the most exciting effects will be the states exist in the interface of the heterostructures can be very different from the composing bulk materials.

7.1 The importance of transition metal oxides

An electron exhibits wavelike and particle-like characteristics. Which aspect predominates in a solid depends on how an electron interacts with its neighbors. According to the Bloch theorem , for instance, an electron placed in a periodic lattice behaves like an extended plane wave. However, when the number of free electrons in a solid becomes comparable to the number of the constituent atoms and the mutual electron- electron interaction becomes strong, electrons may lose their mobility. The dual nature is most apparent in correlated-electron systems, such as the transition-metal oxides in which electron interactions strongly determine electronic properties. In the transition-metal ions, for example, d electrons experience competing forces: Coulomb repulsion tends to localize individual electrons at atomic lattice sites, while hybridization with the oxygen p electron states tends to delocalize the electrons. The subtle balance makes many of the transition-metal oxides excellent resources for studying and taking advantage of the metal-insulator transition that can accompany dramatic changes in a systems electronic properties.

An electron in a solid has three attributes that determine its behavior: charge, spin, and orbital symmetry. One can imagine an orbital, which represents the electrons probability-density distribution, as the shape of an electron cloud in a solid. The charge, spin, and orbital degrees of freedom-and their coupled dynamics can produce complex phases such as liquid-like, crystal like, and liquid-crystal-like states of electrons, and phenomena such as electronic phase separation and pattern formation.

The correlation of electrons in a solid produces a rich variety of states, typically through the interplay between magnetism and electrical conductance. That interplay has itself been a long-standing research topic among condensed matter physicists. But since the discovery of copper-oxide high-temperature superconductors, a more general interest in the metal-insulator transition in a correlated-electron system-has emerged because of the belief that the strong antiferromagnetic correlation which originates in the Mott-insulating CuO_2 sheets and persists into the metallic state , is most responsible for the mechanism of high-Tc superconductivity .

Widespread interest in copper oxides and other correlated- electron systems also led to a rediscovery of the so-called colossal magnetoresistance (CMR) phenomenon, which is a gigantic decrease of resistance induced by application of a magnetic field. This article features some examples of the dramatic phase changes in CMR manganites and other transition-metal oxides that arise from a close interplay among electron properties and their affect on the lattice. Researchers can now control the electronic and magnetic phases of correlated- electron materials in unconventional ways, in some cases with ultrafast response times. Such newly won control offers hope that correlated-electron systems may provide a basis for novel electronics such as spintronics and orbitronics.

7.2   Perovskite Structure

The transitional metal oxides we will discuss are Perovskites. The perovskite structure class is one of the most commonly occurring and important in all of materials science. Physical properties of interest among perovskites include superconductivity, colossal magnetoresistance, ionic conductivity, and a multitude of dielectric properties, which are of great importance in microelectronics and telecommunication. Because of the great flexibility inherent in the perovskite structure there are many different types of distortions which can occur from the ideal structure. These include tilting of the octahedra, displacements of the cations out of the centers of their coordination polyhedra, and distortions of the octahedra driven by electronic factors (i.e. Jahn-Teller distortions). Many of the physical properties of perovskites depend crucially on the details of these distortions, particularly the electronic, magnetic and dielectric properties which are so important for many of the applications of perovskite materials.

The highly versatile ABX_3 perovskite crystal structure is formed by the B cations filling 0.25 of the octahedral holes in the cubic close-packed AX_3 array[51]. In the ideal cubic structure, each A cation is coordinated to twelve X anions and each B cation is coordinated to six X anions. An example of the ideal cubic structure is shown in Fig. 7.1. The substitution of different atoms into the A and B positions is possible if they are of similar size to A and B respectively, and total equivalent oxidation state[52]. Most perovskite structures are distorted and do not have cubic symmetry. Common

distortions such as cation displacements within the octahedra and tilting of the octahedra are related to the properties of the A and B substituted atoms. Factors that contribute to distortion in the structure include radius size effects and the Jahn-Teller effect[51]. Octahedral tilting distortions present in many perovskites was first examined by Goldschmidt in 1926[52]. According to Goldschmidt, the degree of distortion in ABO_3 perovskites can be determined using the following equation:

$$t = [R_A + R_O]/\sqrt{2}[R_B + R_O] \qquad (7.1)$$

where R_A is the ionic radius of A, R_B is the ionic radius of B, and R_O is the ionic radius of oxygen. If the value of t is close to 1, the structure is expected to adopt the ideal cubic symmetry. When the value of t is 0.81 or less and the value of the A site ion is smaller than ideal, and the BO6 octahedra will tilt in order to fill space. Stable perovskite structures have values approximately $0.78 < t < 1.05$. The tolerance factor however, is based on the ionic radius and should only be used as an estimate because perovskites are not exclusively ionic.

Perovkites containing cations such as Cu^{2+} and Mn^{3+} in their octahedral cation site tend to exhibit distortions caused by the Jahn-Teller effect. The Jahn-Teller distortion theorem states that a nonlinear molecule cannot be stable in a degenerate electronic state and must undergo distortion in order to break down the degeneracy and become stable[53]. Distortion caused by the Jahn-Teller effect in perovskites usually involves four of the octahedral

79
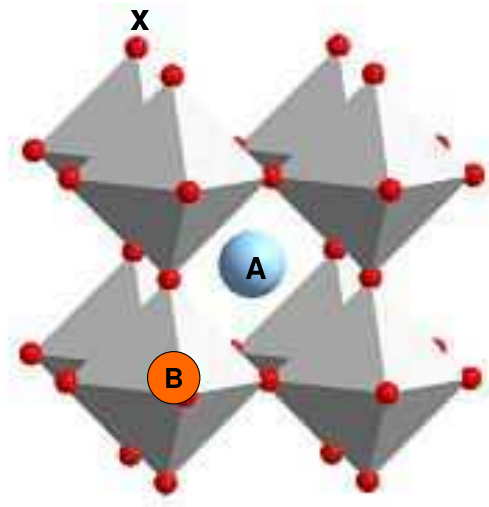
Figure 7.1: Crystal structure of perovskites ABX_3. Transition metal B atoms sit at the center of the diamond cage. A atom is located at the body center of adjacent B atoms. X are anions which are replaced by oxygen atoms in oxides.

bonds contracting and two of the octahedral bond lengthening which gives an elongated octahedral shape. The distortions exhibited by perovskites as a consequence of cation substitution can be used to fine tune and adjust properties of interest. A few of the physical properties of interest in various perovskite systems include conductivity, dielectrics, and colossal magnetoresistance.

7.3 d orbital physics

The atomic orbitals of transition-metal elements are constructed as eigenstates under the spherical potential generated by the transition-metal ion. When the solid is formed, the atomic orbital forms bands due to the periodic potential of atoms. The bandwidth is basically determined from the overlap

of two d orbitals on two adjacent transition metals each. The overlap comes from the tunneling of two adjacent so-called virtual bound states of d orbitals. Because the wave function as compared to the lattice constant in crystals are more localized due to the centripetal repulsive potential $\frac{l(l+1)\hbar^2}{2mr^2}$ ($l = 2$ is the azimuthal quantum number for d orbitals) which makes the effective trapping potential well deeper than s and p orbitals, d-electron systems have in general smaller overlap and hence smaller bandwidths than alkaline metals. In transition-metal compounds, the overlap is often determined by indirect transfer between d orbitals through ligand p orbitals. This means that the bandwidth is determined by the overlap (in other words, hybridization) of the d wave function at a transition metal atom and the p wave function at the adjacent ligand atom if the ligand atoms make bridges between two transition-metal atoms. Because of this indirect transfer through ligand atomic orbitals, the d bandwidth becomes in general even narrower. Another origin of the relatively narrow bandwidth in transition-metal compounds is that $4s$ and $4p$ bands are pushed well above the d band, where screening effects by $4s$ and $4p$ electrons do not work well. This makes the interaction relatively larger than the bandwidth. In any case, because of the narrow bandwidth, tight-binding models constructed from atomic Wannier orbitals provide a good starting point for the transition metal physics. The bands are under the strong influence of anisotropic crystal fields in solids. Because the $3d$ orbital has the total angular momentum L=2, it has fivefold degeneracy (L_z=2,1,0,-1,-2) for each spin and hence a total of tenfold degeneracy including spins. This degeneracy

81
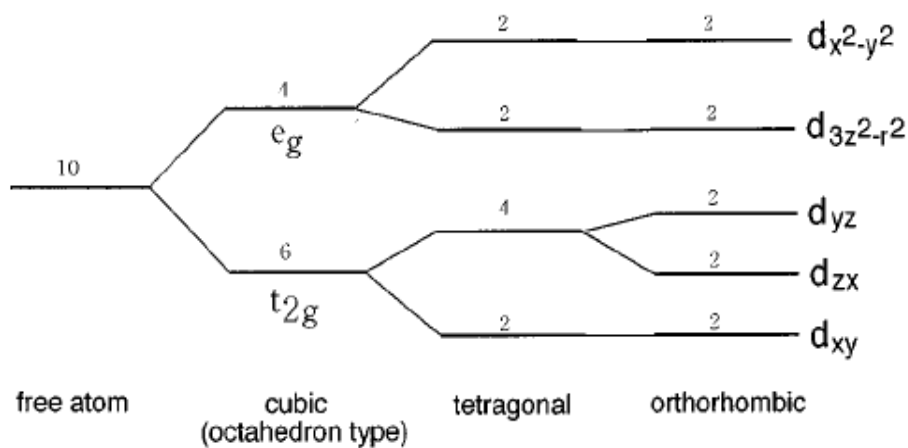
Figure 7.2: Crystal-field splitting of $3d$ orbitals under cubic, tetragonal, and orthorhombic symmetries. For tetragonal symmetry, only the cubic symmetry along z direction is broken and the symmetry along x and y are preserved . For orthorhombic symmetry, the cubic symmetry is completely broken along x, y, z leading to the splitting of t_{2g} orbitals. The numbers cited near the levels are the degeneracy including spins.

is lifted by the anisotropic crystal field. In transition-metal compounds, a transition-metal atom is surrounded by ligand atoms to help in the formation of a solid through the increase in cohesive energy by covalent bonds of the two species. Because the ligand atoms have a strong tendency towards negative valence, the crystal field of electrons in the direction of the ligand atom is higher than in other directions. Fig. 7.2 shows an example of the crystal field splitting , where the cubic lattice symmetry leads to a higher energy level of fourfold degenerate e_g orbital and sixfold degenerate lower orbitals, t_{2g}. When a transition-metal atom is surrounded by ligand atoms with an octahedron configuration, the e_g orbital has anisotropy with larger amplitude in the direction of the principle axes, namely, toward neighboring ligand atoms. The basis of these orbitals may be expanded by $d_{x^2-y^2}$ and $d_{3z^2-r^2}$ orbitals. On the other hand, the t_{2g} orbital has anisotropy with larger amplitude of the wave function toward other directions and may be represented by d_{xy} , d_{yz} , and d_{zx} orbitals. For other lattice structures with other crystal symmetries, such as tetragonal or orthorhombic as in the case of 2D perovskite structure, similar crystal field splitting appears. In the case of tetrahedral surroundings of ligand ions, e_g orbitals lie lower than t_{2g} , in contrast to cubic symmetry or octahedron surroundings.

In general, the relevant electronic orbitals for low energy excitations transition-metal compounds with light transition-metal elements are different from those with heavy ones. In the compounds with light transition-metal elements such as Ti, V, Cr, . . . , only a few bands formed from $3d$ orbitals
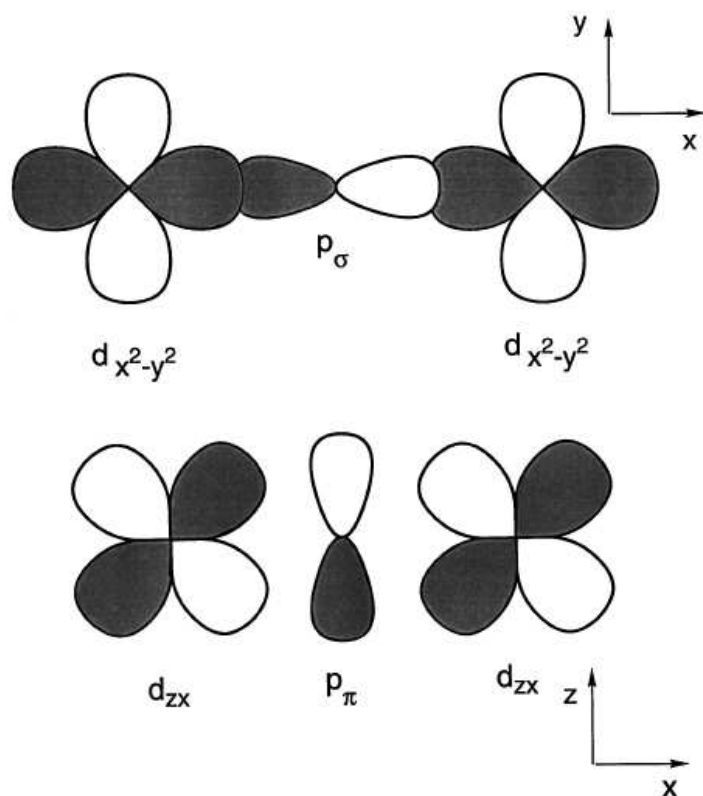
Figure 7.3: Examples of configurations for transition-metal 3d orbitals which are bridged by ligand p orbitals

84

are occupied by electrons per atom. Therefore the t_{2g} orbital (more precisely, the t_{2g} band under the periodic potential) is the relevant band for low-energy excitations in the case of the above mentioned octahedron structure because the Fermi level crosses bands mainly formed by t_{2g} orbitals. By contrast, in transition-metal compounds with heavy transition-metal elements such as Cu and Ni, the t_{2g} band is fully occupied far below the Fermi level, and low-energy excitations are expressed within the eg band, which is formed mainly from eg atomic orbitals. If degenerate t_{2g} or e_g orbitals are filled partially, it generally leads again to degeneracy of the ground state, which frequently induces the Jahn-Teller effect to lift the degeneracy.

Another important difference between light and heavy transition-metal compounds is the level of ligand p orbitals. For example, in the transition-metal oxides, the levels of the relevant $3d$ orbitals and oxygen $2p_\sigma$ orbitals, illustrated in Fig. 7.3, become closer when the transition-metal element is changed from Sc to Cu. This is mainly because the positive nuclear charge increases with this change, which makes the chemical potential of d electrons lower and closer to the p orbital. In fact, in the high-Tc cuprates, the $2p_\sigma$ orbital has a level close to the $3d_{x^2+y^2}$ orbital of Cu. This tendency, as well as the larger overlap of the e_g wave function with the ligand p_σ orbital for geometric reasons, causes a strong hybridization of the e_g and ligand p bands in the late transition metals. Therefore, to understand low-energy excitations on a quantitative level, we have to consider these strong hybridization effects. In contrast, for light transition metal oxides, the oxygen p level becomes far

85

from the $3d$ orbital and additionally the overlap of t_{2g} and p orbitals is weak. Then the oxygen p band is not strongly hybridized with $3d$ band at the Fermi level, and the formal valence of oxygen is kept close to O^{-2}. (More correctly speaking, the oxygen p band is nearly full. However, the real valence of oxygen itself may be larger than -2 because the oxygen p band is hybridized with $3d$, $4s$, and $4p$ orbitals.) Consequently the contribution from the oxygen p band to the wave function at the Fermi level may be ignored in the first stage.

7.4 Electronic interface reconstruction

A central goal of modern materials physics and nanoscience is the control of materials and their interfaces to atomic dimensions. For interfaces between polar and nonpolar layers, this goal is thwarted by a polar catastrophe that forces an interfacial reconstruction. In traditional semiconductors, this reconstruction is achieved by an atomic disordering and stoichiometry change at the interface, but a new option is available in multivalent oxides and the electrons can move so that the electron states are reconstructed.

Let us illustrate with examples to motivate the ideas. The (001) planes in the ABO3 perovskite structure can be divided into alternating layers of AO and BO$_2$ planes. Taking oxygen to have a formal valence of O^{2-}, the A and B cations can take on values of A^{4+}B^{2+}, A^{3+}B^{3+}, A^{2+}B^{4+} or A^{1+}B^{5+}, such that the ABO$_3$ bulk structure remains neutral. Fractional charge values also arise from solid solutions and/or mixed valence states. Just as compound semiconductors made from group IV elements such as Si or Ge have formally

neutral (001) planes, the $A^{2+}B^{4+}O_3$ or IIIV structure (such as $SrTiO_3$) also contains neutral AO and BO_2 (001) planes. An analogue of the IIIV or IIVI semiconductors such as GaN or CdTe that have polar planes is the $A^{3+}B^{3+}O_3$ or IIIIII structure (such as $LaTiO_3$ or $LaAlO_3$), which is composed of +1 AO and -1 BO_2 planes. If we consider joining perovskites from two different charge families with atomic abruptness in an (001) orientation, a polar discontinuity results at the interface. Taking the example of joining $LaAlO_3$ with $SrTiO_3$, two configurations arise, which can be defined by the composition of the layer between AlO_2 and TiO_2 at the interface: $AlO_2/LaO/TiO_2$ or $AlO_2/SrO/TiO_2$. Such a junction between polar and nonpolar planes is very common in oxide heterostructures, and the following discussion applies generally to many perovskite interfaces. Figure 7.4(a),(b)shows how an atomically abrupt interface between polar and neutral layers leads to a polar catastrophe (where the electrostatic potential diverges with thickness) if there is no redistribution of charges at the interface. Unlike conventional semiconductors where each ion has a fixed valence, in complex oxides compositional roughening is not the only option for charge rearrangement: mixed valence charge compensation can occur if electrons can be redistributed at lower energy cost than redistributing ions. Conceptually, one can first construct the interface from neutral atoms and then allow ionization, resulting in the net transfer of half an electron per two-dimensional unit cell (e-/u.c.) from $LaAlO_3$ to $SrTiO_3$ across the interface (Fig. 7.4(c)). This process leaves the overall structure neutral, with the Ti ion at the interface becoming $Ti^{3.5+}$, and the potential no longer diverges.
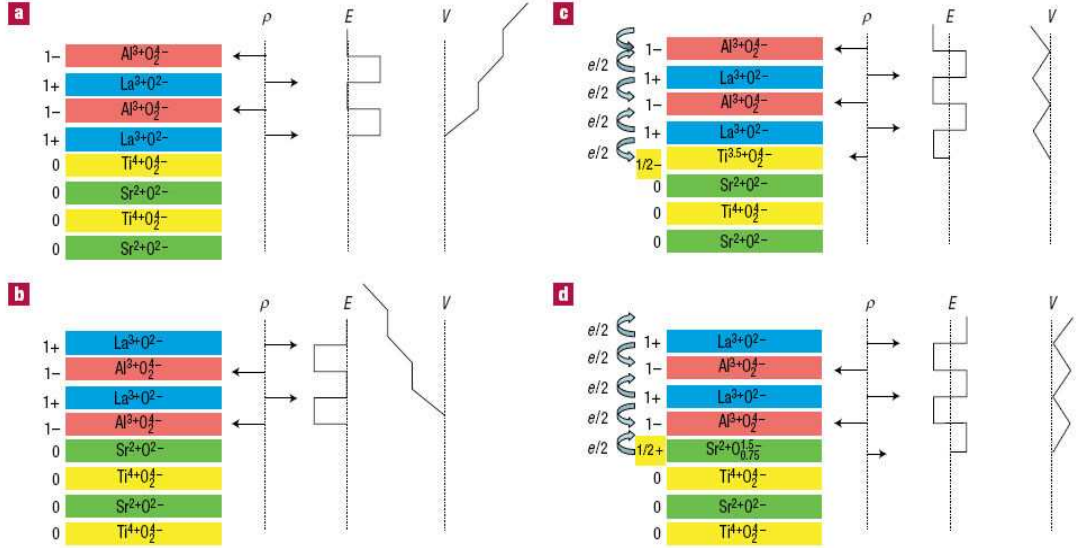
Figure 7.4: The polar catastrophe illustrated for atomically abrupt (001) interfaces between $LaAlO_3$ and $SrTiO_3$. (a) The unreconstructed interface has neutral (001) planes in $SrTiO_3$, but the (001) planes in $LaAlO_3$ have alternating net charges (ρ). If the interface plane is $AlO_2/LaO/TiO_2$, this produces a non-negative electric field (E), leading in turn to an electric potential (V) that diverges with thickness. (b) If the interface is instead placed at the $AlO_2/SrO/TiO_2$ plane, the potential diverges negatively. (c) The divergence catastrophe at the $AlO_2/LaO/TiO_2$ interface can be avoided if half an electron is added to the last Ti layer. This produces an interface dipole that causes the electric field to oscillate about 0 and the potential remains finite. The upper free surface is not shown, but in this simple model the uppermost AlO2 layer would be missing half an electron, which would bring the electric field and potential back to zero at the upper surface. (d) The divergence for the $AlO_2/SrO/TiO_2$ interface can also be avoided by removing half an electron from the SrO plane in the form of oxygen vacancies. The picture is reproduced from the reference [73].

88

The extra half an electron at the $AlO_2/LaO/TiO_2$ (n-type) interface should be physically detectable by transport and direct spectroscopic measurements. Indeed, metallic conductivity and Hall measurements suggest free electrons at the n-type interface. Figure 7.4(d) shows the analogous construction for the $AlO_2/SrO/TiO_2$ interface where the SrO layer must now acquire an extra half a hole per two-dimensional unit cell (e+/u.c.) to maintain charge neutrality, that is, formally it should be p-type. Electrically, however, this interface is insulating. As this positive charge is still electrostatically necessary to avoid the divergence, and there are no available mixed-valence states to compensate for the half a hole (such as $Ti^{4.5+}$, which is energetically inaccessible), an atomic reconstruction is required.

Chapter 8

Quantum Wells in Polar-Nonpolar Oxide Heterojunction Systems

We address the electronic structure of quantum wells in polar-nonpolar oxide heterojunction systems focusing on the case of non-polar $BaVO_3$ wells surrounded by polar $LaTiO_3$ barriers. Our discussion is based on a density functional description using the local spin density approximation with local correlation corrections (LSDA+U). We conclude that a variety of quite different two-dimensional electron systems can occur at interfaces between insulating materials depending on band line-ups and on the geometrical arrangement of polarity discontinuities.[1]

8.1 Introduction

Complex oxide materials exhibit a wide variety of exotic phenomena from high temperature superconductivity[54], to colossal magnetoresistance[55], to electronic and orbital order[2]. Recently, inspired by advances in epitaxial growth techniques, there has been increasing interest[56–62] in making

---

[1]The discussion in this chapter is based on the article: C.-C Joseph Wang, Bhagawan Sahu, Hongki Min, Wei-Cheng Lee, Allan H. MacDonald, arXiv: cond-mat/0810.0798v1, (2008).

progress toward the goal of controlling oxide properties by designing layered structures at the atomic level. The class of artificial materials which has been studied most extensively is ABO_3 perovskites. Already there is evidence for the emergence of superconductivity from non-superconducting materials[57] and magnetism from nonmagnetic materials[58]. One element which distinquishes oxide heterojunction systems from weakly correlated semiconductor heterojunctions is the possibility of exploiting gradients in polarity[63] to help control electronic properties. In this article we study the electronic properties of oxide quantum wells in which the barrier and well materials have very different polarities, using the case of non-polar $BaVO_3$ wells surrounded by polar $LaTiO_3$ barriers as an example.

Our paper is organized as follows. In Section II, we present a qualitative discussion of four possible polar-nonpolar quantum well geometries. We have tested conjectures made in Section II by performing local spin-density-approximation with local-correlation corrections (LSDA+U) calculations for BVO quantum wells in LTO and LTO quantum wells in BVO. Throughout this paper, we use LTO as the shorthand for the perovskites associated with LaO and TiO_2 layers and BVO as the shorthand for the perovskites associated with BaO and VO_2 layers. In Section III, we briefly detail the LSDA+U electronic structure calculation methods we have employed to model LTO/BVO/LTO or BVO/LTO/BVO quantum well systems. The combination (LTO/BVO) was chosen because LTO is polar and BVO is not and because this material combination should not lead to large strains at the interface. Partly for con-

91

venience and partly because multi-quantum-well systems are likely to be of equal experimental interest, we assume periodically repeated quantum wells so that we have a superlattice in the growth direction. In bulk both LTO and BVO are d^1 Mott insulators. We focus on heterojunction systems composed of materials which have the same d-band occupancies in the bulk because more possibilities exist for interface electronic structure compared to the case of heterojunctions between d^1 and d^0 materials such as $LaTiO_3/SrTiO_3$, for which interface metallicity appears to be inevitable. In Section IV we present the results of our *ab initio* electronic structure calculations for the two representative quantum well systems and compare with the conjectures we made in section II. Finally in Section V we briefly summarize our results.

8.2 Polar-Nonpolar quantum well structures

In this section, we discuss four different possible geometries for a polar-nonpolar quantum well system. The main points we wish to make are illustrated in Fig. 8.1 which illustrates approximate charge transfers and electric potentials. Throughout this discussion we use LTO to represent a prototypical d^1 polar perovskite and BVO to represent a prototypical d^1 nonpolar perovskite. We identify two possible geometries for both LTO/BVO/LTO (case (a) and case (c))and BVO/LTO/BVO (case (b) and case (d))quantum well systems. At an interface between two strongly correlated bulk materials we should expect a complex interplay between the ionic potential energy, kinetic energy, and correlation energies of the two materials. By using density

functional theory with local correlations (LSDA+U) we can take into account those energies approximately with a single electron picture. The electronic structure is characterized most crudely by an ionic electron counting picture which neglects hybridization between oxygen and transition metal orbitals and ignores the finite thickness of the various atomic layers. Using this picture, the $La^{+3}O^{-2}$ planes in LTO are positively charged and the $Ti^{+3}O_2^{-4}$ are negatively charged. In bulk BVO on the other hand, the $Ba^{+2}O^{-2}$ and $V^{+4}O_2^{-4}$ planes are neutral in the bulk. The transition-metal ions in both materials then have one electron in the d orbitals to maintain charge neutrality. When we combine polar perovskites with nonpolar ones, the transition-metal layer will distribute the d-charges in a different way to compensate for the nonuniform distribution of ionized layers in this system, as illustrated in Fig. 8.1. We discuss only cases in which the center of the quantum well is a center of inversion symmetry. In each case the number of layers which would have a positive charge in a bulk polar crystal differs from the number of layers which would have a negative charge.

In case (a), we have two BaO layers and one VO_2 layer inserted in the unit cell of a superlattice with six LaO^+ layers but seven TiO_2 layers. The charges in the supercell cannot be neutral if we assume that each TiO_2 is negatively charged as in the bulk LTO states. Instead, we expect that the extra electrons s will be distributed evenly among the TiO_2 layers near the central VO_2 layer. The easiest way to accomplish this is to have the TiO_2 layers next to BaO layers to be $Ti^{+3.5}O_2^{-4}$ rather than $Ti^{+3}O_2^{-4}$, $i.e.$ that

93
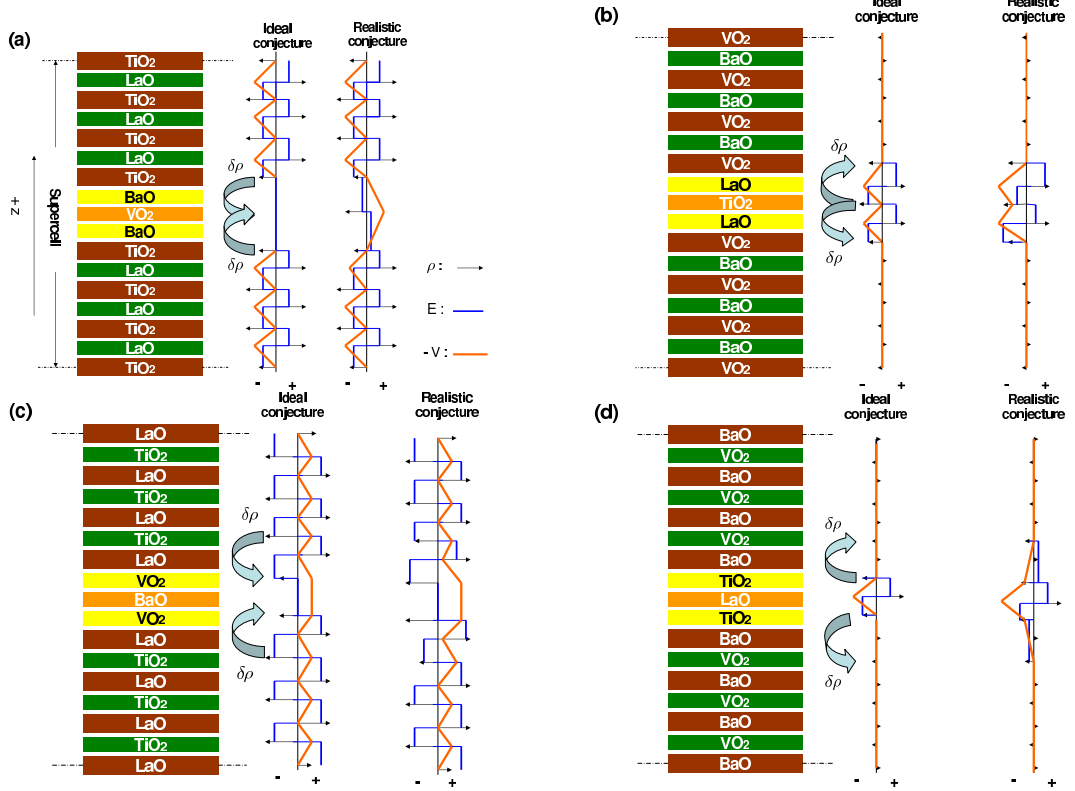
Figure 8.1: Approximate charge density, electric field, and electric potential distributions in different polar-nonpolar quantum well systems with inversion symmetry in the quantum well center. The arrows (black on line) indicate the expected charge densities ρ centered on different atomic layers, the piecewise constant thick lines lines (blue on line) indicate the expected electric fields E between the atomic layers, and the cusped lines (red on line) indicate the expected electric potential $-V(z)$ distribution. The distributions labeled *ideal conjecture* in this figure assign the charge deficiency or excess to the two transition metal layers adjacent to the quantum well whereas the distributions labeled *realistic conjecture* assume additional charge redistribution $\delta\rho$ due to the difference between V and Ti d-orbital energies. The signs $+$ and $-$ stand for the direction of electric field E, the value for ρ, and the potential $-V(z)$.

94

they contain 0.5 d-electrons per Ti rather than 1.0 d-electrons per titanium. This idealized conjecture ignores $d - p$ hybridization as well as the difference between the d-orbital energies on Ti and V sites. In particular a V^{+4} ion should have a lower intrinsic atomic levels than the Ti^{+3} ion. We should expect that charges might react locally to this difference by transferring additional electrons $\delta\rho$ to the VO_2 well from nearby TiO_2 layers. This additional charge transfer partially screens the original atomic energy level difference. These considerations are illustrated schematically in Fig. 8.1. The d-electron system electronic structure reconstructs in this way near the interface in reaction to the electrostatic potentials produced by the bulk crystal layer polarizations. Qualitatively similar considerations would apply to wider BVO quantum wells.

In case (b), we have two LaO^{+} layers and one TiO_2 barrier layer in the middle of the supercell. By the same arguments as case (a), the simplest conjecture is that the VO_2 layers nearest the TiO_2 layers will be negatively charged $(V^{+3.5}O_2^{-4})$ to keep the system neutral. The charge configuration $Ti^{+3}O_2^{-4}$ is maintained by the protection of two surrounding LaO^{+} layers. Therefore, there will be 1.5 d-electrons on V sites in the $V^{+3.5}O_2^{-4}$ layers and 9 d-electrons in the supercell. However, the local physics is different in this case. The electron can respond locally by transferring electrons from the barrier TiO_2 to the VO_2 well layers. The reconstructed potential should therefore be lower in the well region in this case.

In case (c), we switch the ordering of layers from case (a) (BaO $\leftrightarrow$ VO_2 and LaO $\leftrightarrow$ TiO_2). There are 7 positive charged LaO^{+} layers and 6

$Ti^{+3}O_2^{-4}$ layers. To compensate for the charge difference, VO_2 layers have to be negatively charged as $V^{+3.5}O_2^{-4}$ in the idealized conjecture illustrated. Additional charges can transfer from adjacent $Ti^{+3}O_2^{-4}$ to the $V^{+3.5}O_2^{-4}$ layers. The reconstructed potential should therefore be higher in the well region.

Similarly in case (d), the structure has been changed from case (b) by switching the ordering $BaO \leftrightarrow VO_2$ and $LaO \leftrightarrow TiO_2$. There is only one LaO^+ layer in this case. The abutting TiO_2 layers should have the configuration $Ti^{+3.5}O_2^{-4}$ to keep charge neutrality, resulting in a lower reconstructed local potential in the center of the cell. Notice that the magnitude of the additional charge transfer and its spatial distribution expected in the realistic pictures needs to be determined by self-consistent microscopic calculations. In the next section, we will focus on cases (a) and (b) to check the degree to which the qualitative pictures explained here agrees with the results of microscopic DFT calculations and to obtain further insight into the nature of the two-dimensional electron systems which these electronic reconstructions enforce.

8.3   Electronic Structure Calculations

In our *ab initio* electronic structure calculations we have considered symmetric quantum well geometries only, use the experimental atom positions[64, 65] for LTO, and neglect atomic relaxation in the BVO layers. (The room temperature crystal structure of BVO is not known experimentally.) The electronic structure calculations were performed using DFT with LSDA+U as implemented in the software package VASP [66–68]. Projector-augmented

wave pseudopotentials[69] are used to describe the electron-ion interaction. We sample the full superlattice Brillouin zone (BZ) with a $5 \times 5 \times 3$ mesh and used an energy cutoff of 410 eV which we found to be sufficient to reproduce bulk LTO properties. We used PAW pseudopotentials supplied by the VASP code for La, O, Ba, Ti and V but for Ba, Ti and V, we used the one with semicore states treated as valance states. The screened local correlation U in the partially filled d bands of the transition metal elements were treated using the rotationally invariant LSDA+U method due to Dudarev et al.[70]. Since the La f bands lie much higher in energy in experiments[60, 72] we impose a much larger $U_{La} = 11$ eV on La f states to prevent their mixing with d bands at low energy. We chose $U_{Ti} = 3.2$ eV and $J_{Ti} = 0.9$ eV since these values reproduces the Mott-insulating nature of bulk LTO[71] and we take U_V and J_V to be the same as U_{Ti} and J_{Ti}. We have varied U_V to check the robustness of our calculations and find that our conclusions are independent of this LSDA+U parameter.

8.4 LSDA+U quantum-well electronic structure

Case A : $(LaTiO_3)_3/(BaO)_2VO_2/(LaTiO_3)_3TiO_2$

The unit cell of the superlattice consists of a single VO_2 layer at the center of the well surrounded by two BaO layers as illustrated in Fig. 8.2. Because of the smaller p-d energy separation in bulk BVO compared to LTO, this material combination should form a quantum well centered on the VO_2 layer, assuming that the p-bands of the two materials are nearly aligned at the

97
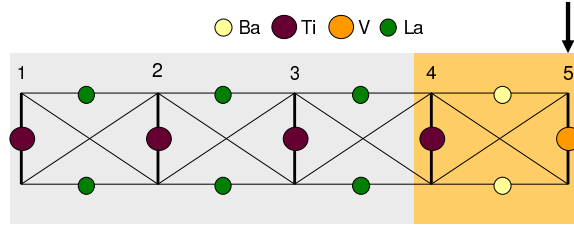
Figure 8.2: (color online) Half of the inversion symmetric unit cell. The quantum well consists of two layers of BaO and a monolayer of VO_2 and is embedded in bulk $LaTiO_3$. The light-orange shadowed region indicating the narrow active region in which the electronic interface reconstruction (EIR) driven by the polar discontinuity takes place. Oxygen atoms are located at the intersections of the checkered lines and form octahedra around the Ti and V atoms. The numbers specify labels for different layers. The downward arrow indicates the location of the VO_2 inversion plane.

interface. In our superlattice the BVO quantum well layers are separated by 7 TiO_2 transition metal layers, each in turn separated by a LaO layer. Half of the inversion symmetric unit cell is shown in Fig. 8.2 in which the VO_2 inversion plane is marked by an arrow. Ti and V in bulk LTO and BVO respectively both have nominal valence charge d^1. In the quantum well structure we study here the number of LaO layers, which are positively charged in the polar LTO crystal, is one smaller than the number of TiO_2 layers. It follows that the total d charge per transition metal summed over all layers is expected to be reduced by 1. Unless the inversion symmetry is broken we should expect the missing d-charge to be symmetrically distributed around the quantum well center. The simplified assumptions of the previous section would divide this valence change between the two TiO_2 layers adjacent to the quantum well.

Fig. 8.3 shows the d-projected DOS at a Ti site and a V site in each

TiO$_2$ and VO$_2$ plane. The states below -1.5 eV are the $d-p$-bonding states between Ti, V atoms and their neighboring oxygens which have dominant p-character, whereas the states near the Fermi level (E = E$_F$) are the antibonding states which have dominant d-character. As we move through the superlattice from TO$_2$ barrier layers to the VO$_2$ we see the DOS evolve from the typical bulk LTO form (layers 1 to 3) to a new form near the heterojunction. In particular, there is a large depletion away from atomic-like d^1-charges in layer 4. The electronic reconstruction which accommodates the band offsets and the polarity discontinuity is evident very strongly in the layers 5 and 6 surrounding the quantum-well layer 4 (layer 6 is not shown in Fig. 8.3 to avoid redundancies because of the inversion symmetry of the system). We also observe that the p-d separation is maintained at the VO$_2$ layer as expected after the electronic reconstruction. The total electron transfer from layer 4 is larger than in the *ideal conjecture*, as expected, and more remote layers participate in the transfer because of oxygen mediated coherence between transition metal orbitals centered on different layers.

Most Mott insulators are orbitally and magnetically ordered. In order to gain some insight into the way in which the magnetic order is disturbed by the quantum well structure, we plot in Fig. 8.4 the spin-resolved d-projected DOS in all layers. In our calculations we find G-type antiferromagnetic (G-AFM) order in which neighboring transition metals ions have opposite spins both within and between layers for the bulk like TiO$_2$ layers. (layers 1, 2, 3 in Fig. 8.4). Layer 4 on the other hand has an overall magnetic moment
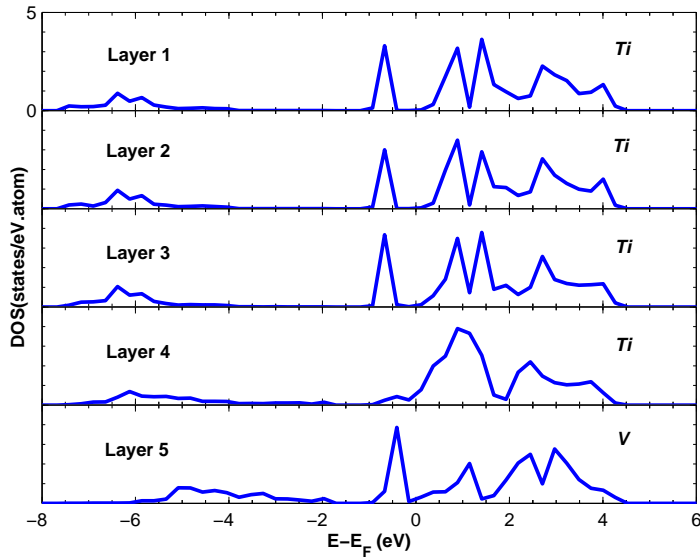
Figure 8.3: Layer-resolved d-projected density of states at Ti and V sites versus energy. The layer labeling is defined in Fig. 8.2.

of around 0.1 μ_B per Ti ion indicating a ferromagnetic layer. Because of the electronic interface reconstruction (EIR), the magnetic order in the VO$_2$ plane changes from AFM to ferromagnetic. The projected moments on each Ti ions in the AFM bulk-like TiO$_2$ layers is calculated to be 0.74 μ_B inside the Ti ionic radius which is fixed in our calculation by the pseudopotential construction. We believe that by enlarging the Ti ionic radius, we can get d-orbital integrated moments close to the 1 μ_B value expected for d^1 Mott insulators. Note that ferromagnetism is induced in the VO$_2$ layer by the two adjacent strongly depopulated and ferromagnetic TiO$_2$ layers.

Fig. 8.5 shows the superlattice band structure along high symmetry directions in the Brillouin zone. The bands (five majority (red) spin bands

and five minority (blue) spin bands), which lie far below the E_F (in the energy range between between -1 eV and -0.6 eV), can be identified as bulk LTO d-charge character bands by comparing with Fig. 8.4 and calculating band-decomposed local charge density contributions. In the supercell, we have 5 bulk TiO_2 layers (layer 1, 2, 3, 7, 8) in our superlattice corresponding in the antiferromagnetic state to 10 full bands (5 spin-up and 5 spin-down). Therefore, there should be ten full bulk like LTO d-bands, identified by the solid circle, in Fig. 8.5. Two full majority spin bands and one full minority spin band (near -1 eV) highlighted by two dashed circles are associated with the d-charges in the VO_2 layers. The two majority bands close to the interface states in energy and are hybridized along the layer-growth direction and delocalized (This interpretation has been verified by separating the charge density contribution of those bands) . Because of this hybridization, the total d-charges ($2.4053 \, e^-$) at the V sites is smaller than the $3 \, e^-$ value which would be implied by a local interpretation of the band structure. It can in general be misleading to estimate the number of charges at transition metal ions by counting the number of reconstructed bands with a particular dominant orbital character. The three partially full bands (one minority band and two majority bands) near the fermi surface E_F are the bands responsible for the charge depletion at the TiO_2 layers adjacent to the quantum well (layer 4 and 6). The momentum k_z dependence of the electronic states is shown in the right panel of Fig. 8.5 (from momentum $(0 , 0, 0)$ at Γ to $(0, 0, k_z)$ at Z). It shows that, the states at the Fermi energy form a two-dimensional electron gas centered on three layers,

101
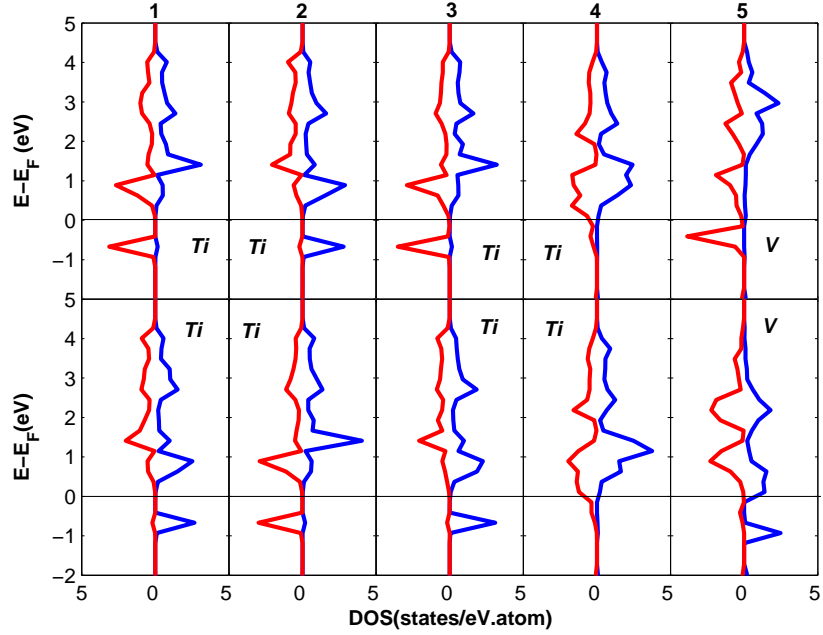
Figure 8.4: Spin and layer resolved densities-of-states versus energy. The labels on top are layer labels as in Fig. 8.2. Since we allow G-type AFM order in the barrier material, there are two distinct transition metal atoms in each layer. The DOS for majority spins and minority spins are represented by red and blue lines respectively and the Fermi level is marked with a horizontal dark line at $E = E_F$.

the active region. Notice that there also appears a flat band between M and X, which corresponds to the direction away from the bonding direction between Ti and O atoms in charge depleting the TiO_2 layers, due to the fact there is negligible tunneling of electrons along this direction. The two dimensional system is metallic in this case and has three partially filled bands.

Since we have discussed the local potential for the electron in case (a) in Fig. 8.1 based on qualitative model in which we assume the charges at each
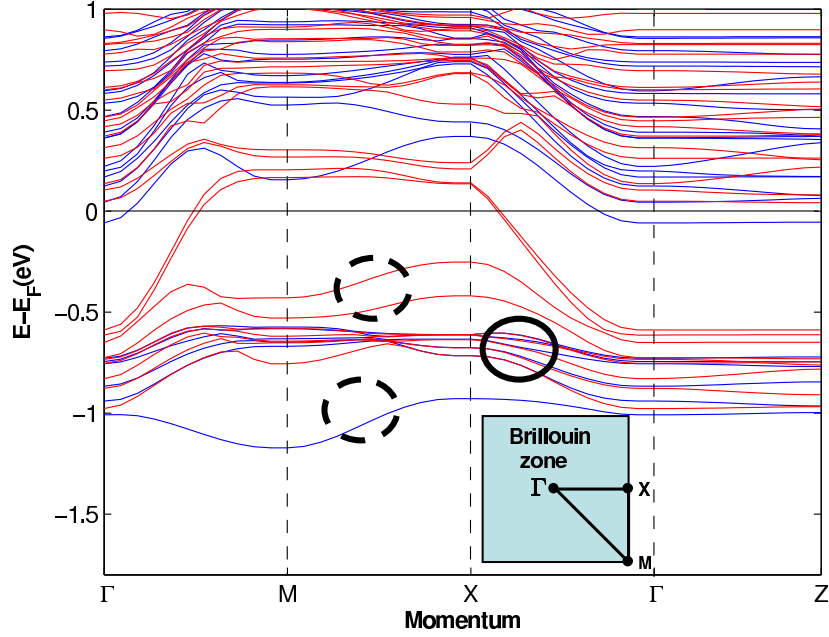
Figure 8.5: Spin-resolved band structure at the Brillouin zone. The horizontal axis represents superlattice crystal momentum. The red solid lines represents the majority-spin bands and the blue ones are the minority-spin bands. The momentum dependence along the layer direction k_z is indicated in the region between the Γ and Z points. The full circle marks the d^1 bands for Ti atoms in LTO bulk states. The dashed circles represents the d bands for V atoms in VO_2. The bands associated with EIR are flat along k_z demonstrating their quasi-two-dimensional character. The shadowed blue square represents the projection of the superlattice Brillouin zone in the plane of the quantum well.

layer are concentrated in a single layer along the layer direction, we would like to examine how the the crude model prediction compares with actual DFT predictions. In Fig. 8.6, the DFT plane-averaged Hartree potential for the electrons is shown. First TiO_2 layer starts at $z = 0$ and layers repeat with a spatial period of 3.96 $\mathring{A}$ and with the central layer ($z = 15.84$ $\mathring{A}$) of the supercell substituted by the VO_2 layer. First LaO layer is located at $z = 1.98$ $\mathring{A}$ and these layers repeat with a period of 3.96 $\mathring{A}$ except that the two layers surrounding the central VO_2 layer correspond instead to BaO layers. By inspecting the variation of the local minima in the potential, we can see that the qualitative behavior anticipated in case (a) in Fig. (8.1) is valid, as shown by the black-dashed line. The electric field in the qualitative model should be considered as a macroscopically averaged electric field between potential minima in the microscopic calculations. Notice that the potential of the VO_2 layer is somewhat lower than anticipated.

In Fig. 8.7, we show the linear electron number density $\lambda(z) \equiv 0.5 \int \rho(x, y, z) dx dy$ along the layer-growth direction. The charge number spatial distribution $\rho(x, y, z)$ is normalized per transverse unit cell which is doubled because of the system's antiferromagnetic order, and includes the total number of electrons contributed by the d-bands between with energies up to 1.5 eV below the Fermi level. (See Fig. 8.5.) The factor 0.5 is used to convert the normalization to d-electrons per transition metal ion, to facilitate comparison with the qualitative picture. The dashed lines represent the boundaries for the transition-metal oxide layers used in this electron number construction. The

104

area under the curve $\lambda(z)$ represent the total number of electrons from all d-bands. We see an apparent charge depletion at the TiO$_2$ layers centered at $z = 11.88$ Å and $z = 19.8$ Å along with large charge accumulation at the VO$_2$ layer. There is only minor charge depletion at second-nearest TiO$_2$ layers ($z = 7.92$ Å and $z = 23.76$ Å) away from VO$_2$ layer. The total charges from the d-bands, 7 e^-, is obtained by adding the number of electrons at each layers and agrees with the qualitative predictions for case (a). The number of electrons in the depleted TiO$_2$ layers is 0.3793. The other layers have small deviation from one electron. The calculation shows a clear deviation from ideal conjecture we made for this case and is closer to the *realistic conjecture*. In general, the charges in the well are mainly transferred from the adjacent TiO$_2$ layers but there is also a minor contribution from other TiO$_2$ layers as shown from the number of electrons in each layers.

Case B : (BaVO$_3$)$_3$/(LaO)$_2$TiO$_2$/(BaVO$_3$)$_3$VO$_2$

In this section, we consider the quantum well structure shown in case (b). In this case, the number of LaO layers, which are positively charged in the polar LTO crystal, is greater than the number of TiO$_2$ layer by one. It follows that the total d-electrons per transition-metal summed over all layers is expected to be increased by 1. Unless the inversion symmetry is broken we should expect the extra d-charge to be symmetrically distributed around the quantum well center.

Fig. 8.8 shows the d-projected DOS at a Ti site and a V site in each
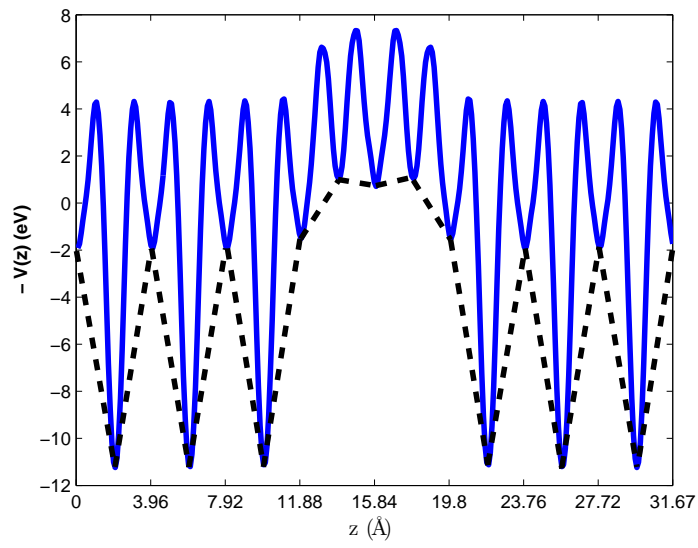
Figure 8.6: Plane averaged Hartree potential along the layer-growth direction z. The blue curve represents the Hartree potential experienced by electrons $-eV(z)$. The dashed line indicates the net potential variation between charge-concentrations centers in each layers.
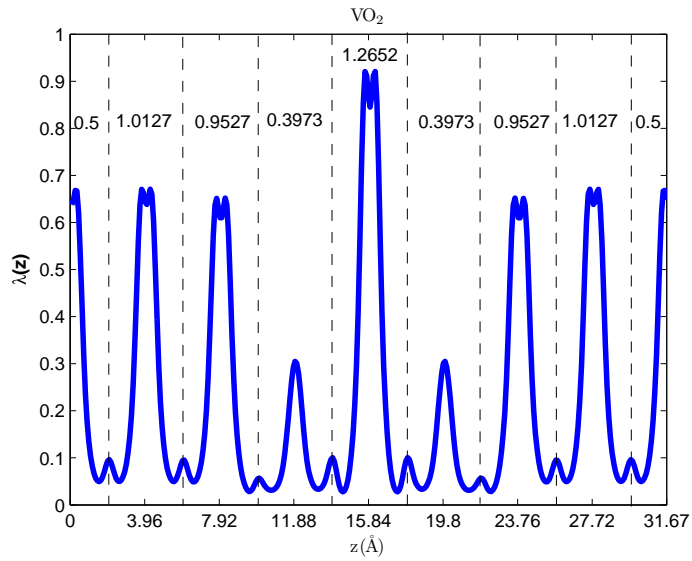
Figure 8.7: Linear electron number density $\lambda(z)$ along layer-growth direction z. The dashed lines represent the boundaries used for the partitioning of density into contributions from different layers. The total number of electrons in each layer contributed by the d-character bands in Fig. 8.5 is indicated by the numerical values between dashed lines. In this case, the total number of electrons in the supercell is seven.
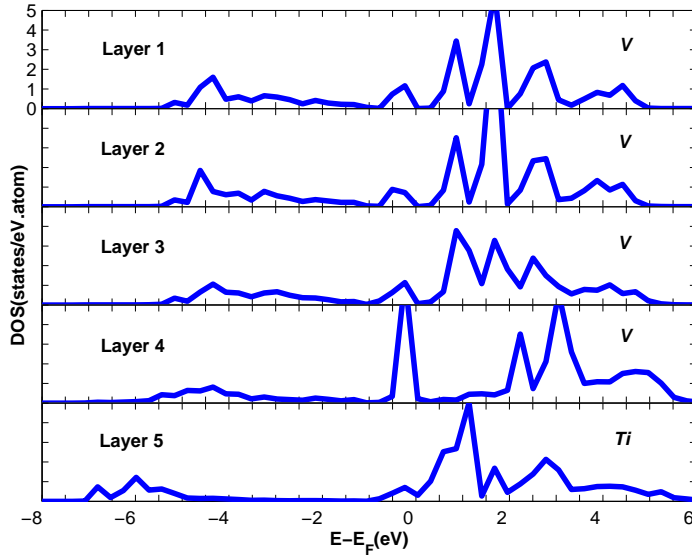
Figure 8.8: Layer-resolved d-projected density of states at Ti and V sites versus energy.

TO$_2$ and VO$_2$ plane. The states below -1 eV are the $p-d$-bonding states between the transition-metal atoms (Ti, V) and the p orbitals of the neighboring oxygens and have dominant p character. The states near the Fermi level (E $=$ E$_F$), on the other hand, have dominant d-character. As we move through the superlattice from the VO$_2$ layers to the TiO$_2$ barrier layer we see the DOS evolve from the typical bulk BVO layer form (layers 1 to 3) to a new form near the heterojunction. In particular, we see a strong peak in DOS in layer 4 near the Fermi energy E_F with 1.6 e^- per V ion in agreement with our conjectures. As far as magnetic order is concerned (Fig. 8.9), we find G-type AFM order in which neighboring transition metals ions have opposite spins both within and between layers for the bulk like VO$_2$ layers (layers 1 and 2). The magnetic

108

orders in layer 3 and 5 are reconstructed to be ferromagnetic with the magnetic moment 0.9755 μ_B per V ion and the moment 0.4750 μ_B per Ti respectively. The magnetic order in layer 4 is ferrimagnetic with a net magnetic moment 0.2170 μ_B. In the corresponding band structure illustrated in Fig. 8.10, we identify three partially filled two-dimensional bands that cross the Fermi level, and sixteen full d-bands. These bands accommodate 9 d-electrons obtained by taking the average d-charges per transition metal ion and summing the charges of all the layers, as illustrated in Fig. 8.12 discussed below. The two majority spin partially-filled bands, and the single minority-spin partially-filled band, are responsible for the extra charge at V sites in layer 4 and 6 as shown in Fig. 8.9. The three full minority-spin bands, which are lower in energy than the partially-filled minority-spin band but closer to the Fermi level than other full minority-spin bands mainly contribute to minority-spin charge concentrated in layers 4, 5, and 6. The wave functions for those bands are strongly hybridized within those layers. The lowest majority-spin band in Fig. 8.10 is mainly of V character in layer 4 but lower in energy due to the more attractive local potential at this site. The peak of the DOS for the minority spin at the V site seems to shift higher toward the Fermi energy than expected. This is due to the fact those states are strongly hybridized with the states at the Ti sites which are shifted toward higher energy, an effect not included in the qualitative analysis. (See the potential profile of the realistic conjecture of case (b) in Fig. 8.1). Other full bands are responsible for BVO bulk states away from the region in which the electronic interface reconstruction occurs.
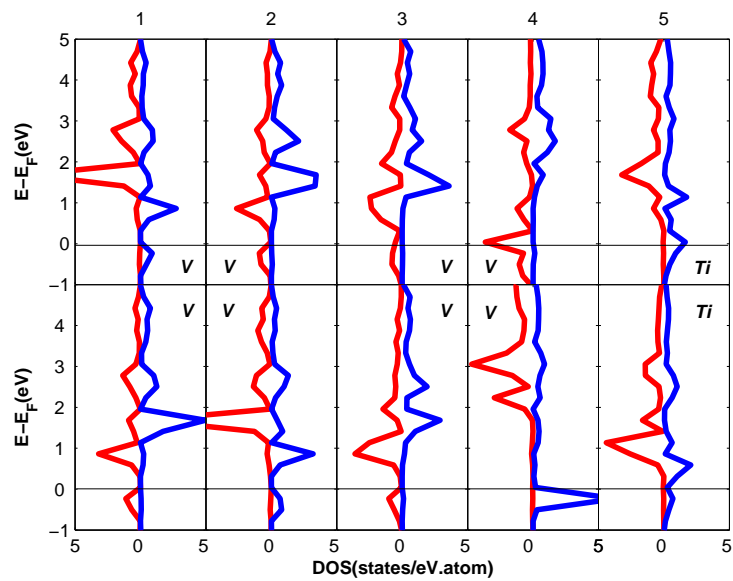
Figure 8.9: Spin and layer resolved densities-of-states versus energy. The labels on top are the layer labels indicated in Fig. 8.2. Since we allow G-type AFM order in the barrier material, there are two distinct transition-metal ions in each layer. The DOS for majority spins and minority spins are represented by red and blue lines respectively.
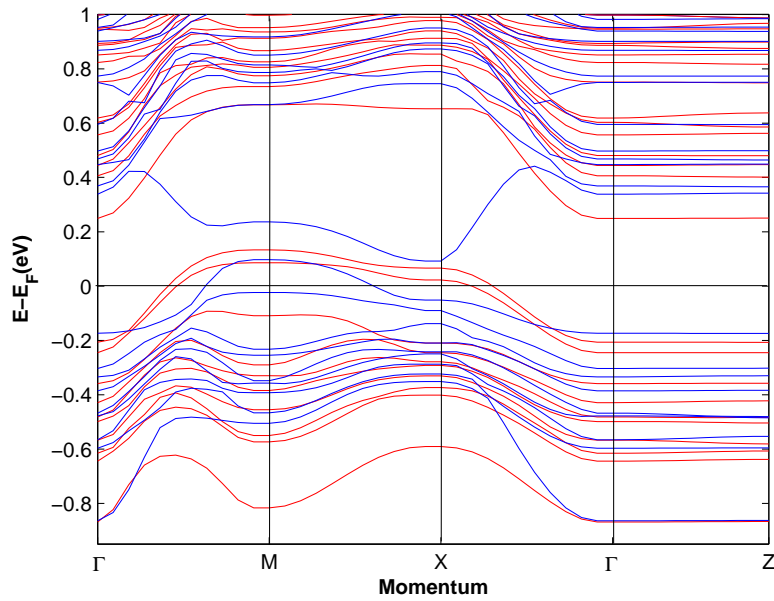
Figure 8.10: Spin-resolved band structure. The horizontal axis represents superlattice crystal momentum. The red solid lines represent the majority-spin bands while the blue lines represent minority-spin bands. The momentum dependence along the layer direction k_z is captured in the region between the Γ and Z points. The three partially occupied bands associated with EIR are flat along k_z, demonstrating their quasi-two-dimensional character.

In Fig. 8.11, we plot plane-averaged Hartree potentials. The first layer starts with VO_2 at $z = 0$. Transition metal layers repeat with a spatial period of 3.96 $\mathring{A}$ with the center ($z = 15.84$ $\mathring{A}$) layer occupied by TiO_2 layer. At $z = 1.98$ $\mathring{A}$, the first BaO layer starts and repeats also at a period of 3.96 $\mathring{A}$; the local minima closest to TiO_2 correspond instead to LaO layers. By inspecting the local minima in the Hartree potential, we can see that the DFT calculations largely verify the scenario of case (b) in Fig. (8.1) except that the dashed line wiggles in the region of bulk BVO. The wiggling may due to the slight difference of the strength of ionic bonding between Ba-O and V-O along the layer direction, which causes the small dipole modification of charge distribution in BVO ionized layers.

In Fig. 8.12, we show the corresponding electron linear number density $\lambda(z) \equiv 0.5 \int \rho(x, y, z) dx dy$ along the layer-growth direction. This charge number spatial distribution $\rho(x, y, z)$ include the total charges contributed from the bands between 0 and - 0.9 eV with respect to Fermi level in Fig. 8.10. We see an apparent charge accumulation (1.5144 e^-) at the TiO_2 layers centered at $z = 11.88$ $\mathring{A}$ and $z = 19.8$ $\mathring{A}$ along with much less charge (0.6295 e^-) at the TiO_2 layer. Remote transition metal layers have small deviations from a d^1 valence. The total amount of charges from the d-bands is 9 e^- by adding the charges at each layer in agreement with our prediction in case (b). The calculation shows small deviations from the ideal conjecture we made for this case and almost the realistic conjecture. In general, the charges in the well are transferred from the TiO_2 layer to adjacent VO_2 layers as discussed in section
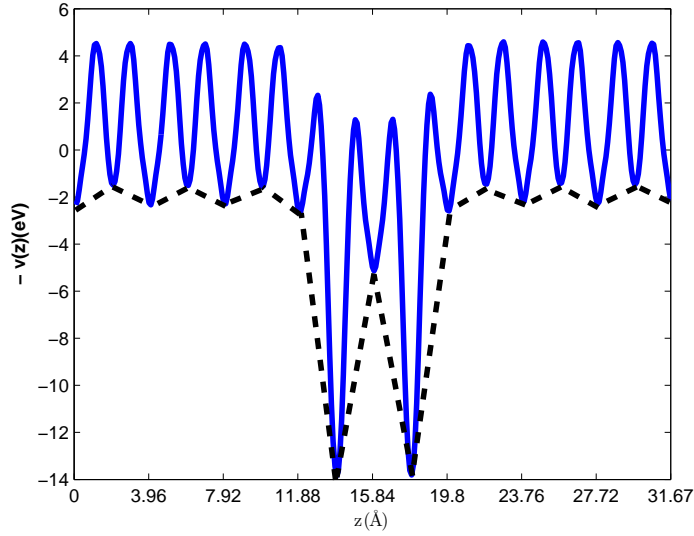
Figure 8.11: Plane averaged Hartree potential along the layer-growth direction z. The solid dashed line indicates the net potential variation between charge-concentrated centers at each layer.

II.

8.5   Summary and Discussion

In this paper we have explored some possibilities for the realization of artificial two-dimensional electron systems by growing quantum wells consisting of a few atomic layers of one layered oxide surrounded by another material. In particular we consider systems which involve heterojunctions between polar insulating perovskites like LTO and nonpolar insulating perovskites like BVO. Perovskites can be viewed as consisting of alternating AO and BO_2 layers where B is a transition metal. The main idea of this paper is that inversion

113
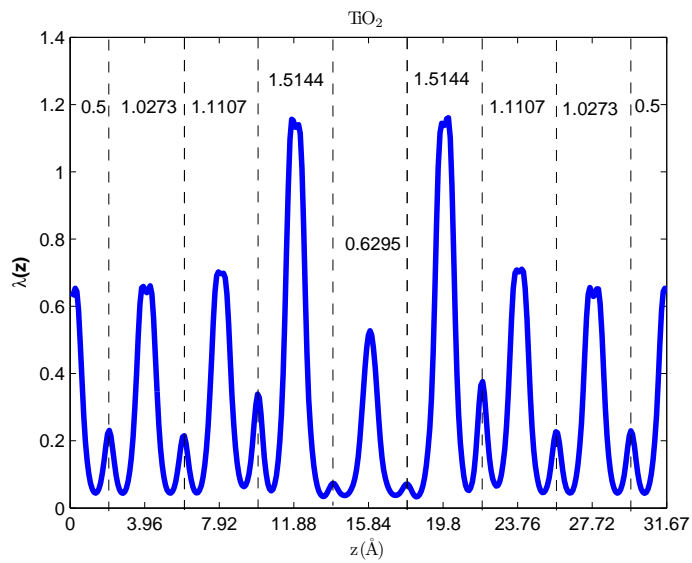
Figure 8.12: Linear electron number density $\lambda(z)$ along layer-growth direction z. The dashed lines represent the boundaries between different layers used in constructing the layer decomposition of this charge density. The numerical numbers between dashed lines in each layers are the total number of electrons from d-derivative bands in Fig. 8.10. In this case, the total number of electrons is nine.

symmetric quantum wells will necessarily have a different number of AO and BO$_2$ layers, and that this will necessarily lead to an electronic reconstruction which induces two-dimensional electron systems near the quantum well when one material is polar and one is nonpolar. Four different cases can be identified, in which the quantum well material is either polar or non-polar and in which it either has an excess AO layer or an excess BO$_2$ layer. The excess layers induce either a unit increase or a unit decrease in the total d-orbital occupancy per transition metal site when summed over all layers. This charge must be localized close to the quantum well to avoid large band shifts due to polarization driven electrostatic potentials. As long as inversion symmetry around the quantum well center is not-broken spontaneously, half of this charge must appear on each half of the quantum well center. Because of the strong-correlation character of the oxide electronic structure, these charges will tend to be localized in half-filled LSDA+U bands which are weakly hybridized so that both cross the Fermi energy.

We have tested and elaborated on this qualitative picture of the electronic structure of polar-nonpolar heterojunction quantum wells in perovskites by performing self-consistent LSDA+U electronic structure calculations for a representative system composed of BVO and LTO without any atomic relaxation at the interface. The LSDA+U calculations capture the interplay between long range polar electrostatic energy and local physics driven by energetic offsets between different transition metal ions and by $p - d$ hybridization. We find that in the two cases we have examined one additional two-dimensional

bands is induced by the energetic offsets. In all cases the quantum well structure creates a two-dimensional metal inside a three dimensional Mott insulator, and alters the character of the magnetic order. The reconstructed magnetic order is ferromagnetic in the active well region and antiferromagnetic in bulk region. The appearance of two-dimensional ferromagnetism in intimate exchange contact with antiferromagnetism is intriguing from the point of view of spintronics.

Because of the complexity of oxide materials, our calculation should be viewed as an exploration of possibilities rather than as predictive in any detailed sense. Among the many sources of uncertainty, the Hubbard U interaction used in our LSDA+U is a phenomenological parameter for which we have chosen a standard bulk values. This value should likely be renormalized near the quantum well. More challenging to account for is the role of inevitable lattice distortions, oxygen stoichiometry variations, and other defects near the interfaces. The interfaces between the thin film oxide and the substrate on which it is grown can also play a complicating role if either the barrier material or the substrate is polar. For a few cases we have explored the influence of lattice distortion effects by allowing the atoms to relax along the layer growth direction in the active region, maintaining U_V=U_{Ti}= 3.2 eV as before. What do we find is that the amount of charge transfer to or from particular layers and the details of the magnetic orders are highly sensitive to ionic relaxation. These complications make the accurate prediction of the electronic reconstruction and the associated magnetic order highly nontrivial.

Further progress in understanding detailed properties of the two-dimensional electron systems we envision which almost certainly require inputs from experiments. The microscopic calculations reported on here can be used as guidance in constructing phenomenological models which can be fit to any data which might emerge from future work. The present paper has addressed d^1 transition metal systems. Considerations similar to those explained here also apply to transition-metal oxides with heavy transition metal elements (Cu, Ni) in which the t_{2g} bands are fully occupied far below the Fermi level, and low-energy excitations are expressed within the e_g bands.

Chapter 9

Summary

In this thesis, we have introduced the applications of many-body physics in fermions and bosons. For bosons, we apply the mean field theory with Gaussian fluctuations (Mean field + RPA) based on Boson coherent state formulation to study vortex dynamics. This approach can be also used to any symmetry breaking phases such as magnetism and superconductivity. For interacting Fermions, density functional theory is one of the powerful and easy way to address the physics of interacting fermions. The DFT picture is exact for ground state properties but it is limited by the approximation employed in the application of the theory. Therefore, searching for the correct form of the functional by other methods(such as quantum Monte Carlo, exact diagonization) has been the active research topics in physics, chemistry , and material sciences.

In the first part of the thesis, we introduce the concepts of Bose Einstein condensation characterized by macroscopic wave function and show the existence of the vortex phases are the direct consequences of the BEC. Then we ask if treating vortices as quantum objects is a reasonable proposal which is discussed in chapter 5 extensively. We derive an effective action for the

vortex translational zero modes of a superfluid by integrating out environmental modes which include phase and density fluctuations of the condensate. When the quantum dynamics of the fluctuations are treated as frozen with negligible Berry phases in adiabatic limit, we confirm the occurrence of vortex Magnus force and adiabatic vortex mass due to compressibility of superfluids in agreement with earlier studies. In addition, we also show the results beyond adiabatic limit in which the quantum dissipative action can be derived and solved analytically. We show that the adiabatic approximation is only valid in a neutral superfluid system with radius R and coherence length ξ when the condition $R \gg \xi$ is satisfied. Furthermore, we also build a numerical discrete model based on discrete mean field Gross-Pitaevskii equation and quantum fluctuations to show the collective vortex cyclotron resonance peaks in the imaginary part of the vortex position-position correlation function. It is demonstrated that well-defined cyclotron peaks can be sustained in the limit $R \gg \xi$ in agreement with our theoretical predictions. With the mapping between discrete Gross-Pitaevskii equation and bosonic single-band Hubbard model, we propose that the adiabatic vortex dynamics can be realized by tuning the ratio between tunneling energy J and on-site interaction energy U such that $UN_a \gg J$ in cold atom systems with optical lattices, in which N_a is the total number of bosonic atoms.

In the second part of the thesis, we switch to the strongly correlated electrons in transitional metal oxides. We first introduce why those materials are important and what is the qualitatively correct functional to describe

the physics in which normal band picture of electrons fails. Then we discuss how the density functional theory under LDA approximation can be modified to treat the system with Hubbard U interaction to describe Mott-insulating physics favoring orbital polarizations. In chapter 8, we apply the DFT to study how to create a low dimensional system in the superlattices made of transition metal oxides. We address the electronic structure of quantum wells in polar-nonpolar oxide heterojunction systems focusing on the case of non-polar $BaVO_3$ wells surrounded by polar $LaTiO_3$ barriers. We conclude that a variety of quite different two-dimensional electron systems can occur at interfaces between insulating materials depending on band line-ups and on the geometrical arrangement of polarity discontinuities.

In conclusion, the many-body physics in complex condensed matters are rich such as broken symmetry phases and excitations, or strongly correlated phases which cannot be described by local order parameters and the interplay between different degree of freedoms. The understanding of emergent phenomena in complex materials are ahead of us to explore.

Appendices

Appendix A

GP equation from wave function formulation

Here we show how the Gross-Pitaevskii equation can be equivalently derived from Hatree approximation from the variational wave function $\Psi(\mathbf{r}_1, \mathbf{r}_2, ...\mathbf{r}_N)$. Assume N bosons will all condense into a single particle state $\phi(\mathbf{r}_1), \phi(\mathbf{r}_2), ...\phi(\mathbf{r}_N)$. Therefore, the normalized variational wave function $\phi(\mathbf{r}_1), \phi(\mathbf{r}_2), ...\phi(\mathbf{r_N})$ is given as the symmetrized product states :

$$\Psi(\mathbf{r}_1, \mathbf{r}_2, ...\mathbf{r}_N) = \Pi_{i=1}^{N}\phi(\mathbf{r}_i). \tag{A.1}$$

The Hamiltonian for the dilute gases in spatial representation can be written as

$$H = H_1 + H_2 = \sum_i [\frac{\hbar^2 \nabla_i^2}{2m} + V(\mathbf{r}_i)] + g \sum_{i<j} \delta(\mathbf{r}_i - \mathbf{r}_j), \tag{A.2}$$

where H_1 is the one-body term and H_2 is the two-body term for the Hamiltonian.

Now we would like to evaluate the energy of the system $\langle\Psi|H|\Psi\rangle$. The one body term for the Hamiltonian $\langle\Psi|H_1|\Psi\rangle$ can be written as

$$\langle\Psi|H_1|\Psi\rangle = \sum_{i=1}^{N} \int d\mathbf{r}_1 d\mathbf{r}_2 ... d\mathbf{r}_N \Pi_j \phi^*(\mathbf{r}_i)[H_{1i}]\Pi_k \phi(\mathbf{r}_k), \tag{A.3}$$

$$= \sum_{i=1}^{N} \int d\mathbf{r}_i \phi^*(\mathbf{r}_i) H_{1i} \phi(\mathbf{r}_i) \int \Pi_{j\neq i} d\mathbf{r}_j \phi^*(\mathbf{r}_j)\phi(\mathbf{r}_j),$$

$$= \sum_{i=1}^{N} \int d\mathbf{r}_i \phi^*(\mathbf{r}_i) H_{1i} \phi(\mathbf{r}_i),$$

$$= N \int d\mathbf{r}_i \phi^*(\mathbf{r}_i) H_{1i} \phi(\mathbf{r}_i),$$

in which $H_{1i} = -\frac{\hbar^2}{2m}\nabla_i^2 + V(\mathbf{r}_i)$ can only act on $\phi(\mathbf{r}_i)$, the normalization $\int d\mathbf{r}_j |\phi(\mathbf{r}_j)|^2 = 1$ for any j is used.

The one body term for the Hamiltonian $\langle \Psi | H_2 | \Psi \rangle$ similarly can be written as

$$\langle \Psi | H_2 | \Psi \rangle = \frac{g}{2} \sum_{i \neq j} \int d\mathbf{r}_1 d\mathbf{r}_2 ... d\mathbf{r}_N \Pi_{k,l} \phi^*(\mathbf{r}_k) \phi(\mathbf{r}_l) \delta(\mathbf{r}_i - \mathbf{r}_j), \qquad (A.4)$$

$$= \frac{g}{2} \sum_{ij(i \neq j)} \int d\mathbf{r}_i d\mathbf{r}_j \delta(\mathbf{r}_i - \mathbf{r}_j) |\phi(\mathbf{r}_i)|^2 |\phi(\mathbf{r}_j)|^2 \int \Pi_{k(\neq i,j)} |\phi(\mathbf{r}_k)|^2,$$

$$= \frac{g}{2} \sum_{ij(i \neq j)} \int d\mathbf{r}_i |\phi(\mathbf{r}_i)|^4,$$

$$= \frac{g}{2} N(N-1) \int d\mathbf{r}_i |\phi(\mathbf{r}_i)|^4,$$

in which $\sum_{i,j(i \neq j)} = N(N-1)$ is used. Therefore, the energy of the state $\Psi(\mathbf{r}_1, \mathbf{r}_2, ...\mathbf{r}_N)$ is given by

$$E = N[\int d\mathbf{r} \phi^*(\mathbf{r})[-\frac{\hbar^2}{2m}\nabla^2 + V(\mathbf{r})]\phi(\mathbf{r}) + \frac{g}{2}(N-1)|\phi(\mathbf{r})|^4] \qquad (A.5)$$

where the dummy index $\mathbf{r}_i$ is replaced by $\mathbf{r}$.

The density $n(\mathbf{r})$ at point $\mathbf{r}$ due to the state $\Psi(\mathbf{r}_1, \mathbf{r}_2, ...\mathbf{r}_N)$ is equal to

$$n(\mathbf{r}) = \int d\mathbf{r}_1 ... d\mathbf{r}_n |\Psi|^2 \sum_i \delta(\mathbf{r} - \mathbf{r}_i), \qquad (A.6)$$

123

$$= \sum_i |\phi(\mathbf{r})|^2 \int \Pi_{j(j\neq i)} d\mathbf{r}_j |\phi(\mathbf{r}_j)|^2 = N|\phi(\mathbf{r})|^2$$

where $\int \Pi_{j(j\neq i)} d\mathbf{r}_j |\phi(\mathbf{r}_j)|^2 = 1$ due to normalization of the wave function ϕ. We can therefore identify the condensate wave function $\Psi(\mathbf{r})$ as

$$\Psi(\mathbf{r}) = \sqrt{N}\phi(\mathbf{r}). \tag{A.7}$$

As a result, the energy in terms of condensate wave function $\Psi(\mathbf{r})$ when $N >> 1$ is given by

$$E[\Psi(\mathbf{r}), \Psi^*(\mathbf{r})] = \int d\mathbf{r}\Psi^*(\mathbf{r})[-\frac{\hbar^2}{2m}\nabla^2 + V(\mathbf{r})]\Psi(\mathbf{r}) + \frac{g}{2}|\Psi(\mathbf{r})|^4. \tag{A.8}$$

Now we want to find the condensate wave function by the minimization of the energy functional $E[\Psi(\mathbf{r}), \Psi^*(\mathbf{r})]$ by varying the fields $\Psi(\mathbf{r}), \Psi^*(\mathbf{r})$ under the constraint that the condensed particle are conserved $\int d\mathbf{r}|\Psi(\mathbf{r})|^2 = N$. This procedure is equivalent to $\delta(E - \mu N) = 0$ where the chemical potential μ is the Lagrange multiplier that ensures the constancy of condensate particle number. By variation with respect to $\Psi^*(\mathbf{r})$, we arrive at the time independent Gross-Pitaevskii equation:

$$-\frac{\hbar^2}{2m}\nabla^2\Psi(\mathbf{r}) + V(\mathbf{r})\Psi(\mathbf{r}) + g|\Psi(\mathbf{r})|^2\Psi(\mathbf{r}) = \mu\Psi(\mathbf{r}). \tag{A.9}$$

Appendix B

Boson coherent state and path integral

B.1 Coherent state

The construction of path integral is to segment the time evolution of a quantum (many-body)Hamiltonian into infinitesimal time slices and to absorb the quantum dynamical phases accumulated during the short-time propagation. Given that many-particle Hamiltonian are conveniently expressed in terms of creation/annihilation operators, it would be natural to search for eigenstates for these operators. This state exists and is called coherent state. After second thought, it turns out it is impossible to have an eigenstate for the creation operator in Fock space with different particle number because the minimum particle number will increase by one which cannot be proportional to original state to operate on. However, annihilation operators do possess eigenstates, known as the bosonic coherent state, which is defined as

$$|\phi> \equiv \exp\left[\sum_\alpha \phi_\alpha a_\alpha^\dagger\right]|0\rangle, \tag{B.1}$$

where $|0\rangle$ is the vacuum state for the particles and ϕ_α are complex numbers which means the probability amplitudes for particles to occupy state α. The bosonic coherent state satisfy the following important properties. First, co-

herent state is the eigenstate of the annihilation operator a_α

$$a_\alpha|\phi\rangle = \phi_\alpha|\phi\rangle, \tag{B.2}$$

which can be easily checked by expanding exponential operator and take advantage of the properties for the operators

$$a^\dagger|...., n_\alpha, ...\rangle = (n_\alpha+1)^{1/2}|...., n_\alpha+1, ...\rangle, a|...., n_\alpha, ...\rangle = n_\alpha^{1/2}|...., n_\alpha-1, ...\rangle. \tag{B.3}$$

Second, the overlap between two coherent states $\langle\phi|\phi'\rangle$ is

$$\langle\phi|\phi'\rangle = e^{\sum_\alpha \phi_\alpha^* \phi_\alpha'} \equiv e^{(\phi_\alpha|\phi_\alpha')}, \tag{B.4}$$

which can also be proved by using the definition eq. (B.2).

The third property is the closure relation in Fock space

$$\int \prod_\alpha \frac{d\phi_\alpha^* d\phi_\alpha}{2i\pi} e^{-(\phi_\alpha|\phi_\alpha)} |\phi\rangle\langle\phi| = 1, \tag{B.5}$$

as can be checked by sandwiching by the vacuum state $\langle 0|....|0\rangle$ in which $d[\phi^*]d[\phi] = \prod_\alpha \frac{d\phi_\alpha^* d\phi_\alpha}{2i\pi}$.

B.2 Action in imaginary time

From statistical physics, we know all the equilibrium properties can be obtained from grand-canonical partition function

$$Z = Tr[e^{-\beta(\hat{H}-\mu\hat{N})}], \tag{B.6}$$

where $\beta = 1/k_B T$ and μ is the chemical potential. The partition function Z in coherent state representation can be expressed as

$$Z = \int d[\phi^*] d[\phi] e^{-(\phi|\phi)} \langle \phi | e^{-\beta(\hat{H} - \mu \hat{N})} | \phi \rangle. \tag{B.7}$$

We observe that the operator $e^{-\beta(\hat{H} - \mu \hat{N})}$ is identical to the quantum mechanical evolution operator $U(t, 0) = e^{-i(\hat{H} - \mu \hat{N})t}/\hbar$ evaluated at the imaginary time $t = -i\hbar\beta$. Put it in another way, we thus want to evaluate the imaginary time evolution operator $U(-i\tau, 0)$ for $\tau = \hbar\beta$. To do so, we split the time interval $[0, \hbar\beta]$ into M steps, with $\tau_m = m\hbar\beta/M$ and $m = 0, 1, ..., M$. and the $\Delta\tau = \hbar\beta/M$. This is Feynman's path-integral formulation of the partition function. At each time step τ_m, we can insert the closure relation of the coherent state $\int d[\phi^*][d\phi] e^{-(\phi|\phi)} |\phi\rangle\langle\phi| = 1$. Therefore, the propagator in imaginary time $\langle \phi_M | e^{-\beta(\hat{H} - \mu \hat{N})} | \phi_0 \rangle$ is rewritten as

$$\langle \phi_M | e^{-\beta(\hat{H} - \mu \hat{N})} | \phi_0 \rangle = \int \prod_{m=1}^{M-1} d[\phi_m^*] d[\phi_m] e^{-(\phi_m|\phi_m)} \prod_{m=1}^{M} \langle \phi_m | e^{-\Delta\tau(\hat{H} - \mu \hat{N})/\hbar} | \phi_{m-1} \rangle. \tag{B.8}$$

We will look at the continuum limit $M \to \infty, \Delta\tau \to 0$, we only need to keep the lowest order term in $\Delta\tau$ for the propagator $\langle \phi_m | e^{-\Delta\tau(\hat{H} - \mu \hat{N})} | \phi_{m-1} \rangle$. Hence,

$$\langle \phi_m | e^{-\Delta\tau(\hat{H} - \mu \hat{N})} | \phi_{m-1} \rangle \simeq \langle \phi_m | \phi_{m-1} \rangle (1 - \Delta\tau H[\phi_m^*, \phi_{m-1}]/\hbar), \tag{B.9}$$

where $\langle \phi_m | \phi_{m-1} \rangle = e^{(\phi_m|\phi_{m-1})}$. Eq. (B.8) then can be manipulated into the suggestive form

$$\langle \phi_M | e^{-\beta(\hat{H} - \mu \hat{N})} | \phi_0 \rangle \tag{B.10}$$

$$= e^{(\phi_M|\phi_M)} \int \prod_{m=1}^{M-1} d[\phi_m^*] d[\phi_m] \exp\left\{ -\frac{1}{\hbar} \sum_{m=1}^{M} \Delta\tau \left(\hbar \frac{(\phi_m|\phi_m) - (\phi_m|\phi_{m-1})}{\Delta\tau} + H[\phi_m^*, \phi_{m-1}] \right) \right\}.$$

127

In the continuum limit $M \rightarrow \infty$, the partition function Z can be written as the functional

$$Z = \int_{\phi(0)=\phi_0}^{\phi(\hbar\beta)=\phi_0} d[\phi^*]d[\phi]e^{-S[\phi^*,\phi]/\hbar}, \tag{B.11}$$

where the so-called Euclidean action is

$$S[\phi^*, \phi] = \int_0^{\hbar\beta} d\tau \{(\phi^*(\tau)|\hbar\frac{\partial}{\partial\tau}|\phi(\tau)) + H[\phi^*(\tau), \phi(\tau)]\}. \tag{B.12}$$

Appendix C

Exchange-correlation hole

The energy of a many-body electronic system can be written in the following way:

$$E = T + V_{ext} + \frac{1}{2} \int \frac{n(\mathbf{r})n(\mathbf{r'})}{|\mathbf{r} - \mathbf{r'}|} d\mathbf{r} d\mathbf{r'} + E_{XC}, \qquad \text{(C.1)}$$

where E_{XC} is defined as the exchange and correlation energy

$$E_{XC} = \frac{1}{2} \int \frac{n(\mathbf{r})n(\mathbf{r'})}{|\mathbf{r} - \mathbf{r'}|} [g(\mathbf{r}, \mathbf{r'}) - 1] d\mathbf{r} d\mathbf{r'} \qquad \text{(C.2)}$$

where $g(\mathbf{r}, \mathbf{r'})$ is the pair correlation function which can be less than one in the presence of exchange and correlation. The exchange- correlation energy can be interpreted as the fact that the electron at position $\mathbf{r}$ with density $n(\mathbf{r})$ sense the exchange correlation hole at $\mathbf{r'}$ with density $n(\mathbf{r'})[|g(\mathbf{r}, \mathbf{r'}) - 1|]$ where $g(\mathbf{r}, \mathbf{r'}) - 1 < 0$. The behavior of the pair correlation function $g(\mathbf{r}, \mathbf{r'})$ can be shown in the following figure.
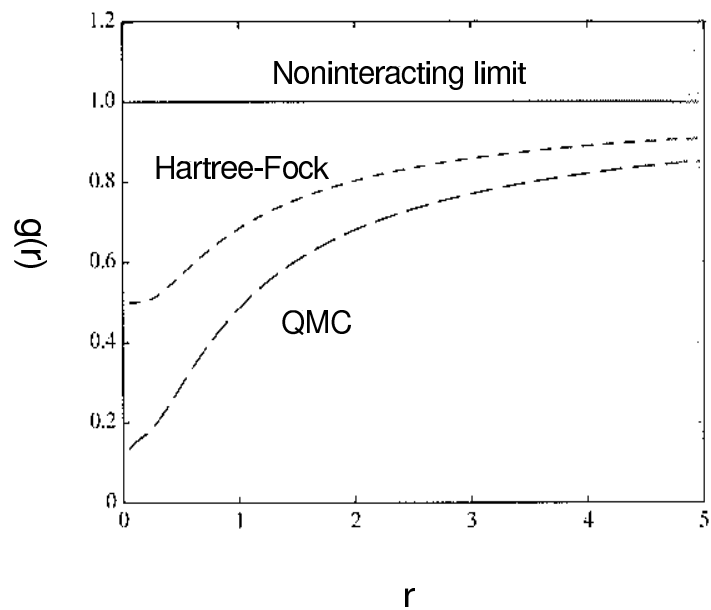
Figure C.1: The pair correlation function $g(r)$ as a function of distance r. The solid line represents the correlation for noninteracting electrons. The middle dashed line presents the correlation drops to 0.5 at the distance $r \longrightarrow 0$ due to the fact that only electrons with opposite spins are allowed. The bottom dashed line demonstrate the additional drops of pair correlation function because of correlation between electrons by Quantum Monte Carlo simulation. The figure is reproduced from the reference [74].

Bibliography

[1] Xiao-Gang Wen, Quantum Field Theory of Many-body Systems (Oxford University Press, 2004).

[2] M. Imada, A. Fujimori, and Y. Tokura, Rev. Mod. Phys. **70**, 1039 (1998).

[3] E.Dagotto, Science, **309**, 257 (2005).

[4] S. Raghu, Xiao-Liang Qi, C. Honerkamp, Shou-Cheng Zhang, Phys. Rev. Let. **100**, 156401 (2008).

[5] Xiao-Liang Qi, Taylor L. Hughes, Srinivas Raghu, Shou-Cheng Zhang, arXiv:0803.3614 (2008).

[6] C. J. Pethick and H. Smith, Bose Einstein Condensation in Dilute Gases (Cambridge University Press, 2008), Second edition, p. 17

[7] Edited by A. Griffin, D. W. Snoke, S. Stringari, Bose Einstein Condensation (Cambridge University Press, New York, 1995), pp.452 462

[8] P. W. Anderson, Rev. Mod. Phys. **38**, 298 (1966).

[9] A. J. Leggett and F. Sols, Found. Phys. **21**, 353 (1991).

[10] A. L. Fetter, Annals of Phys. **70**, 67 (1972).

[11] L. Onsager, Nuovo Cimento Suppl. **6**, 249 (1949).

[12] R.P. Feynman in *Progress in Low Temperature Physics*, edited by C.J. Gorter (North Holland, Amsterdam, 1955), Vol. 1, p. 17.

[13] M.H. Anderson, J.R. Ensher, M.R. Matthews, C.E. Wieman, and E.A. Cornell, Science **269**, 198 (1995).

[14] K. B. Davis, M.-O. Mewes, M.R. Andrews, N.J. van Druten, D.S. Durfee, D.M. Kurn, and W. Ketterle, Phys. Rev. Lett. **75**, 3969-3973 (1995).

[15] A. J. Leggett, Rev. Mod. Phys. **73**, 307-356 (2001).

[16] N. K. Wilkin and J. M. F. Gunn, Phys. Rev. Lett. **84**, 6 (2000); B. Paredes et al., ibid. **87**, 010402 (2001); J. Sinova et al., ibid. **89**, 030403 (2002).

[17] T.-L. Ho, Phys. Rev. Lett. **87**, 060403 (2001);

[18] I. Coddington, P. C. Haljan, P . Engels, V. Schweikhard, S. Tung, and E. A. Cornell, Phys. Rev. A. **70**, 063607 (2004).

[19] A. Fetter, arXiv:0801.2952, (2008)

[20] U. R. Fischer, P. O. Fedichev, and A. Recati , J. Phys. B **37**, 301 (2004).

[21] F. Dalfovo, S. Giorgini, L. P. Pitaevskii, and S. Stringari, Rev. Mod. Phys. 71, 463-512 (1999).

[22] M. Greiner, O. Mandel, T. Esslinger, T. W. Hnsch and I. Bloch, Nature (London) **415**, 39 (2002).

[23] O. Morsch and M. Oberthaler, Rev. Mod. Phys. 78, 179 (2006).

[24] K. W. Madison, F. Chevy, W. Wohlleben, and J. Dalibard, Phy. Rev. Lett. **84**, 806 (2000).

[25] J. R. Abo-Shaeer, C. Raman, J. M. Vogels, and W. Ketterle, Science **292**, 476 (2001).

[26] P. C. Haljan, I. Coddington, P. Engels, and E. A. Cornell, Phy. Rev. Lett. **87**, 210403 (2001).

[27] E. Hodby, G. Hechenblaikner, S. A. Hopkins, O. M. Maragò, and C. J. Foot, Phy. Rev. Lett. **88**, 010405 (2002).

[28] A. A. Burkov and E. Demler, Phys. Rev. Lett. **96**, 180406 (2006).

[29] P. Ao, Snapshots on vortex dynamics, cond-mat/0504222, 2005.

[30] N. B. Kopnin, Vortex dynamics, part IV, in Theory of Nonequilibrium Superconductivity (Clearendon Press, Oxford, 2001).

[31] P. Ao and X.-M.Zhu, Phy. Rev. B. **60**, 6850 (1999).

[32] Q. Niu, P. Ao, and D.J.Thouless, Phy. Rev. Lett. **72**, 1706 (1994).

[33] M. Flaig, U. R. Fischer, Phys. Rev. B **74**, 224503 (2006).

[34] P. Ao, and D. J. Thouless, Phy. Rev. Lett. **70**, 2158 (1993).

[35] P. Nozieres and J. Vinen, Phil. Mag. **14**, 667 (1966).

[36] C. Dasgupta and B.I. Halperin, Phys. Rev. Lett. 47, 1556 (1981); D.R. Nelson, Phys. Rev. Lett. 60, 1973 (1988); M.P.A. Fisher and D.-H. Lee, Phys. Rev. B 39, 2756 (1989); E. Simanek Inhomogeneous Superconductors: Granular and Quantum Effects (Oxford University Press 1994).

[37] R. J. Donnelly Quantized Vortices in Helium II (Cambridge University Press 1991).

[38] J. M. Duan, Phy. Rev. B. **48**, 333 (1993).

[39] D. J. Thouless and J. R. Anglin, Phys. Rev. Lett. **99**, 105301 (2007).

[40] J. L. Gervais and B. Sakita, Phy. Rev. B. **11**, 2943 (1975).

[41] H. B. Braun and D. Loss, Phy. Rev. B. **53**, 3237 (1996).

[42] B. P. Anderson, P. C. Haljan, C. E. Wieman, and E. A. Cornell, Phys. Rev. Lett. **85**, 2857 (2000).

[43] P. Hohenberg and W. Kohn, Phys. Rev. **136**, 864 (1964).

[44] R. G. Parr and W. Yang. Density Functional Theory of Atoms and Molecules (Oxford University Press, 1989).

[45] Perdew J P and Wang Y, Phys. Rev. B **45**, 13244(1992).

[46] D. M. Ceperley and B. J. Alder, Phys. Rev. Lett. 45, 566 (1980).

[47] I. V. Soloyev, P. H. Dederichs, V . I. Anisimov, Phys. Rev. B **50**, 16861 (1994).

[48] V. I. Anisimov, I. V. Solovyev, M. A. Korotin, M. T. Czyzyk, and G. A. Sawatzky, Phys. Rev. B **48**, 16929 (1993).

[49] A. I. Liechtenstein, V. I. Anisimov, and J. Zaanen, Phys. Rev. B **52**, R5467 (1995).

[50] S. L. Dudarev, G. A. Botton, S. Y. Savrasov, C. J. Humphreys, A. P. Sutton, Phys. Rev. B **57**, 1505 (1998).

[51] Woodward, P.M., Acta. Cryst., **B53**, 32-43 (1997).

[52] Crystallography and Chemistry of Perovskites, M. Johnsson and P. Lemmens, in Handbook of Magnetism and Advanced Magnetic Media, Ed. H. Kronmller, John Wiley and Sons, New York, (2006), cond-mat/0506606.

[53] Anthony. R. West, Basic Solid State Chemistry, J.W. and D. Ltd, 55-59;364-366, (1999)

[54] Patrick A. Lee, Naoto Nagaosa, and Xiao-Gang Wen, Rev. Mod. Phys. **78**, 17 (2006).

[55] A. P. Ramirez, J. Phys.: Condens. Matter **9**, 8171-8199 (1997).

[56] A. Ohtomo, D.A. Muller, J.L. Grazul and H.Y. Hwang, Nature **419**, 6905 (2002); A. Ohtomo and H.Y. Hwang, Nature **427**, 423 (2004); H.Y. Hwang, MRS Bulliten **31**, 28 (2006).

[57] N. Reyren , S. Thiel , A. D. Caviglia , L. Fitting Kourkoutis , G. Hammerl , C. Richter , C. W. Schneider , T. Kopp, A.-S. Retschi , D. Jaccard , M. Gabay , D. A. Muller , J.-M. Triscone and J. Mannhart , Science **317**, 1196 (2007).

[58] A. Brinkman , M. Huijben , M. Van Zalk , J. Huijben , U. Zeitler , J. C. Maan , W. G. Van der Wiel , G. Rijnders , D. H. A. Blank and H. Hilgenkamp , Nature Mat. **6**, 493 (2007).

[59] C. H. Ahn, A. Bhattacharya, M. Di Ventra, J. N. Eckstein, C. Daniel Frisbie, M. E. Gershenson, A. M. Goldman, I. H. Inoue, J. Mannhart, Andrew J. Millis, Alberto F. Morpurgo and Douglas Natelson, Rev. Mod. Phys. **78**, 1186 (2006).

[60] Satoshi Okamoto, Andrew J. Millis, and Nicola A. Spaldin, Phys. Rev. Lett. 97. 056802 (2006).

[61] Rossitza Pentcheva and Warren E. Pickett, Phy. Rev. Lett. **99**, 016802 (2007).

[62] W.-C. Lee, A.H. MacDonald, Phys. Rev. B 74, 075106 (2006). ; Phys. Rev. B **76**, 075339 (2007).

136

[63] S. Altieri, L.H. Tjeng, F.C. Voogt, T. Hibma and G.A. Sawatzky, Phys. Rev. B **59** R2517 (1999).; J. van den Brink and G.A. Sawatzky, Europhys. Lett. **50** 447 (2000).

[64] Hyo-Shin Ahn, Do Duc Guong, Jaichan Lee, and Seungwu Han, J. Korean Phy. Soc. 49, 1536 (2006).

[65] M. Cwik, T. Lorenz, J. Baier, R. üller, G. André, F. Bourée, F. Lichtenberg, A. Freimuth, R. Schmitz, E. Müller-Hartmann and M. Braden, Phys. Rev. B **68**, 060401(R) (2003).

[66] G. Kresse, and J. Furthmller, Phys. Rev. B **54**, 11169 (1996).

[67] G. Kresse, and J. Furthmller, Comput. Mater. Sci. **6**, 15 (1996).

[68] G. Kresse, and D. Joubert, Phys. Rev. B **59**, 1758 (1999).

[69] G. Kresse, and J. Hafner, Phys. Rev. B **47**, 558 (1993).

[70] S. L. Dudarev, G. A. Botton, S. Y. Savrasov, C. J. Humphreys and A. P. Sutton, Phys. Rev. B **57**, 1505 (1998).

[71] S. Okatov, A. Poteryaev, and A. Lichtenstein, Europhys. Lett. **70**, 499 (2005).

[72] M. T. Czyzyk and G.A. Sawatzky, Phys. Rev. B **49**, 14211 (1994).

[73] N. Nakagawa, H. Y. Hwang, and D. A. Muller, Nature Mat. **5**, 204 (2006).

[74] J. Kohanoff, Electronic Structure Calculations for Solids and Molecules ,
p. 26(Cambridge University Press, 2006)

Index

Vita

Cheng-Ching (Joseph) Wang was born in Taipei, Taiwan on September 27th, 1975, the elder son of Su-Shim Wang and Mei-Hwa Huang. He received his Bachelor and Master of Science degrees on physics from the National Central University in Taiwan and was commissioned lieutenant in The R.O.C. Marines in 1999. He decommissioned from the Marines in 2001 and worked as a research assistant at National Center for theoretical sciences and National Dong-Hwa University at eastern Taiwan at early 2002. He was accepted to the doctoral program on physics at the University of Texas at Austin on August in 2002. He enjoys dropping by coffee shops at Austin when he runs out of ideas on research.

Permanent address: Department of Physics
The University of Texas at Austin
1 University Station C1600
Austin Texas 78712

This dissertation was typeset with LaTeX† by the author.

---

†LaTeX is a document preparation system developed by Leslie Lamport as a special version of Donald Knuth's TeX Program.